Larger Scale Mining at Kankberg

A rock mechanical investigation of the transition from post-pillar mining to longhole open stoping

Master's thesis

Annabel Rijsenbrij

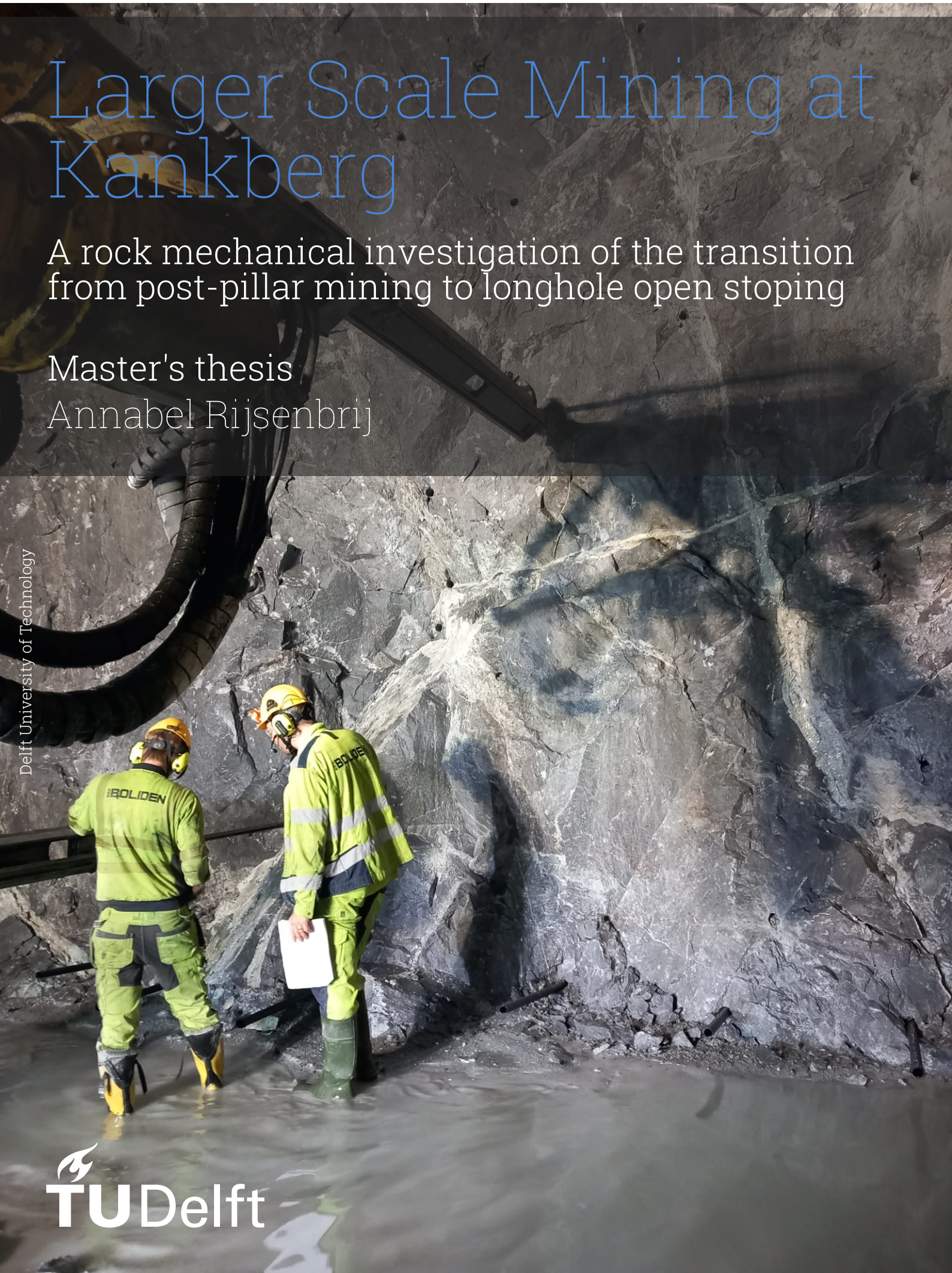

Delft University of Technology

TU Delft

Larger Scale Mining at Kankberg

A rock mechanical investigation of the transition from post-pillar mining to longhole open stoping

by

Annabel Rijsenbrij

Student number:	4703081
Thesis committee:	Dr. ir. Dominique Ngan-Tillard
	Dr. Pierre-Olivier Bruna
	Ir. Daniel Sandström
	Ir. Tim-Oliver Latta
Project Duration:	December, 2023 - August, 2024
Faculty:	Faculty of Civil Engineering and Geosciences, Delft
Company:	Boliden

Cover: Underground in the Kankberg mine

TU Delft

Acknowledgement

This thesis marks the end the eventful era of my student life, during which I got the chance to experience countless small and big adventures thanks to the amazing people around me. It is ending on a high note in the north of Sweden, where I found a third home, next to Spain and the Netherlands.

I want to thank my university supervisors Dominique and Pierre-Olivier for sharing their knowledge and supporting me throughout the project. Special thanks go to Dominique, who spiked my interest in rock mechanics even more during the fieldwork in Tarragona, kept me on my toes during the thesis, and inspires me to dive into the details and keep on studying to become my best self in our field. I will remember to speak up to clearly share my insights, as she taught me. Additionally, I really appreciate Pierre's positive and encouraging way of supervising. His door was always open for a quick question or another explanation about defining paleostress orientations based on conjugate discontinuity sets. He also contributed a lot to the readability of the report by highlighting every single caption that was included in the text and confusing sentence in the draft version. One of the results was that Justin Bieber's 'What do you mean?' was playing on repeat in my head for a week. I hope it is more understandable now.

Of course this thesis would not have been possible without my supervisors from Boliden, Daniel and Tim. I want to thank Daniel wholeheartedly for welcoming me in Sweden and in his team, for giving me the opportunity to move around freely to get to know the company and other mines, and for providing some critical notes towards my work. Moreover, I am grateful for Tim's support during the days when I couldn't see the forest for the trees, for being so approachable for day-to-day questions such that I could keep the speed of the project high and for introducing Skeå and its surroundings to me.

I would like to put Karl-Heinz in the spotlight for inspiring me throughout my studies with his stories to go out and explore the world. He encouraged me to take time for additional experiences, which lead to great opportunities such as working with TU Delft's geothermal well, doing a research project in Ghana (even though Africa is not quite his first choice. I hope I managed to convince him of my positive experiences there) and finishing my studies in Sweden. He taught me the importance of working hard and committing to your goal, and meanwhile staying aware of the 'small-scale' society directly around you and contributing to its growth.

I want to thank my parents for raising me to feel a constant drive to improve myself, my life and the world. Extra thanks for letting me catch my breath in Canelles every now and then. I am grateful for Erik, who tries to keep up and connects the loose ends that I leave while running through life. Thanks a lot to Kata, my role model to become a nerd (in the good way, I think we are slowly getting there), to Joos for our endless discussions in which we try to fathom life, to Carrie for all our videocalls during the last months, and everybody else, thanks for your support!

Un grand merci à Emma, ma colocataire formidable qui m'a motivée ces deux derniers mois de la thèse, qui m'a appris la langue d'un pays où je ne vivrai pas et avec qui j'ai découvert la Suède sous son meilleur jour. À bientôt en Australie!

Och sist men absolut inte minst, tack till alla fantastiska människor som jag fick chansen att lära känna, särskilt Elias, Malin och David. Tack vare er vänlighet har jag inget annat val än att lämna allt bakom mig för att flytta hela vägen till norra Sverige för att leva det svenska livet. Jag ser fram emot att jobba med er, ta promenader till sjön under fikapauserna och göra mycket roliga saker med Bugiganga!

Annabel Rijsenbrij
Canelles, Spain, August 2024

Summary

This project investigates the potential transition from small-scale post-pillar mining to large-scale longhole open stoping in Kankberg, an underground mine in Sweden. Due to increasing instability issues, it has been decided to investigate the feasibility of adopting longhole open stoping, which regular design enables controlling a selection of the mining equipment remotely, ensuring the safety of the miners. Three stoping designs have been created, of which the most geotechnically feasible one is determined. One design option follows the conventional diameters with primary stopes of 10m width and secondary stopes of 15m width. The second design option has both primary and secondary stopes with 15m width. Also in the last design option all stopes have a width of 15m, and the orientation of the stopes is horizontally rotated by 26°.

The targeted ore body is an Au-Te deposit, which is a predominantly felsic intrusion that underwent various types of alteration and subsequently has been intersected by multiple dykes, resulting in a complex geological and geotechnical setting. It has been noted that major failures of the rock mass often occur along east-west striking boundaries between competent and soft rock. A numerical stress model is made in the software Map3D to calculate the stress distribution during and after excavation and execute a stress-induced failure analysis. A structure-induced failure analysis has been performed based on the determined rock mass properties and the characteristics of the occurred major wedge failures.

It was found that the major principal stress does not reach the yield strength of the rock type, therefore not inducing failure. This is explained by the shallow depth of the stope designs, leading to little overburden pressure. Tensile stresses are encountered in the stress model above the access drifts of the first production level, just above the previously mined slices.

A study on structure-induced failure has investigated the geotechnical risk of competence differences at the boundary between competent and weak rock, major fractures, sericite schist and the presence of andesite dykes. Also the bearing capacity of the foundation of the stopes has been evaluated. The study concluded that option 3 has the most favourable design from a geotechnical perspective.

A further investigation of the stability of the stopes was conducted using the Modified Stability Method, which combines stope dimensions with rock type and rock mass parameters and the in-situ stress field. This approach also resulted in a preference for design option 3.

The favoured design option has been modified into design option 4, in order to decrease the geotechnical risks further. Recommendations have been made on the location and length of the stopes, and the location of a selection of the access drifts. Moreover, an optimal horizontal rotation of the stopes could be found by performing further stress distribution calculations. This could reduce the extent of the relaxation zones, without increasing the tensile stresses above the access drifts to a critical level.

Further research is required to gain a deeper insight in the geological and geotechnical conditions and their impact on stope stability, such as the distribution of sericite schist and the persistence of major fractures. Additionally, exploring the use of a refined approach for calculating stress distribution is recommended. Since various modifications of the Stability Method have been developed, it is also suggested to investigate which version would be optimal for Kankberg.

Contents

Preface i

Summary ii

Nomenclature ix

1 Introduction 1

2 Geology and mine design 2
2.1 Geologic history . . . 2
2.2 Ore body . . . 2
2.3 Current mining method: post-pillar mining . . . 6
2.4 Future mining method: longhole open stoping . . . 9

3 Available data, software and theories 15
3.1 Available data . . . 15
3.1.1 Core logging . . . 15
3.1.2 Geologic maps . . . 16
3.1.3 LiDAR scans . . . 17
3.2 Theories . . . 17
3.2.1 Rock stress equations . . . 17
3.2.2 Stress controlled failure criterion per rock type . . . 17
3.2.3 Modified Stability Chart . . . 17
3.3 Software . . . 19
3.3.1 Deswik . . . 19
3.3.2 Gem4D . . . 20
3.3.3 Rocscience . . . 20
3.3.4 Map3D . . . 20
3.3.5 Leapfrog . . . 21

4 Methodology 22
4.1 Rock type, rock mass and major failure characteristics . . . 22
4.2 Stress development due to excavation . . . 23
4.3 Geotechnical challenges . . . 23
4.4 Geotechnical feasibility of the stope designs . . . 24

5 Results 25
5.1 Rock type, rock mass and major failure characteristics . . . 25
5.1.1 Rock mass characteristics . . . 25
5.1.2 Rock type characteristics . . . 26
5.1.3 Characteristics of major failures . . . 29
5.1.4 Results evaluation . . . 36
5.2 Stress development due to excavation . . . 37
5.2.1 Model construction . . . 37
5.2.2 Overall stress changes through steps . . . 37
5.2.3 Differences between models . . . 40
5.2.4 Results evaluation . . . 42
5.3 Geotechnical challenges . . . 43
5.3.1 Stress-induced failure . . . 43
5.3.2 Structure-induced failure . . . 46
5.3.3 Overhang . . . 50
5.3.4 Critical areas . . . 52

5.3.5 Results evaluation . . . 53
5.4 Geotechnical feasibility of the stope designs . . . 54
5.4.1 Stope selection . . . 54
5.4.2 Q'-parameters . . . 54
5.4.3 N'-parameters . . . 54
5.4.4 Stability charts . . . 55
5.4.5 Optimal design option . . . 58
5.4.6 Results evaluation . . . 60

6 Discussion **61**

7 Conclusion **64**

References **66**

A Conversion sheet RMR data to Q parameters **69**

B σ_1 distribution around stopes **72**

C Excel sheets for Modified Stability number determination **75**

List of Figures

2.1 Geological map of the eastern part of the Skellefte district (Wagner and Wenzel, 2007). 3
2.2 Whole ore body (side view). . . . 5
2.3 Gold distribution (red) at 500m depth (top view). . . . 6
2.4 Mine design post-pillar mining. . . . 7
2.5 S310 s13. . . . 8
2.6 S310 s14. . . . 8
2.7 S310 s15. . . . 8
2.8 Rock type legend geological maps. . . . 9
2.9 Longhole open stoping excavation sequence (Fernberg, 2007). . . . 10
2.10 Front, side and top side of stope design 1 (images retrieved from Deswik). . . . 11
2.11 Front, side and top side of stope design 2 (images retrieved from Deswik). . . . 12
2.12 Front, side and top side of stope design 3 (images retrieved from Deswik). . . . 13

3.1 Conversion factor from BRQD to RQD. . . . 16
3.2 LiDAR image of S310 s15. . . . 17
3.3 Graphs for determination of the factors that are required to find N', and the Stability graph (Potvin, 1988, Stewart and Forsyth, 1995). . . . 19
3.4 Gem4D. . . . 20
3.5 Stereonet from Dips, showing poles and corresponding averaged discontinuity orientations. . . . 20
3.6 Building a stope design in Map3D. . . . 21
3.7 Leapfrog. . . . 21

4.1 Stope model visualization in Map3D. . . . 23

5.1 Mean and standard RQD over depth. . . . 25
5.2 Stereonets of poles of all discontinuities combined per mined slice of S310. . . . 26
5.3 Stereonets with discontinuity poles for sericite-quartzite per mined slice of S310. . . . 27
5.4 Stereonets with discontinuity poles for sericite schist per mined slice of S310. . . . 28
5.5 Stereonets with discontinuity poles for quartz-feldspar-porphyry per mined slice of S310. 28
5.6 Stereonets with discontinuity poles for breccia per mined slice of S310. . . . 29
5.7 Stereonets andalusite-quartzite per mined slice of S310. No andalusite-quartzite was encountered in s15. . . . 29
5.8 Top view of slice 13, 14 and 15 in S310, indicating overbreak and failure area division. . 30
5.9 Overbreak that exceeds two meters above the planned roof level, and geology for each slice in area A. The numbered hatched zones in the geologic close-ups correspond to pillars. . . . 31
5.10 Slice 14 area A major fall-outs and corresponding stereonets. . . . 32
5.11 area A major fall-outs and corresponding stereonets. . . . 32
5.12 Geotechnical borehole data in slice 15. . . . 33
5.13 Area B overbreak and geology. The scale starts two meters above the designed roof level. 34
5.14 Slice 13 area B overbreak and geology. . . . 35
5.15 Slice 14 area B overbreak and geology. . . . 35
5.16 Area B major fall-outs and corresponding stereonets. . . . 36
5.17 Stope design options containing the mining sequence (indicated by numbering) in Map3D. 37
5.18 Stress distribution through mining steps 1, 3 and 6 for design option 1 on horizontal grids located one meter above the access drifts. The stope model is seen from the south side. The stress levels are displayed on a scale ranging from 0 MPa (blue) to 80 MPa (red). The arrows point at relaxation zones. . . . 38

5.19 Minor principal stress distribution through mining steps 1, 3 and 6 for design option 1 on horizontal grids located one meter above the access drifts. The stope model is seen from the south side. The stress levels are displayed on a scale ranging from 0 MPa (blue) to -40 MPa (red). The coloured areas indicate tensile stresses. 39
5.20 Stress distribution through mining steps 1, 3 and 6 for design option 1 on vertical grids that are positioned through the access drifts (right grid), the middle of the stopes (middle grid) and at the back end of the stopes (left grid). The stope model is seen from the west side. The stress levels are displayed on a scale ranging from 0 MPa (blue) to 80 MPa (red). The arrows point at relaxation zones. 40
5.21 Stress accumulation and relaxation variation between models after mining step 3, the excavation of the primary stopes of the first production level. Top row: Differential stress. Bottom row: tensile stress. Note the different scale. The grids are positioned at mid-height of the stopes. The arrows point at relaxation zones. 41
5.22 Stress accumulation above stope access drifts after mining step 6. Top row: Differential stress. Bottom row: tensile stress. Note the different scale. The grid level is 1m above the stope access drifts of the first production level. The arrows point at relaxation zones. 42
5.23 Geology (left column) and stress distribution (middle and right column) through mining steps for design option 1. The stress distribution images overlay the geology images. Horizontal grids one meter above the stope access drifts. 44
5.24 Geology (left column) and stress distribution (middle and right column) through mining steps for design option 2. The stress distribution images overlay the geology images. Horizontal grids one meter above the stope access drifts. 45
5.25 Geology (left column) and stress distribution (middle and right column) through mining steps for design option 3. The stress distribution images overlay the geology images. Horizontal grids one meter above the stope access drifts. 46
5.26 Sericite schist (red) - quartz-feldspar-porphyry (dark green) boundary that is prone to failure due to a competence difference between the rock types. 47
5.27 Top view, 1m below the roof of the first production level for each design option. The arrows point at the SERSCH-QFP boundary in the stope walls. 47
5.28 Top view, top of access drifts into second production level for each design option. The black arrow points at the remainder of the previously covered sericite schist formation. The white arrow points at the second sericite schist formation. 48
5.29 Detail of slice S310 s15, underbreak due to incoming fracture. The black lines indicate the area that was planned to be mined. Due to the dissipation of blasting energy through the discontinuity, the rock behind it did not get damaged enough to fail. 48
5.30 Incoming fracture with respect to each design option. The stopes are yellow and slice S310 s15 is red. 49
5.31 Andesite dykes (light green) through access drifts of the designs. 50
5.32 Position of the pillars in the underlying cut-and-fill slice with respect to the different stope designs. The secondary stopes are numbered. 52
5.33 Areas to be investigated further. 53
5.34 Stability graphs following Potvin (1988), design option 1. In case that N' is below 0.1 no dot is presented and the face is assumed to fail. 56
5.35 Stability graphs following Potvin (1988), design option 2. In case that N' is below 0.1 no dot is presented and the face is assumed to fail. 57
5.36 Stability graphs following Potvin (1988), design option 3. In case that N' is below 0.1 no dot is presented and the face is assumed to fail. 58

6.1 Updated design option 3, where the green lines indicate the opted adjustment on the design and the purple line indicates the incoming fracture that cuts through a selection of the stopes in the first production level. 61

6.2 Further geotechnically optimized design option 3, where the stopes are moved such that the cut-and-fill pillar location is more favourable with respect to the secondary stopes. Secondary stope 3* could be added to account for the relocation of the stopes out of that place. The green lines indicate the opted adjustment on the stope location and the purple line indicates the incoming discontinuities that cuts through a selection of the stopes in the first production level. The secondary stopes are numbered. Stope 3* has been added to the design. The eastern primary stope is removed. 62

A.1 Conversion sheet Ja 70
A.2 Conversion sheet Jn 71
A.3 Conversion sheet Jr 71

B.1 σ_1-distribution around the stopes for design option 1. 72
B.2 σ_1-distribution around the stopes for design option 2. 73
B.3 σ_1-distribution around the stopes for design option 3. 74

C.1 Design option 1, western and middle stope. 76
C.2 Design option 1, eastern and secondary stope. 77
C.3 Design option 2, western and middle stope. 78
C.4 Design option 2, eastern and secondary stope. 79
C.5 Design option 3, western and middle stope. 80
C.6 Design option 3, eastern and secondary stope. 81

List of Tables

2.1 Advantages and disadvantages per stope design. 14

3.1 Geotechnical logging values and corresponding explanation for joint fill and joint roughness individually. 16

5.1 Rock mass parameters per rock type 27
5.2 In-situ stress 37
5.3 Colour-coding of the geological model per rock type based on yield strength, where rock types with a low yield strength have a colour towards red and rock types with a high yield strength a colour towards green. 43
5.4 Standardized parameters for occurring rock types to obtain Q' 54
5.5 A-values induced stress for each occurring rock type. 55
5.6 B-values for walls containing sericite-quartzite. 55
5.7 B-values for walls containing sericite schist. 55
5.8 Geotechnical advantages and disadvantages per stope design, desk study and Modified Stability analysis combined. The geotechnical challenges are weighted based on the risk that they impose. 59

Nomenclature

Glossary

Term	Definition
Access drift	Drifts that branch off from main underground infrastructure, such as declines and ramps, to facilitate access to the production areas in the ore bodies.
Backfill	The material used to fill the voids or empty spaces left after ore extraction in an underground mine.
Back wall	The vertical or near-vertical exposed rock surface at the beginning of a stope, where the development enters the stope.
Cemented backfill	A type of backfill material used in underground mining where waste rock, tailings, or other fill materials are mixed with cement or other binding agents to create a stable and supportive fill for mined-out voids or stopes.
Development	Underground drifts, generally outside the ore body, that facilitate access to the ore bearing rock. It includes ramps, declines, and access drifts.
Dilution	Mixing of waste rock with ore.
Front wall	The vertical or near-vertical exposed rock surface at the end of a stope, where the development ends.
Primary stope	A stope that is mined in the ore body without adjacent excavations. It is backfilled with cemented waste rock.
Production level	An underground working level where active ore extraction takes place. It is a specific horizontal or nearly horizontal level within the mine where mining operations are focused on extracting ore from the deposit.
Secondary stope	A stope that is excavated adjacent to or in between already mined and backfilled primary stopes, giving it one or two artificial sidewalls.
Shotcrete	A construction and mining material used to provide a protective or structural coating to surfaces. It is a form of concrete applied pneumatically (sprayed) onto surfaces.
Side wall	The vertical or near-vertical surfaces that form the sides of a stope in an underground mining operation. These walls are the exposed rock faces left after the ore has been extracted from the stope.
Sill pillar	Horizontal pillar that separates production levels from each other.
Overbreak	The fracturing of a larger volume of rock mass during blasting than designed for.
Slice	A horizontal or near-horizontal underground excavated layer in an ore body that is removed in a down-up sequence, where the roof in the present slice will be the floor in the next one.
Stope	A vertical or near-vertical underground cavity or void created as a result of the extraction of ore between two sublevels. The stope is the primary working area in this method, where ore is drilled, blasted, and removed.
Stope face	Stope wall.

Term	Definition
Sublevel	A horizontal or nearly horizontal underground level or working area that is located between the main levels of a mine and provides access to the ore body for drilling, blasting, and ore extraction.
Underbreak	The fracturing of a smaller volume of rock mass during blasting than designed for.

Abbreviations

Abbreviation	Definition
RQD	Rock Quality Designation
BRQD	Boliden Rock Quality Designation
RMR	Rock Mass Rating
SRF	Stress Reduction Factor
QFP	Quartz-feldspar-porphyry
SERSCH	Sericite schist

1

Introduction

The Kankberg mine owned by Boliden and located in Västerbotten, Sweden, is an underground gold mine that has been operating since 2012. The targeted ore is located in an alteration zone of volcanic material. It is mined using the post-pillar mining method. Whilst the general direction of mining is upwards, multiple production levels are active within one ore body due to sill pillars. Historically, the mine operated with a very low reinforcement plan and little disruption during mining. At date, worsening geological and geotechnical conditions, especially in the upper mine, reduce current production rates and impose safety risks. Currently, extensive reinforcement measures are used to prevent the formation of wedge fall-outs from the roof and through the pillars. This results in a decrease in productivity, mining pace, and economic viability.

This project aims to investigate the feasibility of changing from small scale mining towards larger scale sublevel longhole open stoping, which increases the safety of a selection of the independent mining operations, namely the mucking and hauling, can be controlled remotely. Three preliminary stope layout designs are provided by the mine planning department. Each design will be analysed from a geotechnical perspective. Therefore, the main research question will be: *Which stoping design will be most feasible from a geotechnical perspective?*

A large database of geological data is available and used to model the rock type distribution in the area of interest. However, geotechnical data in the area of interest is scarce, which complicates the classification of the rock mass. In order to execute a rock mass classification the available geotechnical data has been analysed, after which a structural analysis and a stress distribution study have been performed. These components are combined in a geotechnical pre-feasibility study that investigates the stability of the stopes. Four subquestions are formulated to answer the main research question:

1. What are the rock type, rock mass and major failure characteristics in the area of interest?
2. How will the stress distribution in the rock mass develop during excavation?
3. Which areas in the stope design are prone to geotechnical challenges?

First, the geological history of the area is discussed and the ore body features are explained. This is followed by a description of each stope design option. Chapter 3 provides an overview of the data that is available at the initiation of the project, the applied theories and the used softwares. Chapter 4 covers the methodology that is used to address each specific sub-question, followed by the presentation of results corresponding to each sub-question. Chapter 6 covers an overall discussion of the project and its results and lastly, a conclusion is stated.

2

Geology and mine design

2.1. Geologic history

The Fennoscandian Peninsula, encompassing Norway, Sweden and Finland, consists primarily of strongly metamorphosed Archean and Proterozoic rock formations (Blom, 2017). It is subdivided into seven geological domains, of which the Svecofennian domain covers most of Sweden. This domain is predominantly influenced by the Svecofennian orogeny caused by the opening of the Svecofennian sea. The orogeny took place during the Paleoproterozoic, approximately from 2 to 1.8 Ga (SGU, 2020). It consisted of four major stages leading to accretion, extension, collision and gravitational collapse, respectively (Korja et al., 2006). These processes were accompanied by metamorphism, volcanic activity and sedimentation (Nironen, 1997, Lahtinen et al., 2009). Overall, the orogeny induced a semi-continuous subduction zone with a NW-SE strike (Bogdanova et al., 2015, Lahtinen et al., 2023). The sedimentary and volcanic formations that were formed on top of the Paleoproterozoic layers have mostly been eroded by the glaciers that covered the Fennoscandian Shield during the Quaternary ice ages (Guitreau et al., 2014, Sadeghi et al., 2013).

The Skellefte district, in which the Kankberg mine is located, is a mineral-rich area located in the Svecofennian domain. It consists of meta-volcanic, meta-sedimentary and meta-intrusive material (Guitreau et al., 2014). The volcanic and plutonic basement rocks are mainly (ultra)mafic and are partly metamorphosed into greenstone belts. This basement is covered by the meta-volcanic Skellefte Group and the meta-sedimentary Fargfors Group in the Skellefte district (Tavakoli et al., 2012). The primarily felsic Skellefte Group formed 1.90-1.88 Ga by a volcanic arc system caused by the occurring subduction and extensional processes, leading to a large collection of volcanogenic massive sulfide ore deposits that are of interest for the mining industry (Guitreau et al., 2014, Nordfeldt et al., 2019). Kankberg is located in the Skellefte Group (Figure 2.1)(Wagner and Wenzel, 2007). The Skellefte Group has been covered by the Vargfors Group, which was formed consists of fine-grained clastic meta-sedimentary layers and basalt (Dehghannejad et al., 2012, Tavakoli et al., 2012). Plate tectonics and the intrusion of mafic dykes lead to alteration of the rock mass. The primary structural geometry of the area is characterized by extensional faults with a WNW – ESE strike that intersect with faults running NE – SW, that have both been formed during the extensional periods in the Paleoproterozoic (Dehghannejad et al., 2012, Bauer et al., 2011). Later compression caused the faults to reactivate and reverse (Bauer et al., 2011). The most recent major deformation took place approximately 1.80 Ga and lead to an E-W compression (Bergman, 2001). This was accompanied by the mineralization of gold out of gold-bearing fluids with the same orientation (Bark and Weihed, 2012). Since the Proterozoic no major changes have occurred to the Skellefte district (Pabst, 2022).

2.2. Ore body

The Åkulla Au-Te deposit, which is targeted by the Kankberg mine, is a predominantly felsic intrusion that underwent various types of alteration, resulting in a complex geology (Figure 2.2). Sericitisation and silicification are alteration types that are associated with present Au-mineralisations. Sericitisation

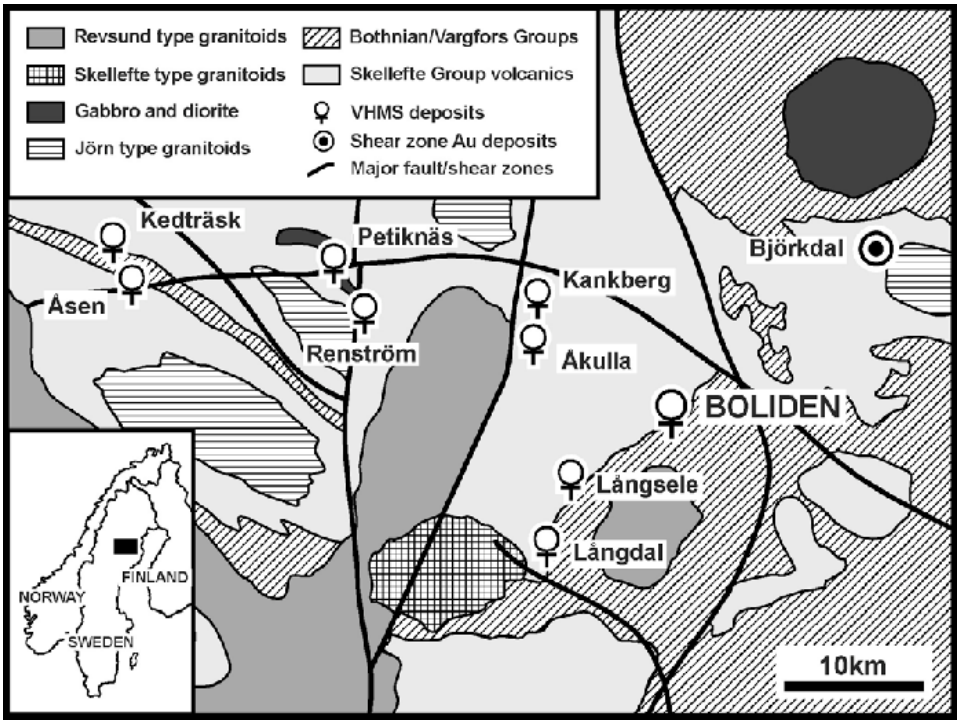

Figure 2.1: Geological map of the eastern part of the Skellefte district (Wagner and Wenzel, 2007).

is the hydrothermal alteration of orthoclase or plagioclase feldspars. The sericite rocks in the Kankberg mine are associated with the presence of muscovite. Silicification is an hydrothermal alteration where silica (SiO_2) replaces original material in the rock. The characteristics of the most important rock types will be explained (Jönsson et al., 1999, Latta, 2024, Blomberg, 2024, Ragnarsson, 2024).

Dacite

Dacite is a silica-rich volcanic rock that experienced rapid solidification. It is the base rock in which the intrusion deposited. The massive fine-grained rock has an average UCS of 143 MPa. Due to the absence of aperture and fill in the joints, dacite does barely pose geotechnical problems. The infrastructure of the mine is located in this rock. Low reinforcement is needed to ensure its stability. When approaching the Au-Te deposit the rock is altered into sericite-quartzite.

Sericite-quartzite

Sericite-quartzite is highly present in the intrusion. The schistosity is poorly to well developed and andalusite alteration is sometimes present. The rock has an average UCS of 125 MPa. Creep takes place when the in-situ stress environment experiences changes. The possible presence of sericite schist within the sericite-quartzite might affect the stability of the rock mass.

Sericite schist

Sericite schist is an altered rock mainly composed of sericite, although it can also include muscovite minerals that can reach up to 1 cm in size. The foliated rock has an average UCS of 104 MPa. Even though it occurs in minor quantities, it poses stability issues. The rock is highly deformable, and instabilities are caused by the foliation and the present joints. Moreover, failures take place at interfaces between sericite schist and competent rock types. Due to these features, the rock type generally requires heavier reinforcement. However, one of the reinforcement elements, shotcrete, does not stick the sericite schist due to low adhesion and detachment along the foliation planes .

Chlorite-quartzite

Chlorite-quartzite is an alteration rock that was formed under high availability of chlorite. It shows many similarities to sericite-quartzite, e.g. an equal average UCS of 125 MPa, and the occurrence of creep. A distinct feature is the presence of chlorite in the rock joints, which exhibits greater slipperiness compared to sericite.

Andalusite-quartzite

Andalusite-quartzite is a massive homogeneous rock type with a UCS of 235 MPa. It is the silicate alteration of Al-rich material and contains an abundancy of aluminium silicate minerals, like andalusite and topaz. The rock is very competent and no deformation is observed when the convergence of the roof is measured, leading to a low need for rock reinforcement. One issue with andalusite-quartzite is its poor drillability, caused by its hardness. This often results in delays in production cycles for drilling and bolting. Also, the joints are occasionally filled with muscovite and sporadically with talc, which could lead to instability of the rock mass. The presence of these joint fills strongly reduces the friction coefficient in the joints, which could result in fall-outs.

Quartz-feldspar-porphyry

Quartz-feldspar-porphyry is a strongly silicified coherent metamorphic rock with an average UCS of 306 MPa. Different levels of brecciation can occur, where greater extents of autoclastic and hydrothermal brecciation, are associated with increased alteration to sericite and a higher abundance of clasts. The presence of topaz and andalusite within this rock ranges from being non-existent to frequently observed, both within the matrix and in the form of distinct crystals. While quartz veins are a common feature in this rock, the occurrence of muscovite is rare. While this rock typically does not present significant geotechnical challenges, it is prone to absorb energy over time due to its homogeneity and mechanical properties. This could lead to a risk of sudden release of energy in the form of rock bursts.

Breccia

Several generations of brecciation are present. The material is very heterogeneous and the matrix is often strongly silicified and cut by quartz veins. Some parts are polymict, some altered or zoned, making it a challenge to assign stability values to it. The material has an average UCS of 203 MPa. Due to its highly brittle character, it is prone to microfractures, which can lead to pillar impairment. This issue is usually intensified by blasting. At freshly blasted faces small rock bursts often take place. Another issue is that the high strength of the material complicates the installment of rock bolts, as it reduces the drilling rate.

Dykes

Multiple dykes have intruded the area. The volcanic material is basaltic-andasitic, which is locally altered. The dykes are generally less than one meter wide. Their intrusion has caused local alteration to mainly chlorite and fuchsite, which developed into veins. Moreover, the presence of a dyke facilitates movement in the rock mass, which could create stability issues. This is especially critical if the dyke intersects a pillar.

Metal lenses

Massive sulfide lenses are present in the highly sulfidic rocks. They consist of chalcopyrite (copper), galena (lead), sphalerite (zinc), gold or pyrite. These lenses can cause geotechnical issues, as they can act as a slip planes. A result is that the stability of the rock mass is generally lower in zones with high mineral grades. Moreover, blast rounds are often seen an issue around metal lenses as the fragmentation size tends to be too large for the processing plant. This can lead to increased costs (i.e. machinery, labor, fuel) and additional crushing.

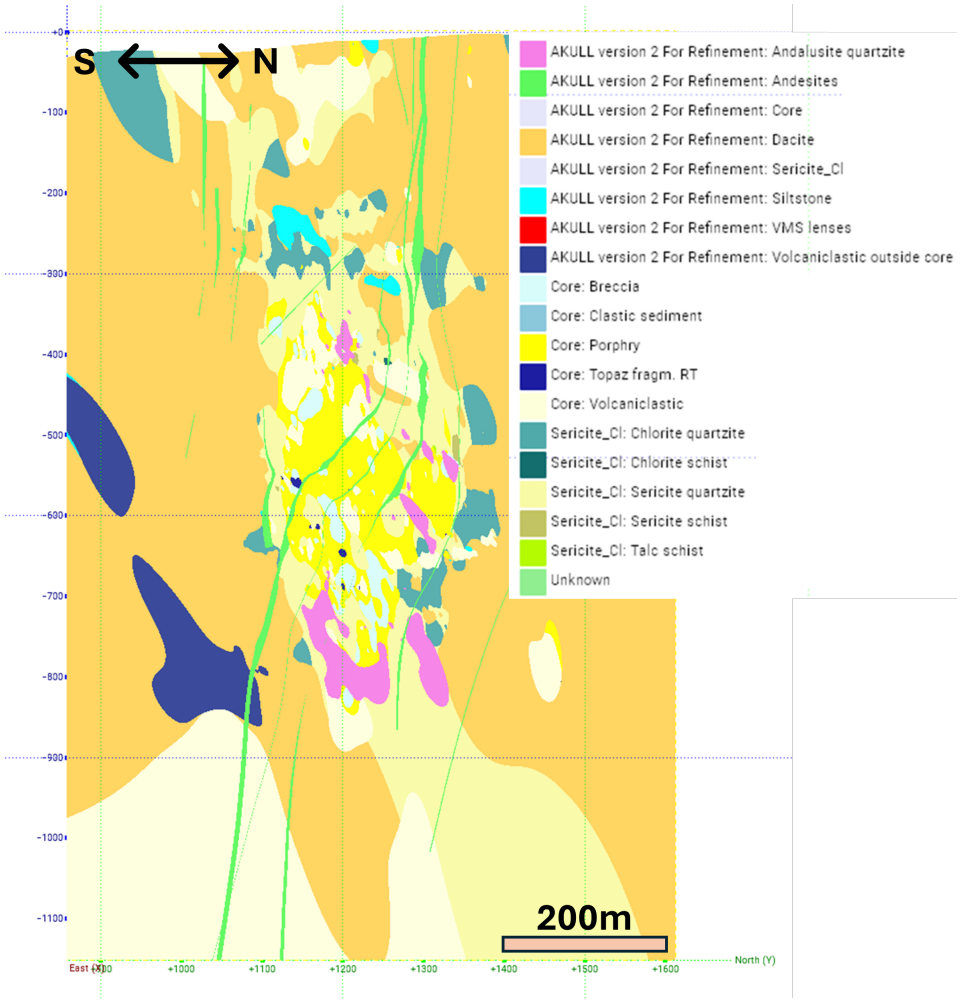

Figure 2.2: Whole ore body (side view).

The ore body extends from just below the surface to a depth of about 800m with an orientation of approximately 298/80 and a width of 200m maximum. It extends in a roughly east-west direction (Figure 2.3). This finds its origin in the direction of the paleostresses under which the ore has been formed. σ_1 was oriented in east-west direction induced by plate tectonics. Fractures were formed in the host rock parallel to the major principal stress direction, through which the ore-forming fluids were transported. Minerals from the fluids were deposited along the fracture walls or in cavities and porous spaces within the rock, which resulted in an east-west striking structural geometry of the ore body (Groves et al., 2018). The gold presence does not depend on a specific rock type, but it appears to be distributed randomly (Figure 2.3). This is due to the various depositional processes of the mineral in this area.

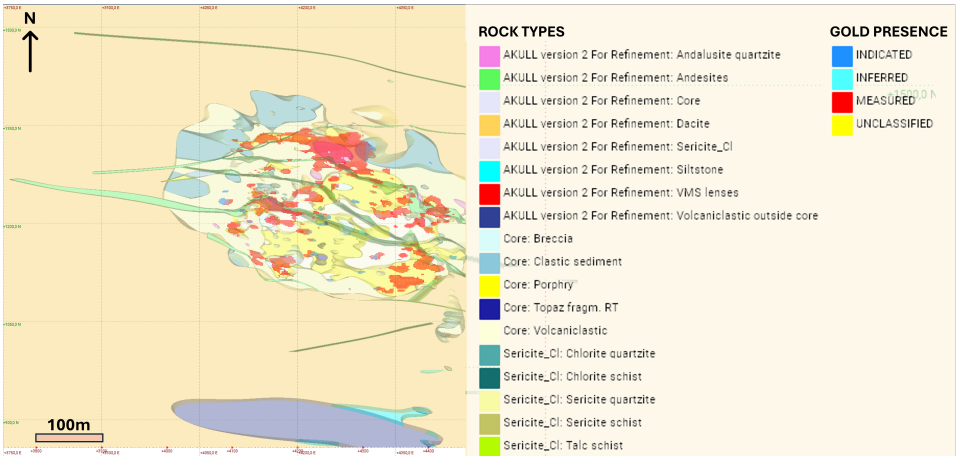

Figure 2.3: Gold distribution (red) at 500m depth (top view).

2.3. Current mining method: post-pillar mining

Currently, the ore is being mined using post-pillar mining, which is a selective underground mining method usually applied for high-grade and steeply dipping mineral deposits. This method starts at the bottom of an ore body and progresses upwards while excavating the material slice by slice. The pillars have design dimensions of 6m x 6m x 6m and the drifts are designed to have a width of 10m, height of 6m and theoretically unrestricted length (Figure 2.4c). After the hauling of the blasted material, rock reinforcement in form of fibre reinforced shotcrete and rock bolts is installed. Once the complete slice has been excavated, the drifts are backfilled with unconsolidated residual rock (waste rock), after which the next production slice is excavated. The machinery will drive on the backfilled material of the previous slice. The production rooms are reached through the development drifts, which are located outside of the ore body (Figure 2.4a). Access to each slice will be through drifts with different inclinations starting from a ramp at mid-height of a set of slices, an etage (Figure 2.4b) (Hustrulid and Bullock, 2007). In the Kankberg mine, the etages consist of six slices, each indicated according to the depth of the ramp towards an etage and whether they are located in the northern or southern ramp (N/S...) and the slice number (s..), e.g. S310 s14. The numbering of the slices restarts above a sill pillar, which is a horizontal layer of intact rock that will not been mined before all production units are mined.

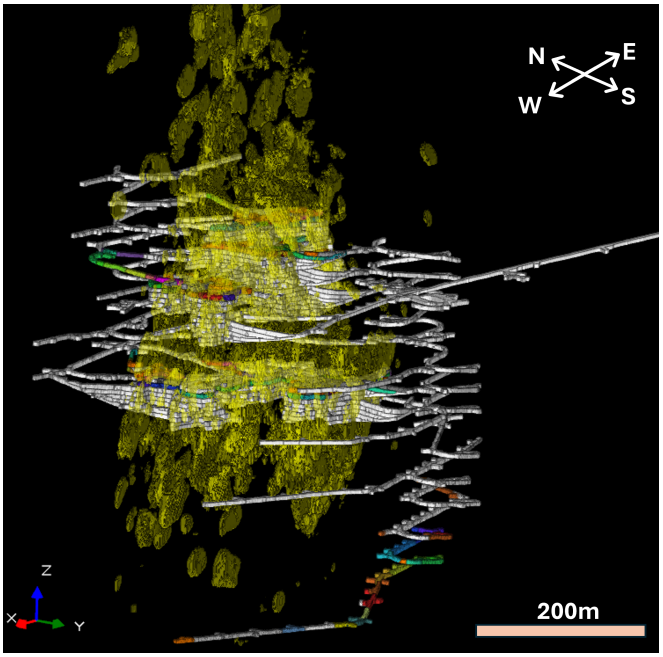

(a) Mined-out and back-filled areas of the Kankberg mine (side view).

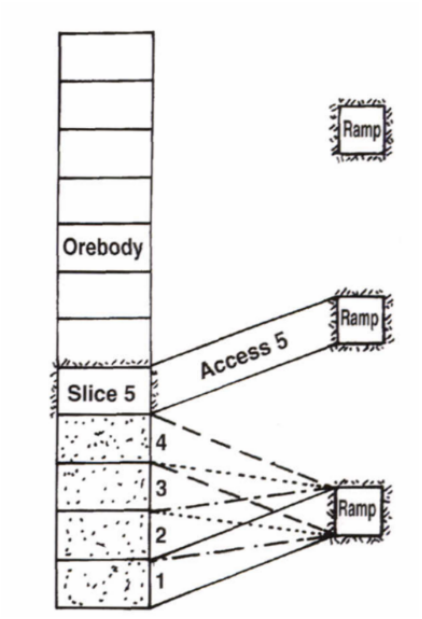

(b) Ramp access for cut-and-fill mining (side view) (Hustrulid and Bullock, 2007).

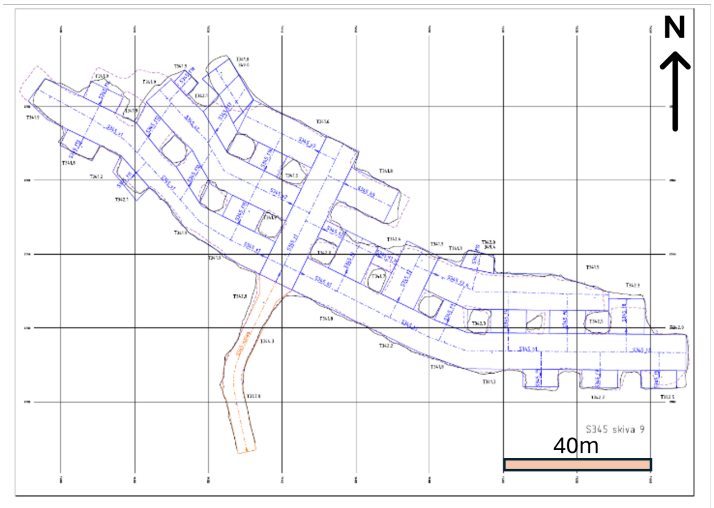

(c) Slice design (top view).

Figure 2.4: Mine design post-pillar mining.

While the mining of the ore progresses upwards, worsening geotechnical conditions are encountered, which affect the production pace and mined profile of drifts in S310 (Figure 2.5a, 2.6a, 2.7a and 2.8). Sharp rock mass contacts from extremely competent to soft and highly schistose rock types such as sericite schist induce challenges regarding roof stability and and profile alignment. From slice 11 upwards, major wedge fall-outs have occurred in each production level. The bolt length has constantly been increased up to the point where 5m bolts are installed in a tight pattern as systematic reinforcement rather than as mitigation measure. Figure 2.5b, 2.6b and 2.7b show the overbreak of the roof of slice 13 to 15, where blue corresponds to the planned roof level and the other colours to the amount of overbreak. The LiDAR image of slice 15 (Figure 2.7b) does not show the full extent of the wedge fall-out, since the area was inaccessible and could not be scanned. This wedge is expected to reach at least three meters higher.

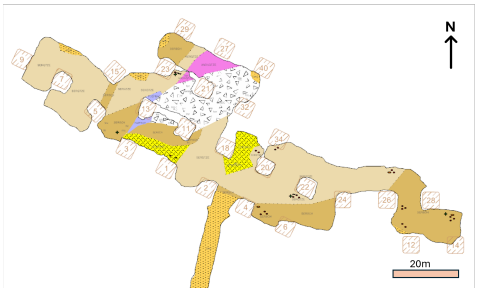

(a) Geology S310 s13.

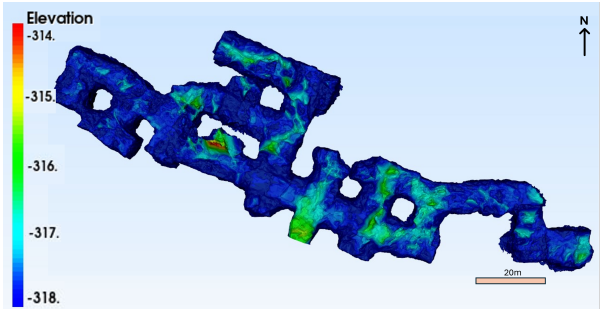

(b) Overbreak S310 s13 after excavation.

Figure 2.5: S310 s13.

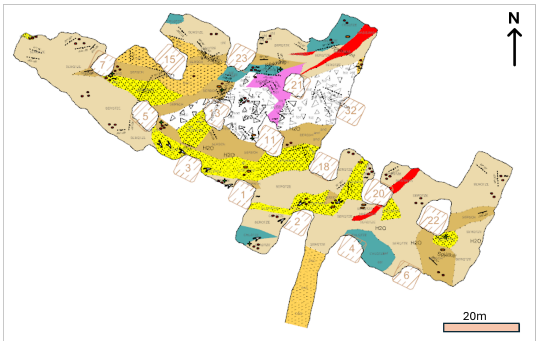

(a) Geology S310 s14.

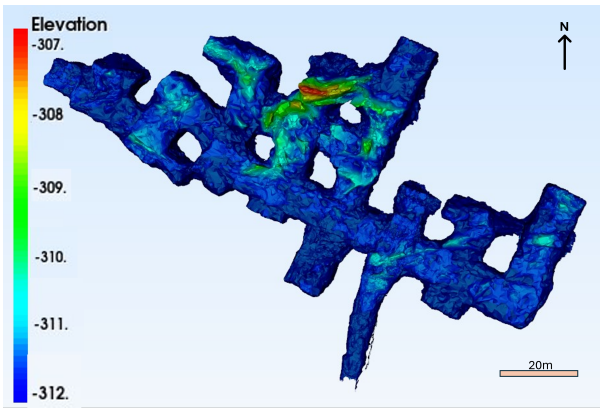

(b) Overbreak S310 s14 after excavation.

Figure 2.6: S310 s14.

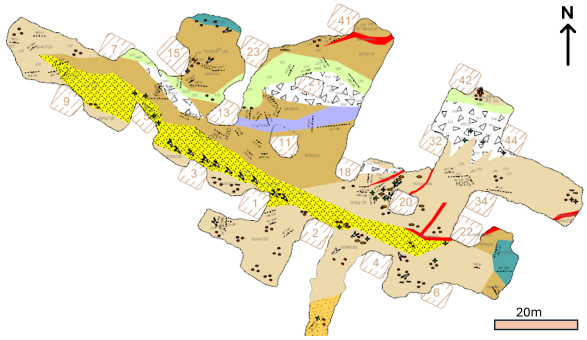

(a) Geology S310 s15.

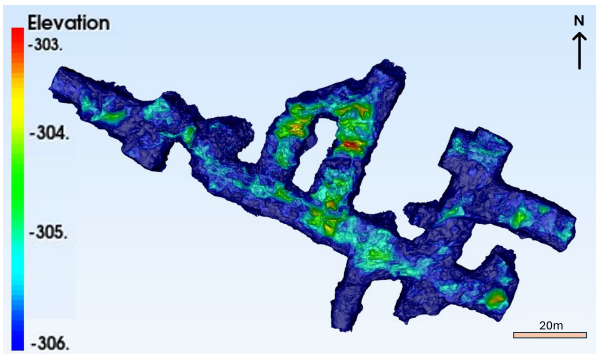

(b) Overbreak S310 s15 after excavation, before major wedge fallout.

Figure 2.7: S310 s15.

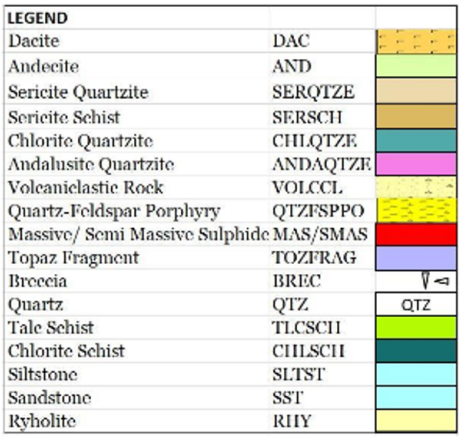

Figure 2.8: Rock type legend geological maps.

2.4. Future mining method: longhole open stoping

Due to the current stability issues it has been decided to investigate the option to change from post-pillar mining to longhole open stoping. This large scale mining method also works from the bottom of the steep ore body upwards and uses backfill for the mined areas. It consists of stopes with a height of approximately 25m for excavation of the ore. This results in increased productivity and the possibility of remote mucking and hauling, or even automating the process, due to the regular stope design. Moreover, no large (>14m) intersections are required, making reinforcement easier and limiting the size of wedge fall-outs, both of which enhance safety. However, increased dilution of waste material with ore will occur due to less selective mining.

The mining method differentiates between primary and secondary stopes, which are alternating each other in horizontal direction. First, the development drifts are created through the ore body at the floor level of the stopes and above them. The upper drift is used to drill the blastholes, install the rock bolts to keep the stope ceiling stable after blasting and backfill the stope. The lower drift is used for mucking out the blasted rock material. After the creation of the development drifts, the primary stopes are excavated and backfilled with cemented waste rock, resulting in a solid body. During this process the secondary stopes at the sides of the primary stope operate as pillars. Once two levels of primary stopes on each side of a secondary stope are backfilled, the secondary stope will be mined and backfilled with loose material (Figure 2.9). During this step the cemented backfill in the primary stopes acts as pillars. Stopes can be mined simultaneously at different levels, which leads to high productivity rates. Mining through sublevel open stoping initiates at 288 meter depth.

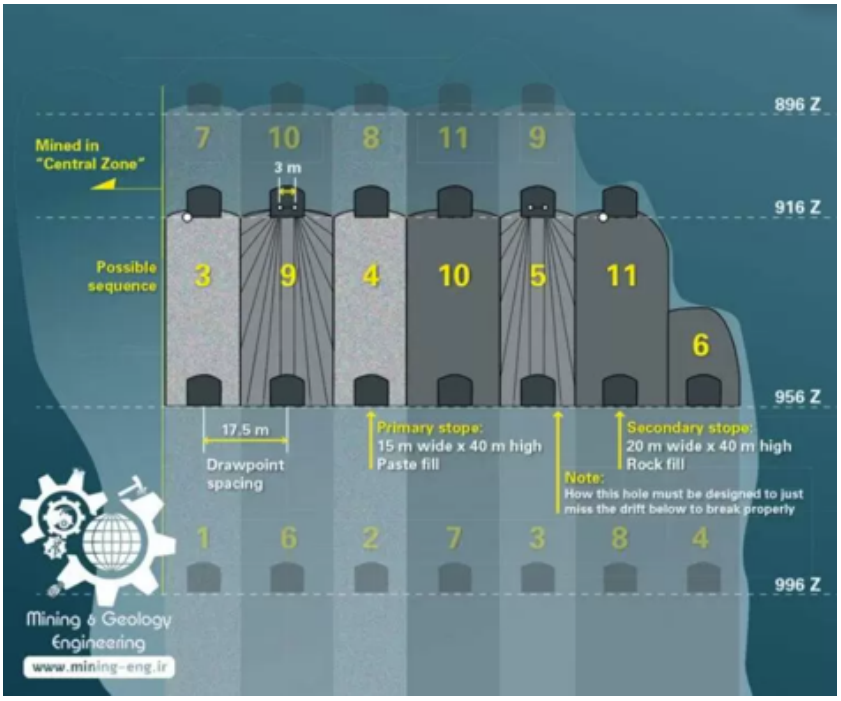

Figure 2.9: Longhole open stoping excavation sequence (Fernberg, 2007).

Three possible designs for the longhole open stoping section in the Kankberg mine have been created by the mine planning department. They will be evaluated geotechnically in order to determine the most feasible option.

Design 1

The first design is based on the Stope Optimizer option from Deswik. The feature generates an optimized stope design by considering the implemented geological model containing the ore distribution and incorporating specific predefined criteria, like stope dimensions. This model has been further refined manually, leading to the design in Figure 2.10. The width of the primary stopes (dark green) is 10m and the width of the secondary stopes (light blue) is 15m. Their height is 25m. Two outer secondary stopes (light green) have been reduced in width to account for decreasing grades. The front and back faces of the stopes are parallel to the horizontal direction of the ore body (Figure 2.10c). Vertically, the front wall is inclined under an angle, following the ore. The back wall of the stopes are vertical(Figure 2.10b). The stopes are oriented under an angle with respect to the underlying slices (Figure 2.10d).

Advantages of this model are the highest possible extraction of ore and the smaller primary stopes than secondary stopes. This leads to a low need for backfill cement, which reduces the costs.

Disadvantages of this model are the dimensions of the primary stopes and the orientation of the stopes with respect to the underlying slices. The primary stopes are not always aligned above a pre-existing pillar due to their relatively small width, which could lead to excessive overhang, leading to instability of the bottom production level, which could affect all stopes.

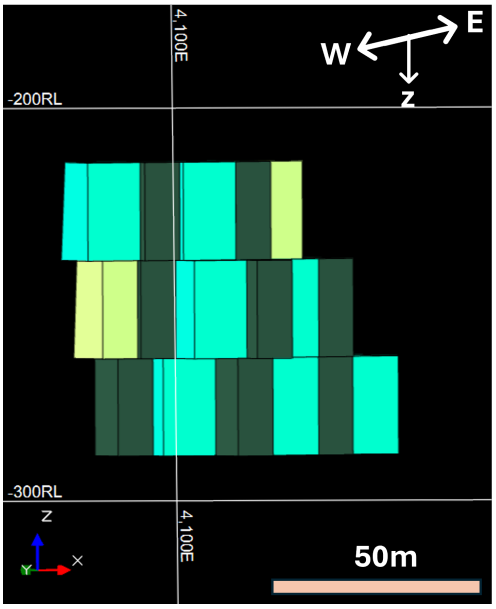

(a) Front view without ore body.

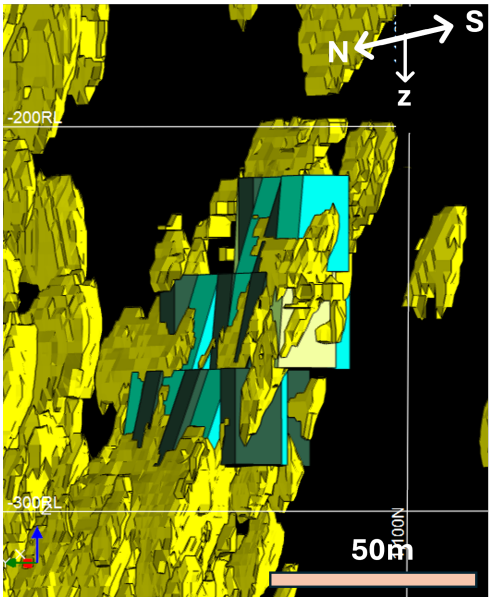

(b) Side view with ore body.

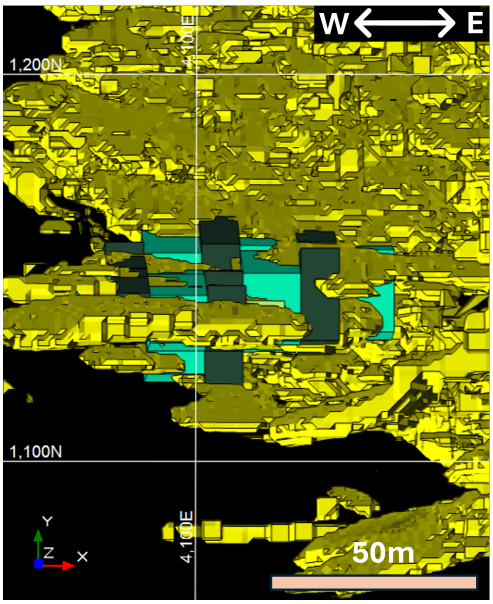

(c) Top view of with ore body.

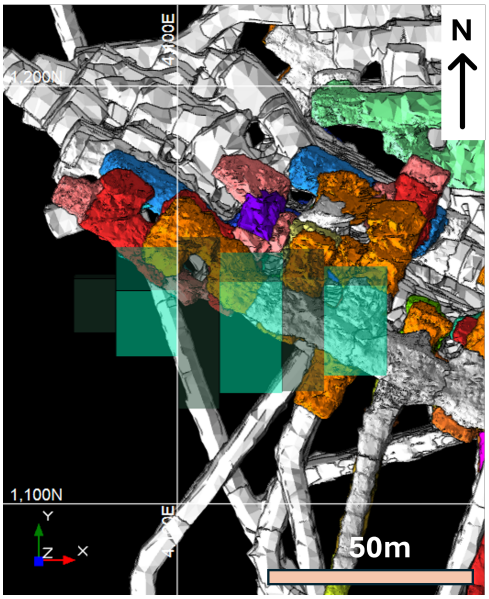

(d) Stopes with respect to underlying slices.

Figure 2.10: Front, side and top side of stope design 1 (images retrieved from Deswik).

Design 2

To compensate for the above-mentioned overhang issue, the second design has primary and secondary stopes with an equal width of 15m. As the distance between pillars in the post-pillar mining is 10m, a stope with a width of 15m serving as a pillar will always overlay an underlying pillar, which improves the bearing capacity of its foundation and reduces overhang. Moreover, due to the smaller amount of stopes, less access drifts are needed which leads to a reduction of required reinforcement and labor. A financial disadvantage of this design is that much more backfill cement will be required, as the primary stopes will have a larger volume.

(a) Front view without ore body.

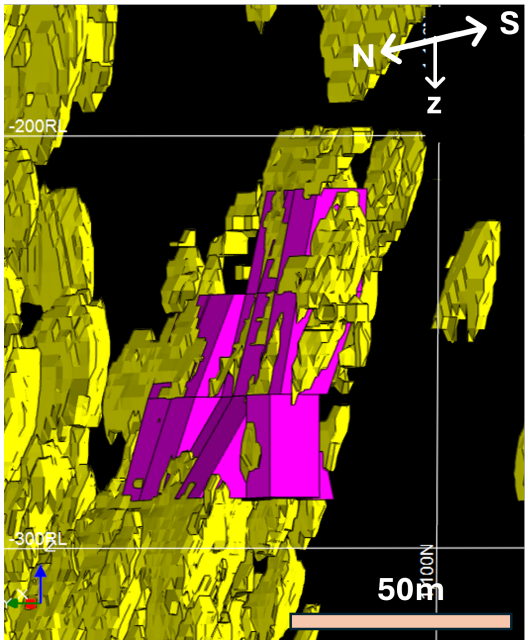

(b) Side view with ore body.

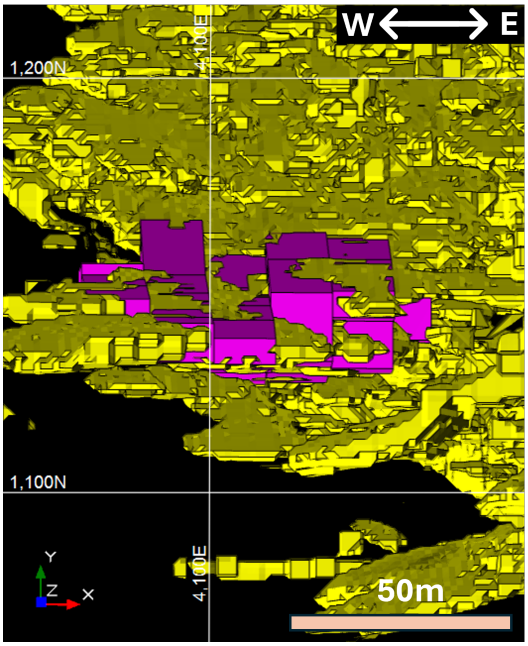

(c) Top view of with ore body.

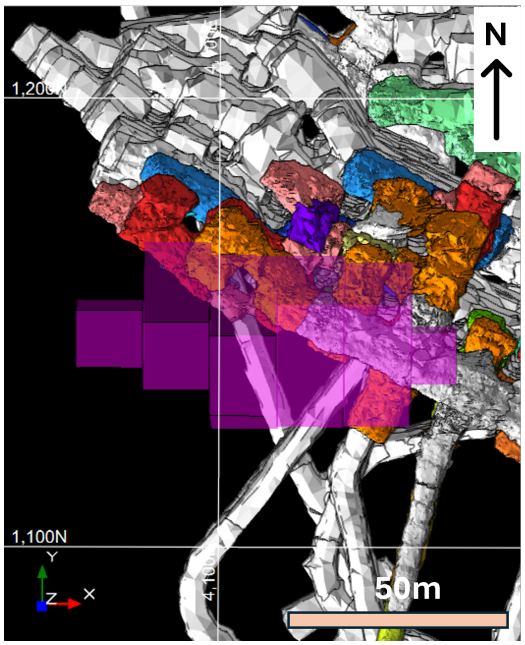

(d) Stopes with respect to underlying slices.

Figure 2.11: Front, side and top side of stope design 2 (images retrieved from Deswik).

Design 3

To further improve the stability of the stopes, they can be orientated along the previous mining orientation, giving them a strike of 26°. This will ensure their placement above a pillar in the underlying slices, which increases the bearing capacity of their foundation and reduces overhang (Figure 2.12d). Consequently, the stopes will no longer align with the horizontal orientation of the ore body, as shown in Figure 2.12c. While this adjustment improves stability, it reduces production optimization, leading to less ore extraction and increased mining of waste material.

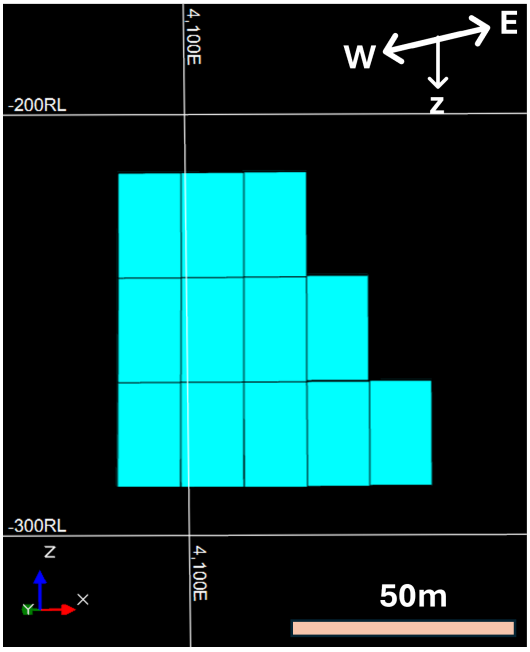

(a) Front view without ore body.

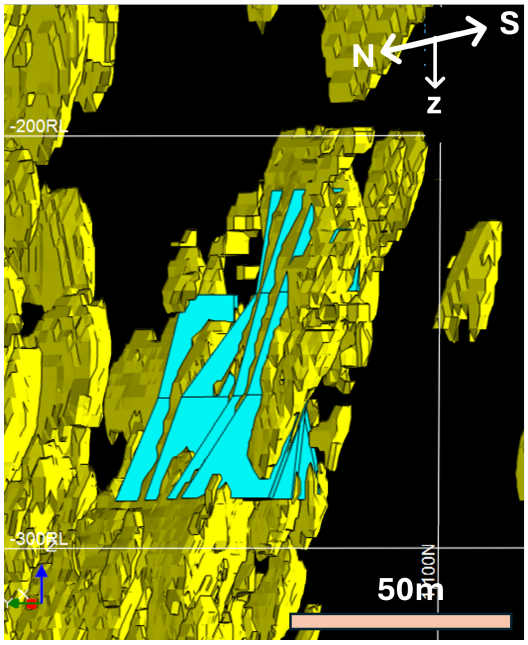

(b) Side view with ore body.

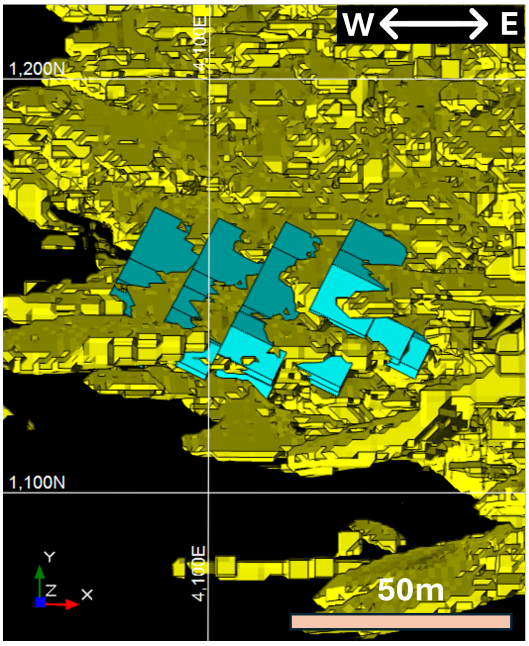

(c) Top view of with ore body.

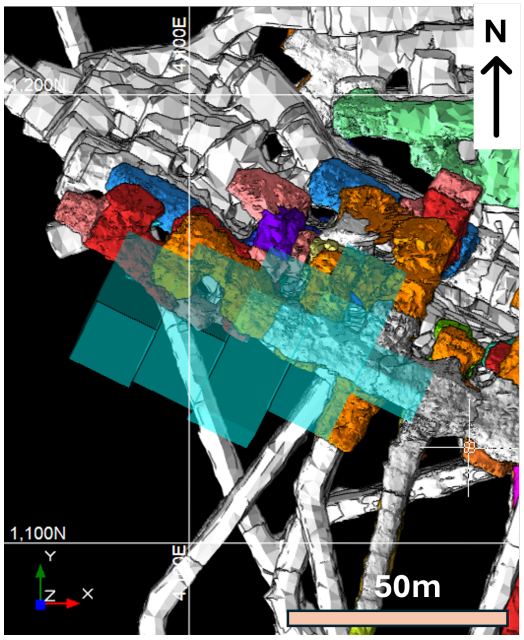

(d) Stopes with respect to underlying slices.

Figure 2.12: Front, side and top side of stope design 3 (images retrieved from Deswik).

Table 2.1 summarizes the advantages and disadvantages per stope design option. Design 1 is financially the most advantageous, and design 3 has geotechnically the best features.

	Advantages	Disadvantages
Design 1	Optimal ore extraction Low need for backfill cement	Susceptible to excessive overhang
Design 2	Reduced susceptibility to excessive overhang Less drift development required	High need for backfill cement Reduced ore extraction
Design 3	Further reduced susceptibility to excessive overhang Less drift development required	High need for backfill cement Further reduced ore extraction

Table 2.1: Advantages and disadvantages per stope design.

3

Available data, software and theories

3.1. Available data

3.1.1. Core logging

During the lifespan of the mine many boreholes have been drilled that have been investigated geologically, covering the occurring rock types, the associated minerals in the rock types and joints, and the core loss. This led to an extensive geological database on rock type distribution through and around the ore body. A smaller amount of boreholes has also been investigated geotechnically, providing among others UCS, BRQD and RMR values. Also the individual parameters that were used to determine the RMR are available, which are more of interest for this project than the RMR itself.

Boliden Rock Quality Designation (BRQD)

The Rock Quality Designation (RQD) is a rock mass classification system and evaluates the rock quality based on drill core logs. It reflects the amount of discontinuities in the rock mass and is defined as the percentage of the core that consists of pieces longer than 10 cm (Equation 3.1). An advantage of this method is that it provides a quick and simple way to classify the rock mass quality. A downside is that only the fracture frequency is taken into account, while multiple criteria, such as rock strength, fracture orientation and condition, and groundwater presence, affect the quality of the rock mass (Haldar, 2018, Deere et al., 1967, Deere and Deere, 1988).

$$RQD[\%] = \frac{\sum \textit{Core pieces > 10 cm}}{\textit{Total core length}} * 100\% \tag{3.1}$$

The RQD provides an insight in the degree of naturally induced joints in a rock core. The Kankberg cores are logged above ground, which requires the transportation of the cores and therefore leads to mechanically induced fractures. The Boliden Rock Quality Designation (BRQD) accounts for both natural and mechanical fractures. Conversion factors between the RQD and BRQD have been determined manually for different values, which were then used to create a best fit through the points (Figure 3.1). The equation that generates this graph is used for conversion of BRQD to RQD values (Equation 3.2).

$$RQD = BRQD * (-8 * 10^{-5} * BRQD^2 + 0.006 * BRQD + 1.2) \tag{3.2}$$

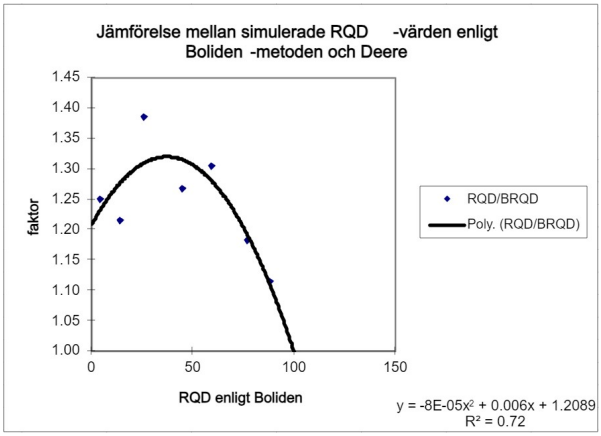

Figure 3.1: Conversion factor from BRQD to RQD.

Rock Mass Rating (RMR)

The Rock Mass Rating (RMR) is a rock mass classification system designed by Bieniawski (1976) for tunnels and mines. It takes multiple criteria into account, leading to a rock mass grade of 0-100. The RMR is based on five parameters: the strength of the intact rock material (UCS), the RQD, the presence of groundwater, and the discontinuity spacing and condition. Also the orientation of the discontinuities with respect to the excavation influences the rock mass grade, which can be taken into account when determining the RMR (Bieniawski, 1976, Bieniawski, 1989). This, however, has not been done by Boliden, since the boreholes are not oriented. The BRQD is converted to the RQD as explained in Section 3.1.1, so the standard RMR is retrieved. Not only the RMR values are available, but also the values for the parameters that are used to determine it, like joint fill and joint type. Specific logging values are attributed to different grades of joint fill and roughness individually. An example could be a borehole section of certain length with joints with a fill value 1 and roughness value 2, indicating a joint fill of 1-5 mm and a slickensided joint surface (Table 3.1) (Sjöberg and Sjöström, 2000).

	Joint fill (Ja)	Joint roughness (Jr)
0	0 mm	Rough
1	0-1 mm	Slightly rough
2	1-5 mm	Slickensided/biotitic/chloritic/altered
3	5-100 mm	Slickensided/slippery/talcic/altered
4	>100 mm	Gouge/clay/strongly altered

Table 3.1: Geotechnical logging values and corresponding explanation for joint fill and joint roughness individually.

Geological model

The geologically logged boreholes are implemented and interpolated in the software Leapfrog, which results in a geological model. The complexity of the heavily altered geology and presence of different alteration products (topaz, andalusite, sericite and chlorite) in varying abundances complicates the manual and therefore subjective logging of cores. An example is the rock types sericite-quartzite and sericite schist, which show similar features and can therefore accidentally be interchanged during the logging of the core. However, only rocks that show many similarities in appearance and therefore behaviour can be interchanged, which leads to a geological model that properly differentiates between soft ductile and hard brittle rock types, but might deviate from reality in rock type distribution within these classes.

3.1.2. Geologic maps

The geologic maps are compiled based on underground observations of the rock mass (Figure 2.5a, 2.6a, 2.7a and 2.8). The rock type determination is complicated by various aspects, leading to decreased precision of the maps. When shotcrete is applied before the geologist has visited the room, the rock mass is covered and cannot be examined. Only the lowest 1.5m of the walls are uncovered, which can be used to get an insight in the present rock types. Another complication is caused by the

absence of reinforcement. As the company's policy prohibits being under an unreinforced roof, certain faces cannot be approached close enough with a UV-lamp, which is used to determine the presence of topaz or andalusite alteration in the rock and needs to be within 30cm of the rock mass.

3.1.3. LiDAR scans

From S310 slice 13 onwards the excavated slices have been scanned using Leica Totalstations with high resolution point clouds (Figure 3.2). These scans show the failures in the roof in detail and could be used to determine the corresponding joint set orientations.

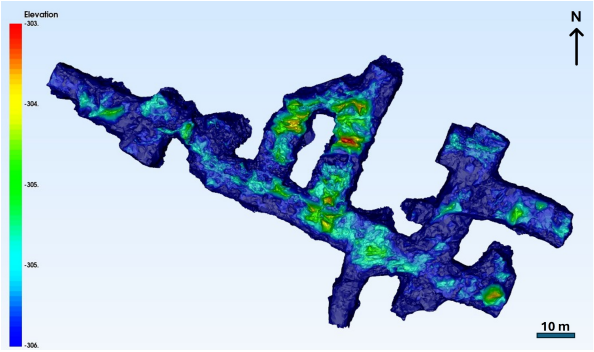

Figure 3.2: LiDAR image of S310 s15.

3.2. Theories

3.2.1. Rock stress equations

The in situ stress ratio between the horizontal and vertical stresses in the Scandinavian subsurface are deviating from the general stress ratios as a result of the induced pressure by the ice caps during the ice ages. The standardized stress equations for Scandinavia are the following (Larsson, 2019):

$$\sigma_H = 10.4 + 0.0446z \tag{3.3}$$

$$\sigma_h = 5 + 0.0286z \tag{3.4}$$

$$\sigma_v = \rho g z \tag{3.5}$$

3.2.2. Stress controlled failure criterion per rock type

Stress controlled failure may occur at an excavation surface as a result of reduced σ_3, which leads to internal tensile fracturing. Slabbing and spalling already develops in unconfined rock for σ_1-values below the UCS (Diederichs, 2003, Martin, 2005). Scholz (1968) found that plastic deformation initiates at 36-57% of the UCS, depending on the rock type. Also the loading rate influences the required stress level for plastic deformation, as higher loading rates lead to an average yield strength of 0.45*UCS, where lower loading rates show a yield strength of 0.35*UCS (Brace et al., 1966). The generally applied lower bound value for plastic deformation is 0.4*UCS, which is also used in this project (Martin et al., 1998, Scholz, 1968, Martin, 2005). For confined conditions, the equation is as follows (Martin, 1997):

$$\sigma_c = 0.4 * UCS + 1.5 * \sigma_3 \tag{3.6}$$

3.2.3. Modified Stability Chart

To investigate the stability of each surface of the open stopes the Modified Stability Chart from Potvin (1988) is used (Figure 3.3d). It links the hydraulic radius (m) to the Modified Stability Number (N'), which has a logarithmic axis. The hydraulic radius reflects the size and shape of the surface of the stope, as it is the ratio of the excavation surface to the perimeter of the exposed surface (Equation 3.7).

$$m = \frac{L * H}{2(L + H)} \tag{3.7}$$

The Modified Stability Number (N') represents the ability of a free surface to stand up under a given stress. The method makes use of the modified Q-system (Q'), which is another rock mass classification method that provides a value for the rock mass stability of an underground excavation in a jointed rock mass. Q' depends on four variables, namely the RQD of the rock mass, the number of joint sets (J_n), the joint roughness number (J_r) and the joint alteration number (J_a) (Equation 3.8). If the conditions of the joints are different, the parameters of the most unfavourable joint are used for the calculation. These parameters are inferred from the collected core log data for the determination of the RMR. The sheets that are used for converting the RMR data to the required Q' data can be found in Appendix A.

$$Q' = \frac{RQD}{J_n} * \frac{J_r}{J_a} \tag{3.8}$$

The Modified Stability Number combines Q' with the rock stress factor (A), the joint orientation factor (B), and the surface inclination factor (C) (Equation 3.9). The rock stress factor is calculated by dividing the UCS of the present rock type in the wall over the maximum stress exerted on the wall. This ratio is then used in the graph in Figure 3.3c, from which the rock stress factor can be determined. The maximum induced stress in a wall is derived from a numerical stress model obtained using the software Map3D, which will be explained in Section 3.3.4. The joint orientation factor relates the orientation of discontinuities to the orientation of the free stope faces and is determined using Figure 3.3b, which combines the effects of the dip angle difference and strike difference between the stope wall and the discontinuity. In case of multiple discontinuity sets, the most unfavorable discontinuity orientation with respect to the stope face should be considered. Lastly, the surface inclination factor accounts for the influence of the stope face angle relative to the horizontal, as there is an increased potential for instability for smaller angles. Equation 3.10 shows the calculation of factor C (Potvin, 1988, (Mawdesley et al., 2001b)).

$$N' = Q' * A * B * C \tag{3.9}$$

$$C = 8 - 6 * cos(\textit{angle of stope face inclination}) \tag{3.10}$$

Stewart and Forsyth (1995) subdivided the Modified Stability Chart (Figure 3.3d) into four zones, with the following definitions:

- **Stable**: The surface under consideration should be essentially self supporting. Dilution is estimated to be less than 10%.
- **Transition zone**: The surface under consideration should require some form of support. If support cannot be placed due to access constraints, some failure with associated dilution should be anticipated. However, a stable unsupported configuration should eventually be attained. Dilution is estimated to fall in the range of 10% to 30%.
- **Stable with support**: The surface under consideration will require extensive and heavy support. If due to access constraints support cannot be placed, a stable configuration may be reached only after a relatively large and probably unacceptable failure with associated excessive dilution and/or ore loss. Dilution is expected to be greater than 30%.
- **Collapse**: The surface under consideration is probably unsupportable and will fail and continue to fail until the void is completely filled or surface breakthrough occurs, i.e. a true caving situation.

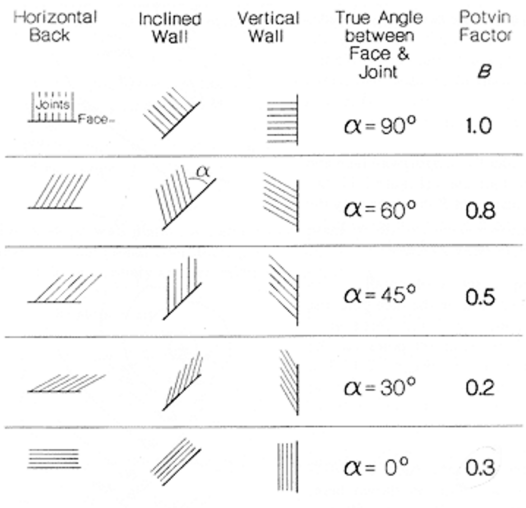

(a) Effect of discontinuity orientation versus face orientation.

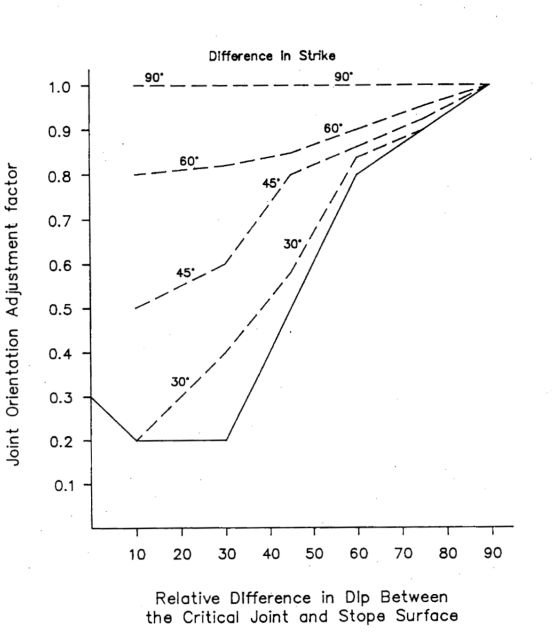

(b) Determination of joint orientation factor.

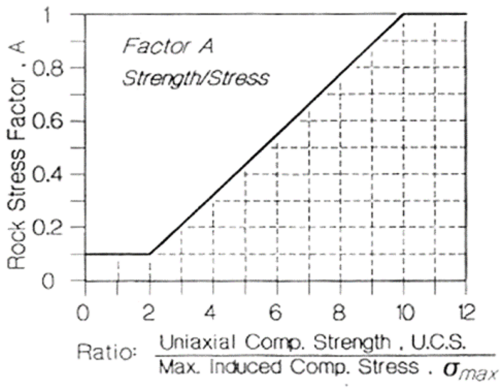

(c) Determination of rock stress factor.

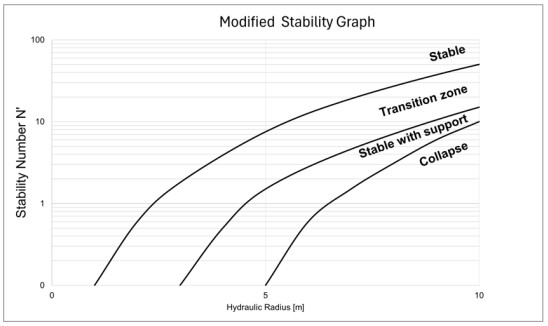

(d) Modified stability chart.

Figure 3.3: Graphs for determination of the factors that are required to find N', and the Stability graph (Potvin, 1988, Stewart and Forsyth, 1995).

3.3. Software

3.3.1. Deswik

Deswik is a software that is widely used in the mining industry and offers advanced planning, design and scheduling tools that assist in optimizing mining operations. In this project it is mainly used as visualisation program. It shows the already excavated and backfilled slices, the designs for the open stoping and the ore body. It is used for exporting the stope designs to implement them in Gem4D (Section 3.3.2) and Map3D (Section 3.3.4).

3.3.2. Gem4D

Gem4D 64-bit Beta version 1.8.6.5 is a software that is used for data visualisation and analysis. Boreholes are visualized as 3-dimensional tubes that show geological or geotechnical properties (Figure 3.4a). The program can also be used to identify the orientations of fractures that caused local failure. After implementing the LiDAR scans and setting the colour scale to 'elevation', any overbreak of the roof can easily be spotted. Setting the colour scale to 'poly dip direction' allows for the determination of fracture orientations (Figure 3.4b). The retrieval of these orientations is accomplished through a manual process that involves estimating the dip angle and selecting two distinct points along the failure plane. A circular shape is then generated between these points, which should align accurately with the failure plane. In case of a misalignment, the circle is recreated with either an adjusted dip angle or alternative points. This procedure is repeated for the largest feasible number of failure planes.

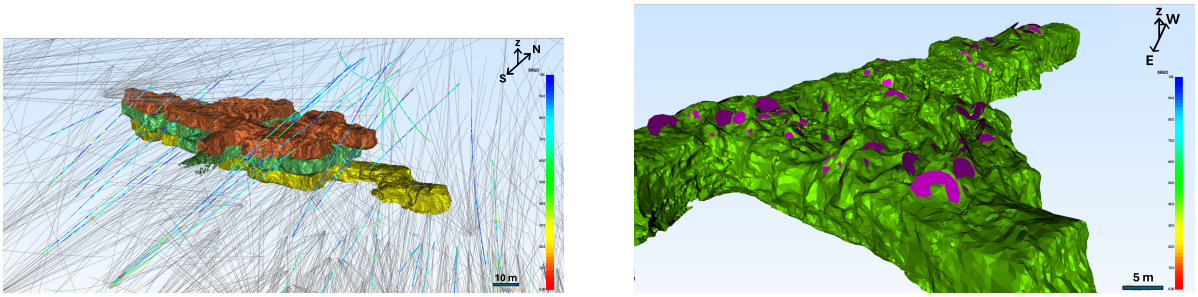

(a) Borehole visualisation around slices in Gem4D.

(b) Discontinuity orientation determination in Gem4D.

Figure 3.4: Gem4D.

3.3.3. Rocscience

Rocscience is a software that consists of various geotechnical engineering software tools for analyzing both soil and rock stability. For this project, the tool 'Dips' has been used.

Dips

Dips is a program that creates stereonets out of provided joint orientation data. After collecting the orientations of the failure planes in Gem4D, the data is implemented in Dips and stereonets containing the poles of the discontinuities are retrieved. A kinematic analysis on the roof can be executed by setting the failure mode to 'planar sliding (no limits)', the Slope Dip to zero and define a friction angle to visualize a friction cone on the stereonet (Figure 3.5).

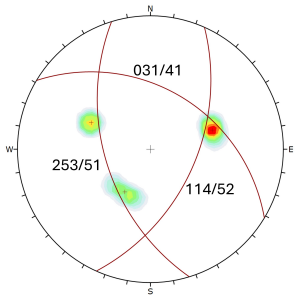

Figure 3.5: Stereonet from Dips, showing poles and corresponding averaged discontinuity orientations.

3.3.4. Map3D

Map3D is an elasto-plastic numerical modelling software that models mining-induced stresses in the subsurface. There are six input categories, namely the geometry of the mining model, the geology, the pre-mining stress state, the constitutive model type (elastic or elasto-plastic), the material properties (strength and stiffness) and the numerical approximation (the element size). There are three output categories: stresses, strains and displacements. Since the incorporation of geological units spikes the computation time of the software, homogeneity and isotropy are generally assumed. After implementing

the design of the excavation, the mining sequence of the to be excavated bodies is determined. The pre-mining stress state and the stiffness parameter are added, and multiple grids are distributed through the design. Subsequently, linear elastic simulations are performed by the software and stress distributions are retrieved.

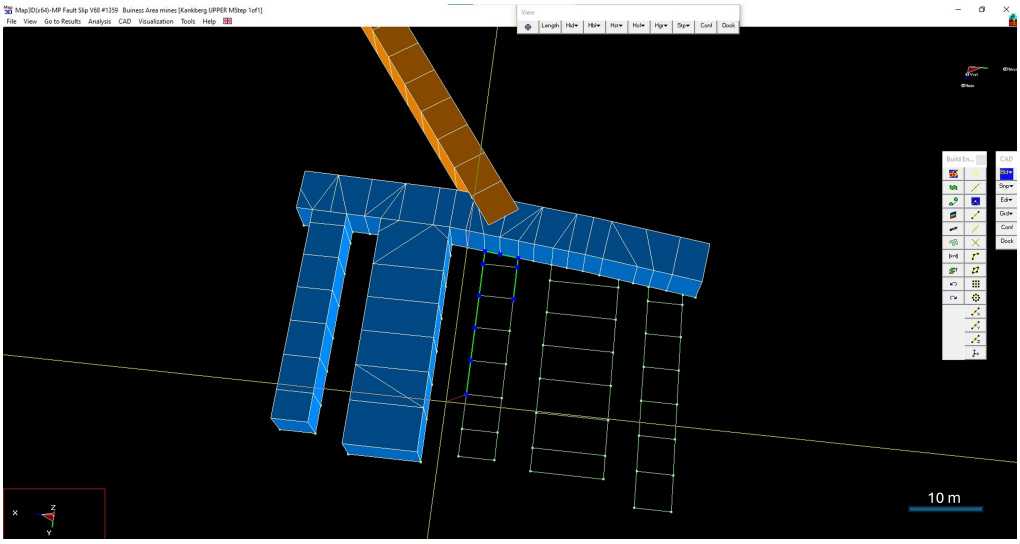

Figure 3.6: Building a stope design in Map3D.

3.3.5. Leapfrog

Leapfrog is a 3D geological modeling tool, enabling the creation of both categorical and numerical models (Figure 3.7). It integrates data from various sources, such as drillholes, points, and surfaces, directly into the modelling process. In this project, it is used to visualize the geological model of the mine and integrate it with the stope design models.

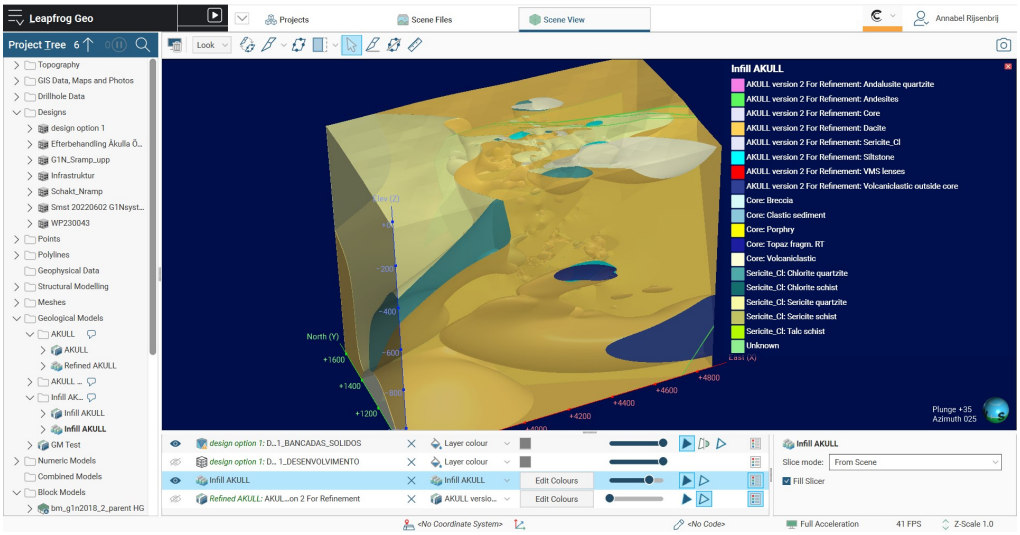

Figure 3.7: Leapfrog.

4

Methodology

In this chapter the methodology to answer each research question is explained.

4.1. Rock type, rock mass and major failure characteristics

BRQD, RMR and joint characteristics

As the area of interest has been investigated more thoroughly geologically than geotechnically, the objective is to supplement the geotechnical database by assigning standardized geotechnical parameter values to each occurring rock type. To gain insight in the spatial development in the rock fracturing, the available BRQD data is plotted against depth. Also, the mean and standard deviation of the BRQD and RQD, and the fracture characteristics are determined per rock type. The rock mass is described by converting the BRQD to RQD values and plotting them with respect to depth. The main discontinuity directions are determined and the hydrogeological situation is described.

Structural analysis

A structural analysis was performed to map the discontinuity orientations per rock type. This process has been carried out manually using Gem4D on the available LiDAR scans. It is assumed that the paleostress conditions are consistent across the area of interest, allowing for the assumption that predominant structures identified in a particular formation are likely to recur in other areas with the same rock type. Additionally, the condition of the discontinuities was investigated. The parameters used to determine the RMR regarding joint surface and filling have been analyzed for each rock type and included in the rock descriptions.

Failure criteria determination

To determine the failure criteria per rock type, a differentiation is made between stress controlled failure (often spalling or slabbing) and gravity driven failure. The stress controlled failure criterion is defined to be equal to the yield strength of a rock type, which is calculated as 0.4*UCS (Section 3.2.2). The gravity driven structurally controlled failure is analysed by mapping the orientations of the discontinuities that formed a failed block. The determination of the orientations is executed in Gem4D. Stereonets are created in Dips, which show the poles and the corresponding averaged discontinuity orientation per pole cluster. The retrieved stereonets are compared to investigate the presence of a recurring pattern regarding the orientation of the discontinuities and the method of failure (free fall or sliding). In case of sliding, a friction cone is plotted in the stereonet. The corresponding friction angle is based on the characteristics of the involved discontinuities, which are determined based on visual observations and boreholes that intersect the wedge failures. Additionally, the averaged joint surface and infill conditions for each rock type are analysed using geotechnically logged boreholes.

4.2. Stress development due to excavation

To determine the impact of the excavations on the local stress distribution, the software Map3D is used (see Section 3.3.4). The mine designs are built in the software and the in-situ stresses are calculated using the equations of Section 3.2.1. Homogeneity, isotropy and linear elasticity are assumed. The mining sequence is implemented based on the standard excavation order for open stoping, as explained in Section 2.4. Horizontally, grids are placed one meter above each access drift to investigate the effect of the excavation on the stress distribution in the roof of the access drifts, and in the middle of each stope to examine the stress distributions around them when not disturbed by the proximity of the access drifts. Vertical grids are placed in the middle of the design intersecting the stopes and the access drifts, and in the hanging wall (Figure 4.1b). Using the guideline of making the element size one fourth of the smallest object in the design and having pillars between the access drifts with a width of 5m, the result is a maximum element size of 1.25m. This is maintained to minimize the computation time. A sequence of mining steps has been implemented in the model to investigate the change in stress regime throughout the mining. The results for a selection of steps will be displayed. This includes step 1, where only access drifts have been excavated, step 3, after which a selection of the primary stopes has been mined, and step 6, after all mining is completed. The differential and tensile stress distributions are retrieved.

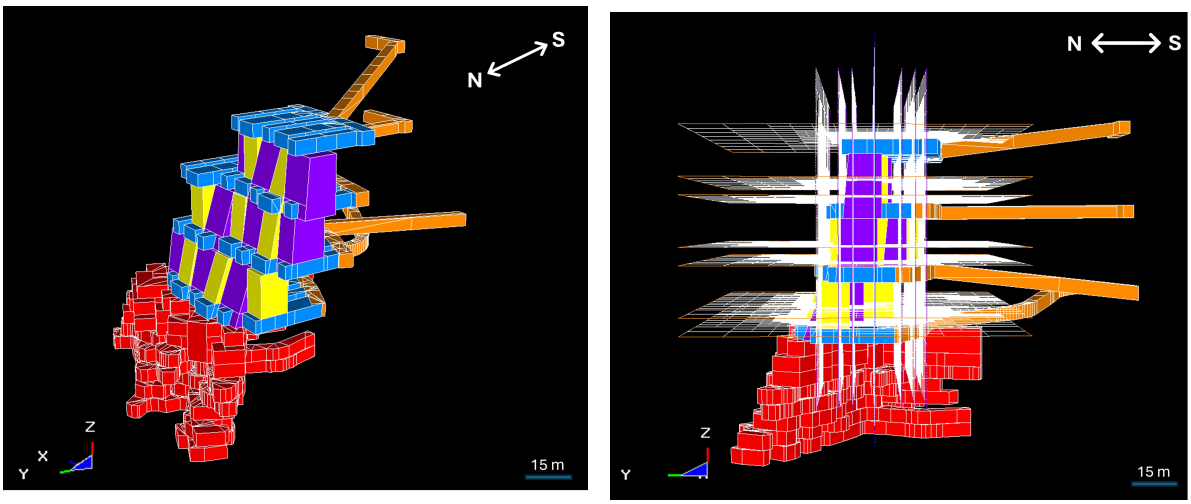

(a) Side view of the stope design.

(b) Grid plane distribution.

Figure 4.1: Stope model visualization in Map3D.

4.3. Geotechnical challenges

To determine which geotechnical challenges could be faced, a distinction is made between stress-controlled failure and structurally-controlled failure. To determine the likelihood of stress-controlled failure, the stress distribution model of each stope design option is compared to the geological model. This is done for the same selection of steps in the excavation sequence of which the results were shown in research question 2, namely step 1, 3 and 6. It is assessed whether areas subjected to high stresses contain weak rock types. This analysis is conducted at each grid location within the stress distribution model. The rock types in the geological model are coloured according to their yield strength, from red to green with increasing yield strength values. For structurally-controlled failure, which occurs in low-stress areas where the clamping force of discontinuities is reduced, the geology in and around the stope design models is investigated. First, the boundaries between weak and strong rock are identified and their orientation relative to the major principal stress direction is checked, as such configurations are known to cause failure. Afterwards, other possible stability issues are investigated and their effect on each stope design option is compared.

4.4. Geotechnical feasibility of the stope designs

To assess the geotechnical feasibility of the designs, the stability of a selection of stopes is analyzed for each model using the Modified Stability Method (see Section 3.2.3), which is widely used in the mining industry (Mortazavi and Osserbay, 2021). The BRQD has been translated to the RQD using Equation 3.1. The joint roughness number (J_r) and joint alteration number (J_a), are derived by modifying and implementing the values obtained for the RMR, as described in Section 3.2.3. The modification of these values is based on conversion charts between RMR and Q-parameters (Appendix A). The joint set number (J_n) is determined using the executed structural analysis, which provided discontinuity sets per rock type.

The rock stress factor (A) is determined using the σ_1-values provided by the numerical model that is created in Map3D, as explained in Section 3.3.4. To find the orientation factor (B), the most unfavourably oriented discontinuity set relative to each stope wall is identified. Subsequently, B is derived by implementing the orientation of this discontinuity in Figure 3.3b. To determine the gravity factor (C), Equation 3.10 is used. The hydraulic radius m is found by using Equation 3.7. In case of a stope with an inclined wall, the stope measurements are taken at its midpoint. The Modified Stability Number N' is calculated according to Equation 3.8 for each face of a stope. The outcomes concerning the roof, the least favourable scenario among the sidewalls, and the least favourable one among the front and back wall are plotted in the Modified Stability Chart (Figure 3.3d), which provides the stability of the stope. The calculations have been executed for the normal scenario and a bad case scenario where one standard deviation is subtracted from the RQD and other Q' parameters.

After executing the Modified Stability Method on the stope designs, the results are supplemented with the found geotechnical challenges to determine which design is most feasible.

5 Results

5.1. Rock type, rock mass and major failure characteristics

5.1.1. Rock mass characteristics

An analysis of the average RQD and its standard deviation through the rock mass has been executed. No trend in the mean RQD over depth through the ore body can be distinguished (Figure 5.1). Also the orientations of the present discontinuities just below the area of interest have been mapped. The stereonets of mined slices 13, 14 and 15 show two recurring discontinuity pole clusters with an average orientation of 182/48 and 358/49 (Figure 5.2).

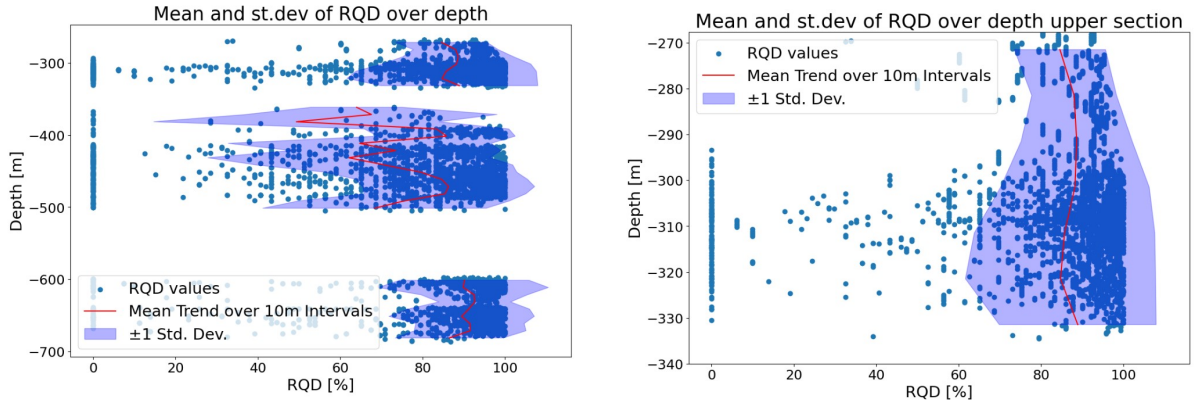

(a) RQD over the whole depth of the mine.

(b) Close-up of the area of interest.

Figure 5.1: Mean and standard RQD over depth.

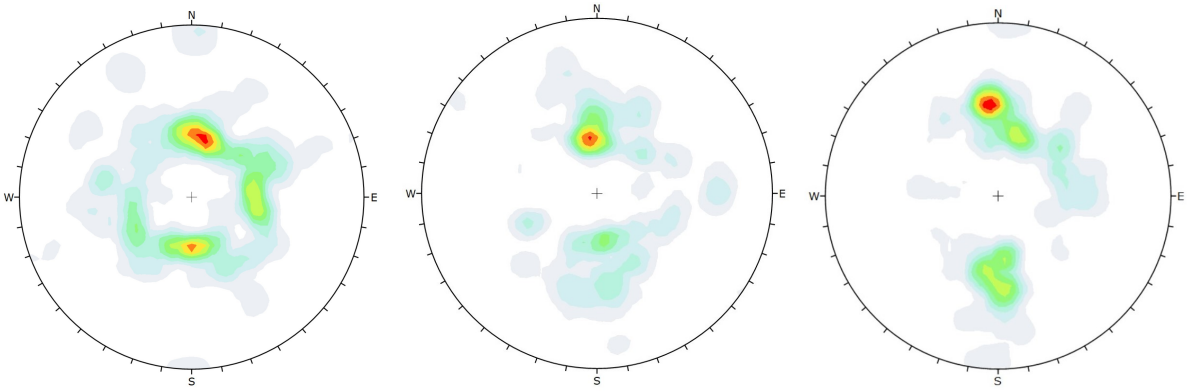

(a) Slice S310 s13. **(b)** Slice S310 s14. **(c)** Slice S310 s15.

Figure 5.2: Stereonets of poles of all discontinuities combined per mined slice of S310.

No hydrogeological investigation has been executed in the mine, but since no significant water inflow is observed, pressure build-up, wash-out of infill of the joints and other negative effects of water presence can be neglected.

5.1.2. Rock type characteristics

In this section, the geotechnical characteristics of each rock type are discussed. The average UCS, BRQD, discontinuity orientation, surface roughness and filling, and failure criteria are covered. Table 5.1 summarizes the findings per rock type. The discontinuity orientations are presented in order of frequency, from most (1) to least (5) common, and are colour-coded based on their corresponding dip direction. The pink and yellow clusters form a conjugate pair running with WNW-ESE strike. The orange-blue conjugate pair has a roughly E-W strike. Both pairs are formed during the Paleoproterozoic (Chapter 2.1). Since the ore body is formed in the same time period, these discontinuity sets are assumed to be found throughout the entire body in the rock types in which they are encountered. Due to the rotation of the principal stresses, shearing forces are applied on the pink-yellow conjugate discontinuity set. These discontinuities are deemed more unstable than the blue-orange cluster, which is not prone to shear.

	SERQTZE	SERSCH	QFP	BREC	ANDAQTZE
UCS [MPa]	125	104	306	203	235
σ_{crit} [MPa]	50	42	122	81	94
BRQD [%]	77 ± 19	61 ± 27	65 ± 19	76 ± 15	80 ± 14
RQD [%]	90 ± 19	73 ± 30	81 ± 21	85 ± 17	92 ± 9
RMR [-]	67 ± 11	56 ± 13	71 ± 11	69 ± 11	73 ± 10
Discontinuity cluster 1 orientation	177/37	003/52	003/33	278/38	005/45
Discontinuity cluster 2 orientation	025/36	354/33	175/46	005/34	182/62
Discontinuity cluster 3 orientation	-	280/41	-	184/46	-
Discontinuity cluster 4 orientation	-	202/41	-	-	-
Discontinuity cluster 5 orientation	-	178/53	-	-	-
Joint roughness					
Rough [%]	10.5	9.8	47.0	6.5	33.1
Slightly rough/discoloured [%]	42.3	16.1	30.3	56.7	39.4
Slickensided/biotitic/chloritic/altered [%]	41.6	55.8	19.6	30.0	22.8
Slickensided/slippery/talcic/altered [%]	4.0	16.1	2.8	3.9	4.2
Gouge/clay/strongly altered [%]	1.6	2.1	0.4	2.9	0.5
Joint fill					
0 mm [%]	9.2	6.3	39.2	10.4	23.3
0-1 mm [%]	83.9	73.0	53.7	80.1	70.6
1-5 mm [%]	6.5	19.8	7.0	9.4	5.8
5 - 100 mm [%]	0.4	0.8	0.1	0	0.5
>100 mm [%]	0	0	0	0	0

Table 5.1: Rock mass parameters per rock type

Sericite-quartzite/chlorite-quartzite

Sericite-quartzite has an average UCS of 125 MPa, and therefore a stress controlled failure criterion of 50 MPa (Equation 3.6). The rock has a BRQD of 77% with a standard deviation of 19%, giving an RQD of 90% and a standard deviation of 19%. The main discontinuity orientation is 177/37. The less apparent discontinuity set has an orientation of 025/36. Half of the joints have a rough to slightly rough surface, whereas only 6% contains infill with a very low friction angle (Table 5.1). Sericite-quartzite and chlorite-quartzite show high similarities and are therefore treated as equivalent to each other.

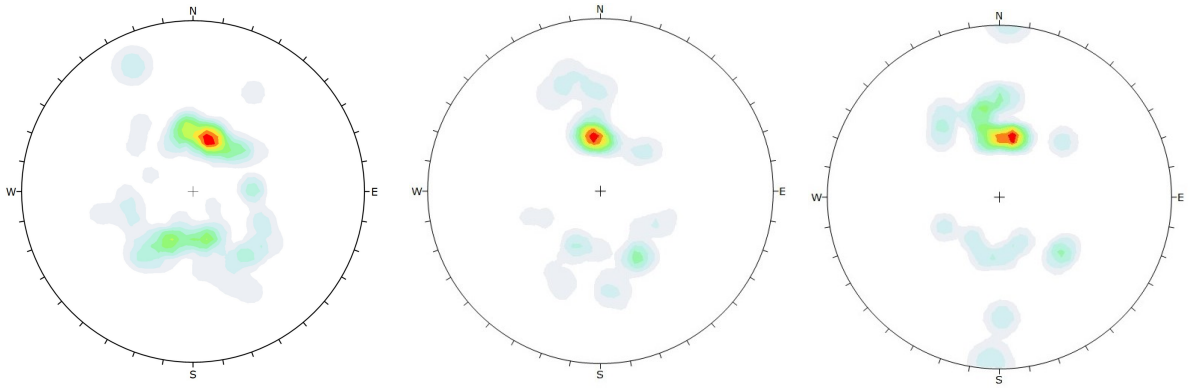

(a) Sericite-quartzite orientations S310 s13. **(b)** Sericite-quartzite orientations S310 s14. **(c)** Sericite-quartzite orientations S310 s15.

Figure 5.3: Stereonets with discontinuity poles for sericite-quartzite per mined slice of S310.

Sericite schist

Sericite schist has an average UCS of 104 MPa and a stress controlled failure criterion of 46 MPa. Its BRQD is 61% with a standard deviation of 27%, which gives an RQD of 73% with a standard deviation of

30%. The orientation of the main discontinuity cluster is 003/52. Apart from this cluster, four other, less pronounced clusters can be distinguished with an orientation of 354/33, 280/41, 202/41, and 178/53. Only 26% of the joints is (slightly) rough, whereas 18% contains infill with a very low friction angle. This, combined with 20% of the joints having an infill of 1-5mm thickness, results in the most unstable joint conditions compared to the other rock types.

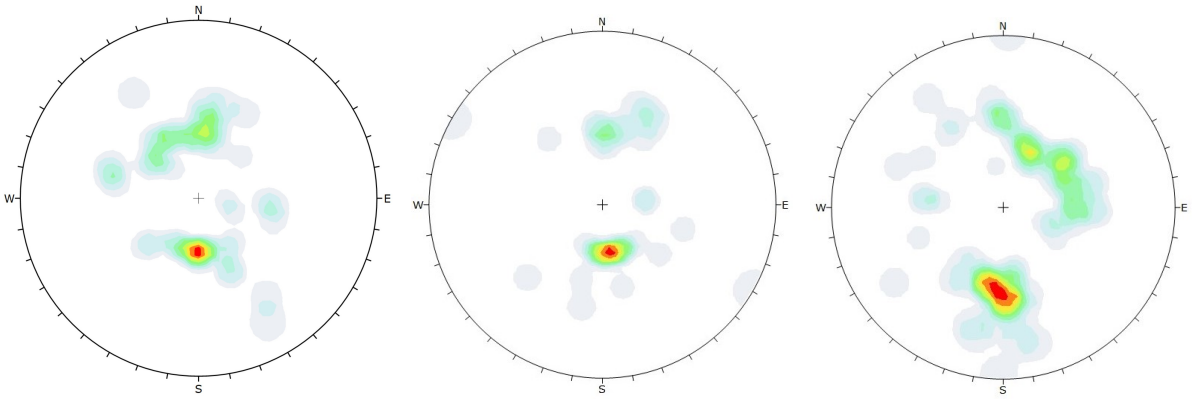

(a) Sericite schist orientations S310 s13. **(b)** Sericite schist orientations S310 s14. **(c)** Sericite schist orientations S310 s15.

Figure 5.4: Stereonets with discontinuity poles for sericite schist per mined slice of S310.

Quartz-feldspar-porphyry

Quartz-feldspar-porphyry has an average UCS of 306 MPa and a stress controlled failure criterion of 122 MPa. It has a mean BRQD of 65% with a standard deviation of 19%, giving an RQD of 81 ± 21%. The main discontinuity cluster and its conjugate set have an orientation of 003/33 and 175/46, respectively. 77% of the joints is rough to very rough and 93% of the joints has an infill of less than 1 mm, which results in very good joint conditions inducing the stability of the rock.

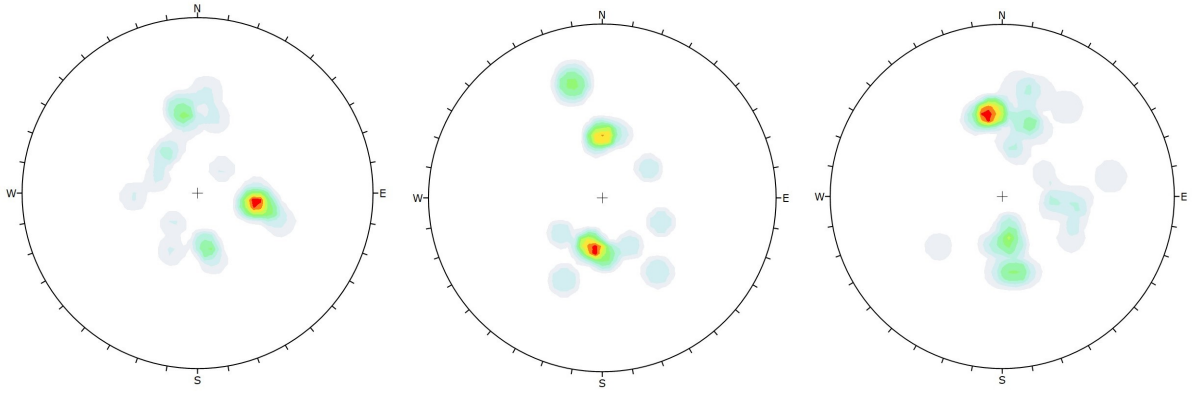

(a) Quartz-Feldspar-Phorphyry orientations S310 s13. **(b)** Quartz-Feldspar-Phorphyry orientations S310 s14. **(c)** Quartz-Feldspar-Phorphyry orientations S310 s15.

Figure 5.5: Stereonets with discontinuity poles for quartz-feldspar-porphyry per mined slice of S310.

Breccia

Breccia has an average UCS of 203 MPa and a yield strength of 81 MPa. The rock type has an average BRQD of 76% with a standard deviation of 15% and an RQD of 85 ± 17%. Three discontinuity clusters with an orientation of 278/38, 005/34 and 184/46 from more to less pronounced can be identified. More than half of the joints are rough to slightly rough. However, 3% are gauges, which is a relatively high amount with respect to the other rock types. 90% of the joints have an infill of less than 1 mm thickness.

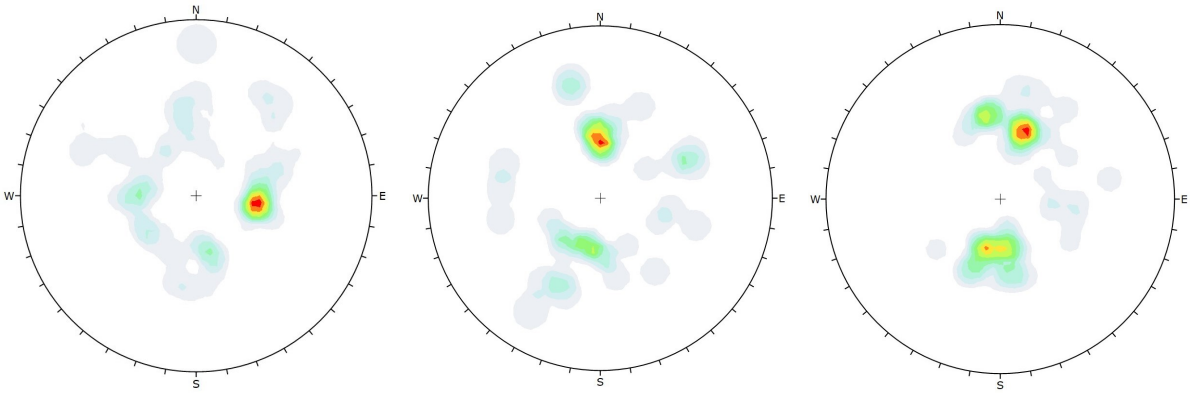

(a) Breccia orientations S310 s13. **(b)** Breccia orientations S310 s14. **(c)** Breccia orientations S310 s15.

Figure 5.6: Stereonets with discontinuity poles for breccia per mined slice of S310.

Andalusite-quartzite

Andalusite-quartzite has a mean UCS of 235 MPa and a corresponding yield strength of 94 MPa. The rock has a relatively high BRQD of 80%, with a standard deviation of 14%. The RQD has a mean of 92% with a standard deviation of 9%. The main discontinuity orientations are 005/45 and 182/62. No andalusite-quartzite has been geologically mapped in slice 15, so no stereonet could be retrieved for this slice. Almost 75% of the joints are slightly rough to rough and the same amount has an infill of less than 1 mm. The high BRQD and favourable joint conditions make the rock overall very stable.

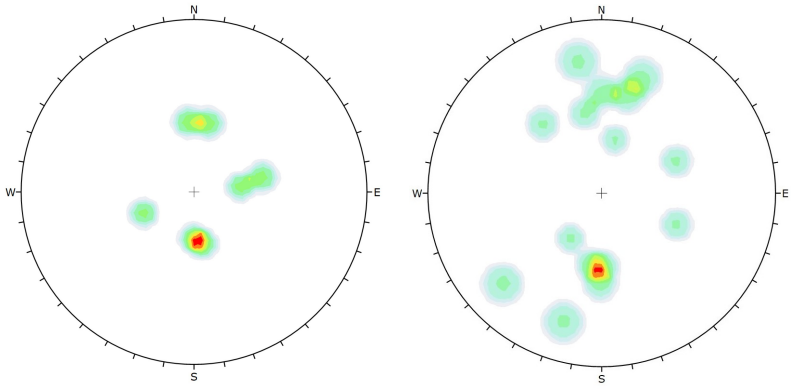

(a) Andalusite-quartzite orientations S310 s13. **(b)** Andalusite-quartzite orientations S310 s14.

Figure 5.7: Stereonets andalusite-quartzite per mined slice of S310. No andalusite-quartzite was encountered in s15.

5.1.3. Characteristics of major failures

To gain deeper understanding of the conditions leading to significant failures, the characteristics of the wedge fall-outs in S310 are identified. An overbreak is classified as 'major' if it extends upwards more than two meters beyond the roof level. Based on the observed overbreak, two areas have been established that are consistent across the different slices and within which the characteristics of the major failures have been analyzed (Figure 5.8).

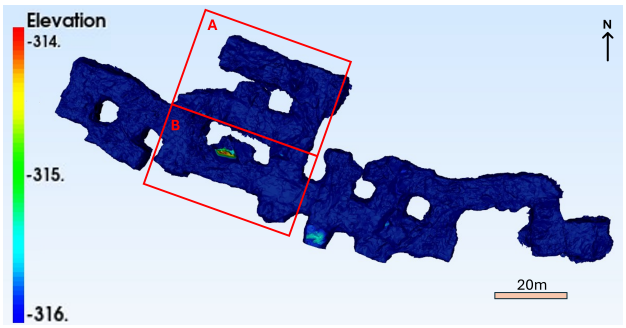

(a) Area division in slice 13 ($z_{roof} = -318m$).

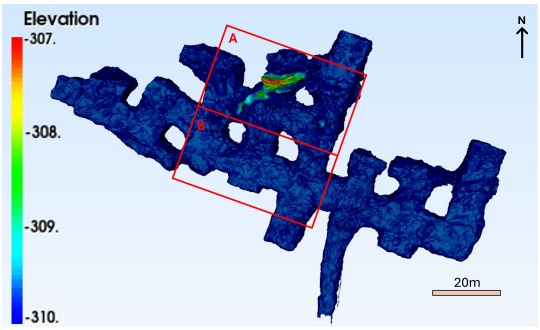

(b) Area division in slice 14 ($z_{roof} = -312m$).

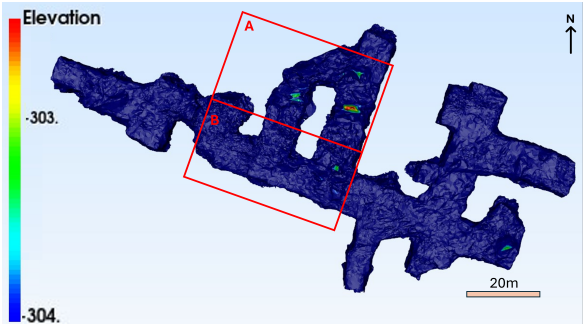

(c) Area division in slice 15 ($z_{roof} = -306m$).

Figure 5.8: Top view of slice 13, 14 and 15 in S310, indicating overbreak and failure area division.

Area A

Comparing the overbreak in area A in each slice and the in-situ geology indicates that major failure takes place around the boundary between competent (breccia, andalusite-quartzite) and weak rock (sericite schist, sericite-/chlorite-quartzite) with a roughly east-west orientation, and in areas with a large open span width after excavation (Figure 5.9). In area A of slice 13 there is no weak-competent rock boundary with an east-west strike, and no major failure took place. In slice 15 major failure took place on the south side of pillar 21, connecting the two wedges at its sides (Figure 5.9e). This area was inaccessible for LiDAR scanning, so the failure is not visualized to its full extent. In slice 16 the nature of the wedge failure was observed. No LiDAR scans are available yet due to the ongoing mining, but it was seen that the outer boundaries of the wedge are formed by two major failure planes with a steep dip angle, which indicate failure through free fall by gravity. One of the major failure planes follows the boundary between sericite schist and the competent rock type, while the other is located in the competent rock. The rock mass that is enclosed by the major failure planes is divided by less extensive fractures into blocks with an average volume of approximately $3.5m^3$. They fail through free fall by gravity or sliding over time, unravelling the wedge upward. Pure shear between the rock types caused the competent, brittle rock to fracture, while the sericite schist reacted ductile. Due to inaccessibility of the area and the absence of a LiDAR scan, the orientation of the fractures could not be determined. Most of the discontinuities in the fractured zone are covered in muscovite, resulting in a low friction angle. The wedge continues approximately 5m above the roof of slice 16. This indicates that the discontinuity at the boundary between the sericite schist and andalusite-quartzite has a vertical persistence of at least 25m. In strike direction, the discontinuity continues approximately 20m. The fractured zone in the andalusite-quartzite has a width of approximately 10m.

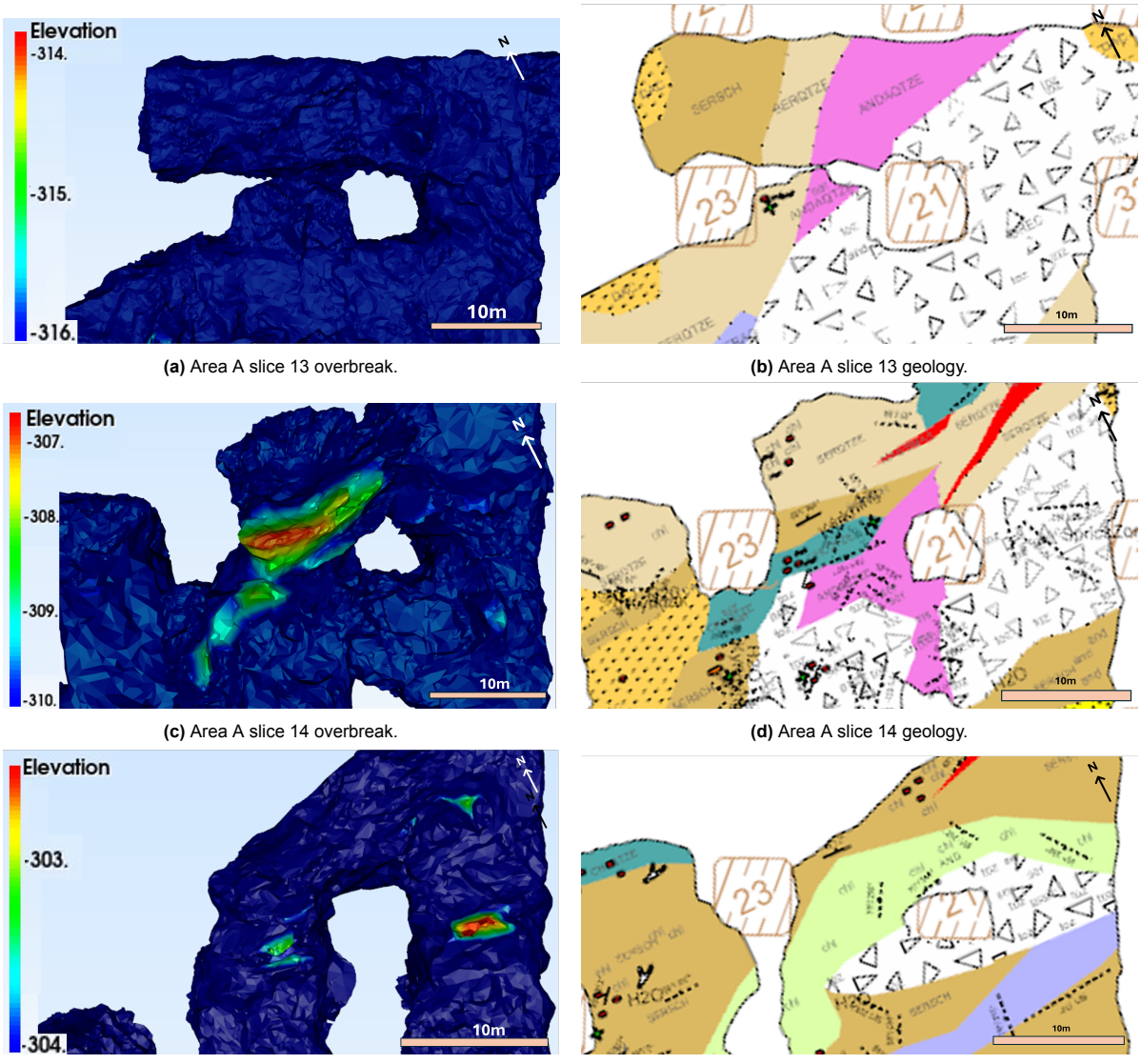

(a) Area A slice 13 overbreak.

(b) Area A slice 13 geology.

(c) Area A slice 14 overbreak.

(d) Area A slice 14 geology.

(e) Area A slice 15 overbreak.

(f) Area A slice 15 geology.

Figure 5.9: Overbreak that exceeds two meters above the planned roof level, and geology for each slice in area A. The numbered hatched zones in the geologic close-ups correspond to pillars.

All stereonets that correspond to the wedge fall-outs in area A of slice 14 and 15 show one or two prominent discontinuities with a roughly east-west strike (Figure 5.10 and 5.11). The wedges are cut off by one or multiple less distinguished discontinuities. All stereonets show failure through falling instead of sliding.

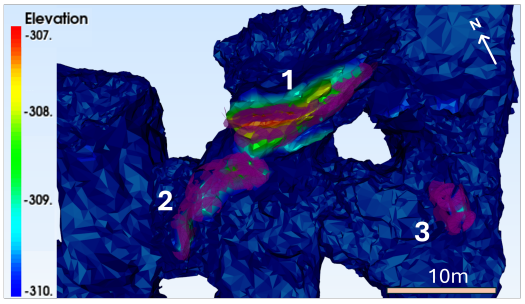

(a) Area A slice 14 overbreak. Note the orientation of the north.

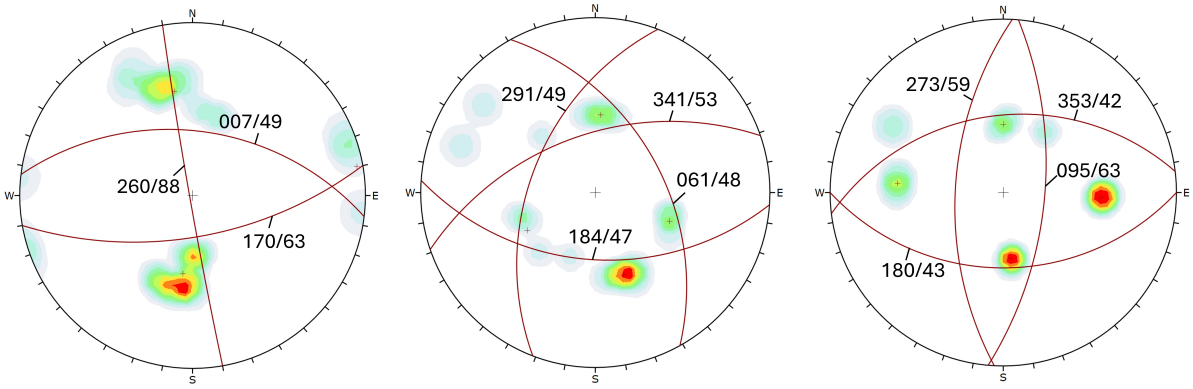

(b) Stereonet fall-out 14.A.1. **(c)** Stereonet fall-out 14.A.2. **(d)** Stereonet fall-out 14.A.3.

Figure 5.10: Slice 14 area A major fall-outs and corresponding stereonets.

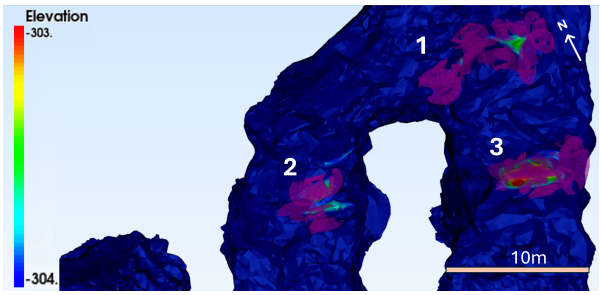

(a) Area A slice 15 overbreak. Note the orientation of the north.

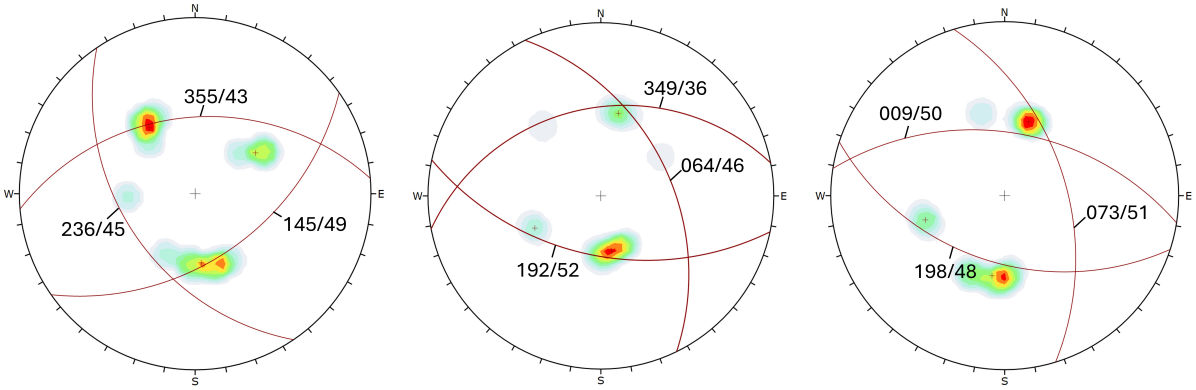

(b) Stereonet fall-out 15.A.1. **(c)** Stereonet fall-out 15.A.2. **(d)** Stereonet fall-out 15.A.3.

Figure 5.11: area A major fall-outs and corresponding stereonets.

Of the boreholes intersecting area A that were logged for geotechnical purposes, unfortunately only

one directly crosses the wedge failure in slice 15 (Figure 5.12). A second borehole, positioned higher, cuts through slice 16 (Figure 5.12a). Notably low BRQD values are distinguished in the failure zone (Figure 5.12b). The joint surfaces are logged as slickensided with a minimal infill of 0-1mm (Figures 5.12c and 5.12d). However, visits to the area of failure indicated that the infill was considerably more substantial, as extensive muscovite sheets of several centimeters thick were encountered in the failure planes.

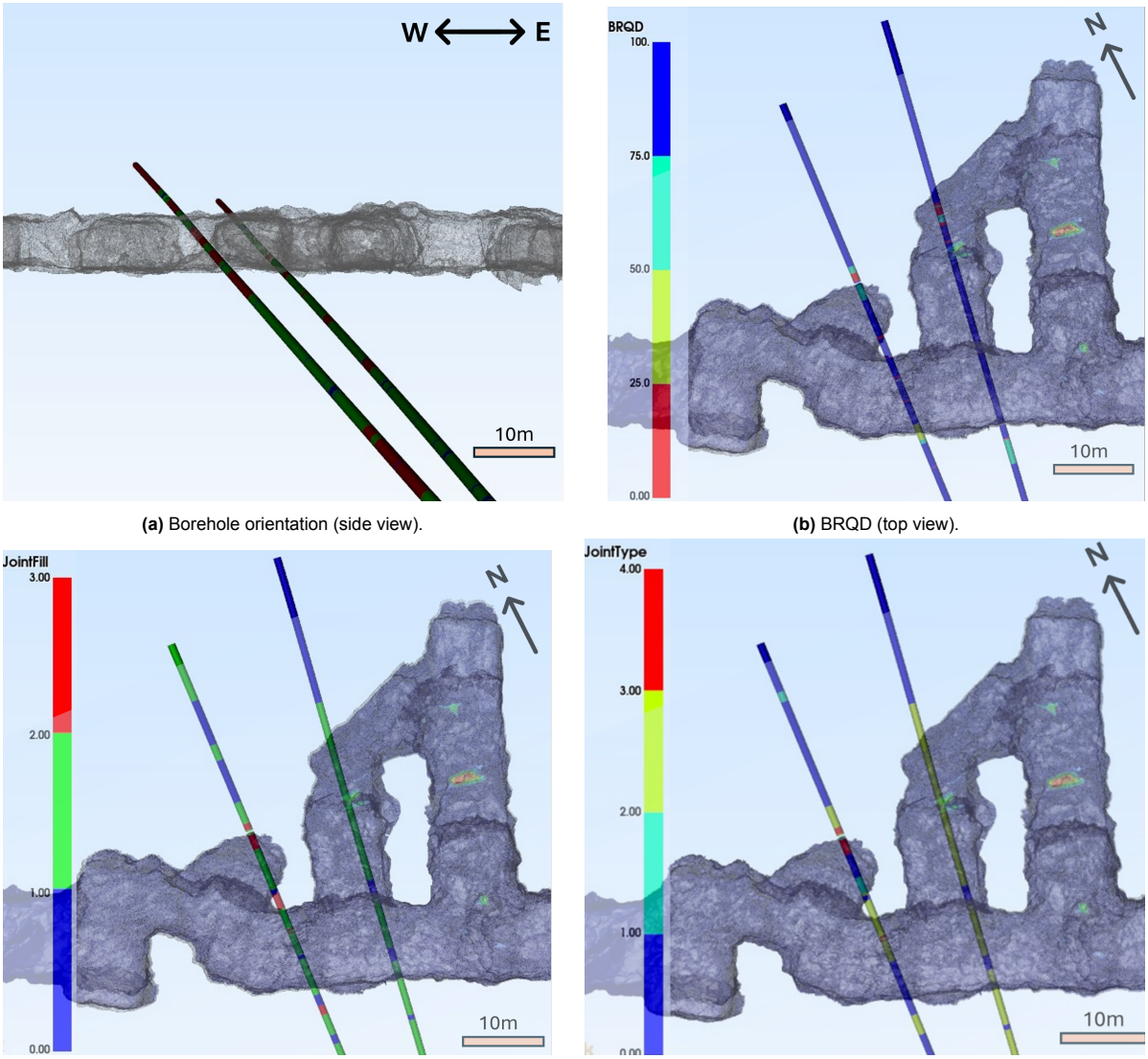

(a) Borehole orientation (side view).

(b) BRQD (top view).

(c) Joint fill (See Table 3.1 for scale value explanation).

(d) Joint roughness (See Table 3.1 for scale value explanation).

Figure 5.12: Geotechnical borehole data in slice 15.

Section B

Also in area B of slice 13, 14 and 15 the fall-outs take place at the boundaries between weak and competent rock (Figure 5.13). Again, the fall-outs take place at the boundaries between sericite schist and quartz-feldspar-porphyry and breccia in excavated areas with a large span width.

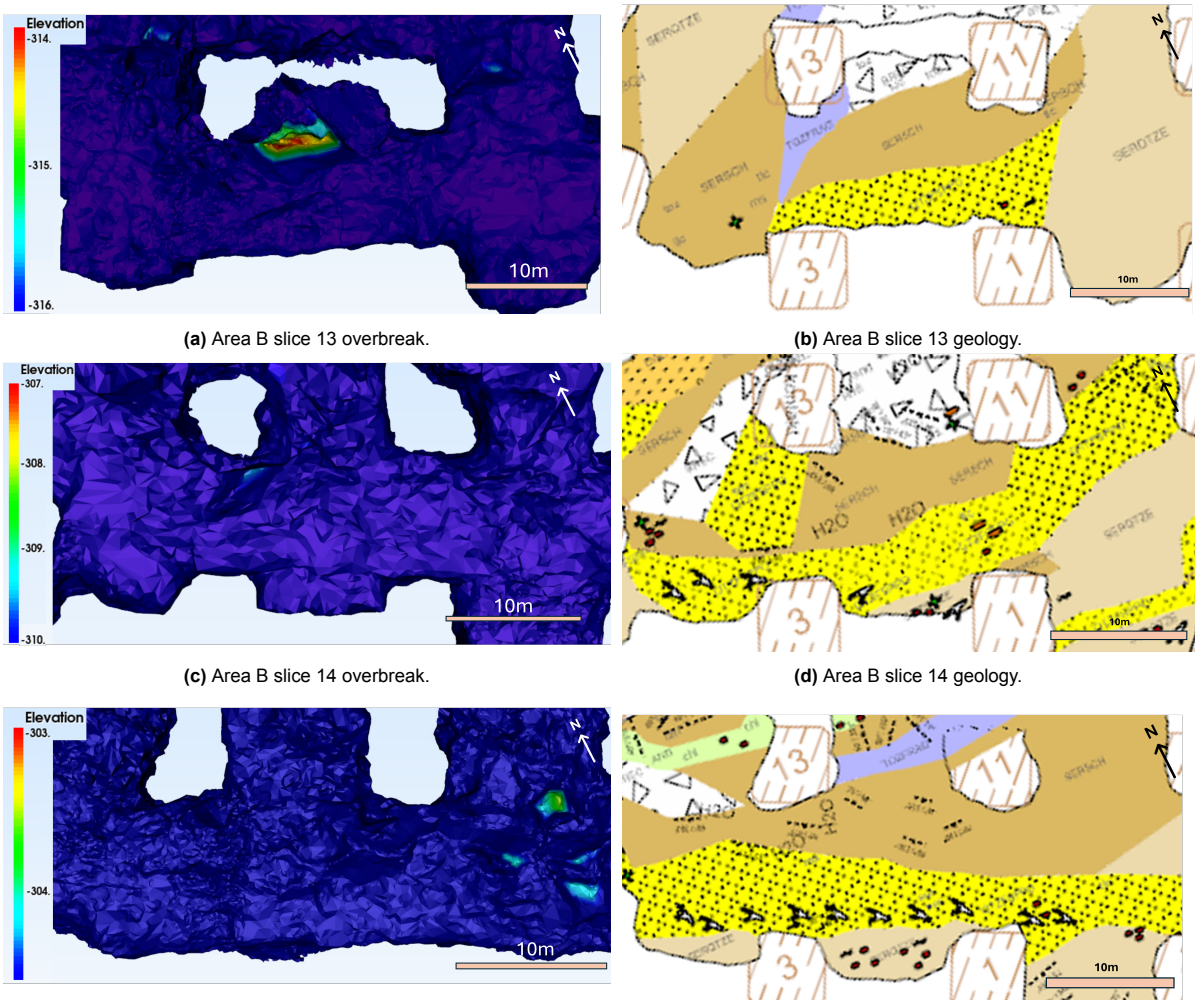

(a) Area B slice 13 overbreak.

(b) Area B slice 13 geology.

(c) Area B slice 14 overbreak.

(d) Area B slice 14 geology.

(e) Area B slice 15 overbreak.

(f) Area B slice 15 geology.

Figure 5.13: Area B overbreak and geology. The scale starts two meters above the designed roof level.

In contrast to the stereonets of area A, those for area B lack a clear pattern, though most show one or two discontinuities with a rough east-west strike (Figure 5.16). All stereonets indicate failure through free fall by gravity. The northern side of failure 13.B.1 does not display a smooth plane, but rather exhibits a step-wise reduction in height that appears jagged, as if the mass has been ripped off under its weight. This complicated the definition of a failure plane. It was chosen to average a plane over the ripped area. No geotechnically logged boreholes intersect area B.

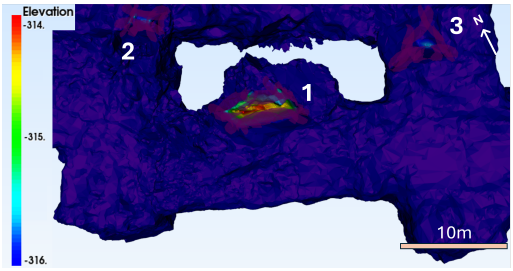

(a) Area B slice 13 overbreak. Note the orientation of the north.

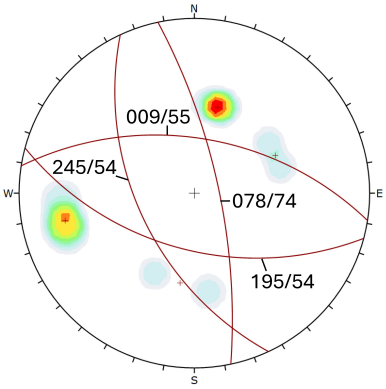

(b) Stereonet fall-out 13.B.1.

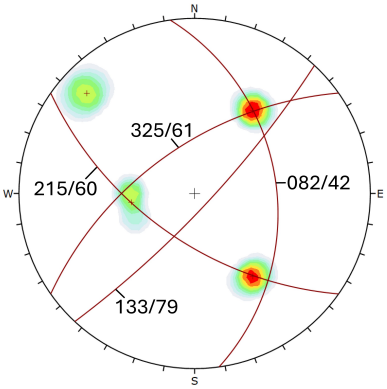

(c) Stereonet fall-out 13.B.2.

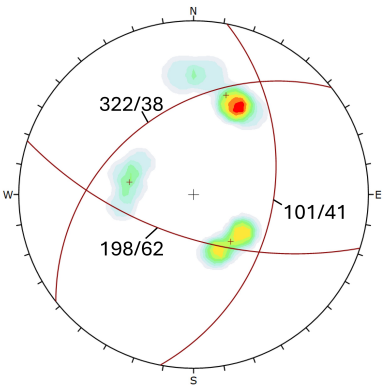

(d) Stereonet fall-out 13.B.3.

Figure 5.14: Slice 13 area B overbreak and geology.

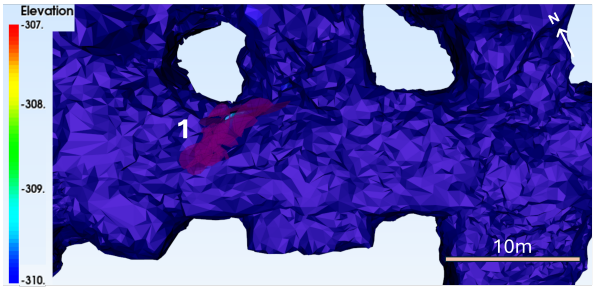

(a) Area B slice 14 overbreak. Note the orientation of the north.

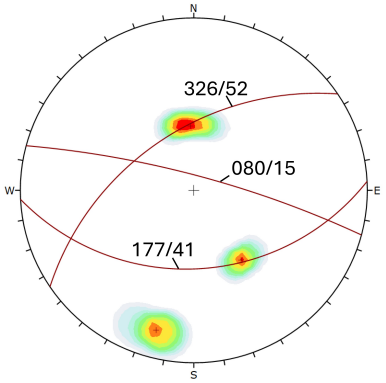

(b) Stereonet fall-out 14.B.1.

Figure 5.15: Slice 14 area B overbreak and geology.

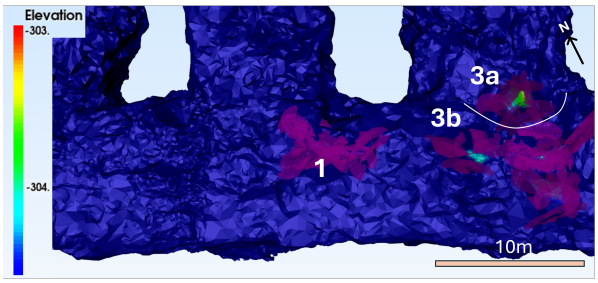

(a) Area B slice 15 overbreak. Note the orientation of the north.

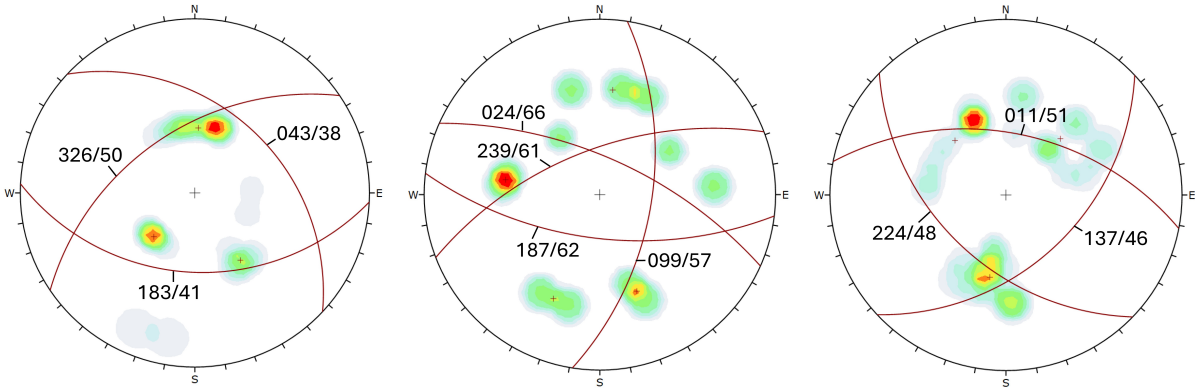

(b) Stereonet fall-out 15.B.1. **(c)** Stereonet fall-out 15.B.3a. **(d)** Stereonet fall-out 15.B.3b.

Figure 5.16: Area B major fall-outs and corresponding stereonets.

5.1.4. Results evaluation

In this section sub-question 1: 'What are the rock type, rock mass and major failure characteristics in the area of interest?' was answered. Two conjugate discontinuity sets were found. One has a WNW-ESE strike and one a roughly E-W strike, which corresponds to the discontinuity sets described by literature. Since the current stress field exerts shear forces on the WNW-ESE set, this cluster has a higher risk of being unstable. However, the discontinuities associated with a major wedge fall-out predominantly exhibit a roughly east-west striking orientation. It was established that major fall-outs are associated with boundaries between competent and weak rock in large excavated intersections, where one major failure plane is oriented at the boundary between sericite schist and andalusite-quartzite and the other failure planes in the andalusite-quartzite, creating blocks that lead to the unravelling of the rock mass in the wedge through time. The major discontinuities enclosing the wedge failure have a persistence of at least 25 meters. No information is available regarding variations in the width of the fractured zone.

Boundaries between competent and weak rock that are not aligned along an east-west strike also occur. The absence of failure could be attributed to the clamping force exerted by the major primary stress, which has a component that is oriented perpendicular to the boundary and therefore stabilizes the rock mass.

5.2. Stress development due to excavation

5.2.1. Model construction

In the construction of the model in Map3D, two categories are important: the pre-mining stress state and the mining design with its sequence. Since a homogeneous geology is assumed by the model, no rock mass parameters are taken into account. The assumption of linear elasticity and isotropy leads to the implementation of an averaged Young's Modulus of 60 GPa and Poisson's ratio of 0.25 (Purser et al., 2021, Heapa et al., 2020, Wiles, 2012).

Pre-mining stress state

Using Equation 3.3, 3.4 and 3.5 to determine the in-situ stress distribution before mining for z=310m and $\rho = 2.8 * 10^3 kg/m^3$ results in the stresses listed in Table 5.2. These are the initial conditions that are implemented in the numerical model.

Stress	value [MPa]	orientation
σ_1	24.2	east-west
σ_2	13.9	north-south
σ_3	8.7	vertical

Table 5.2: In-situ stress

Mining sequence

As explained in Section 2.4, a certain mining sequence is followed for the excavation and backfilling of the stopes. The designs have been divided into six mining steps each. The development of the access drifts (orange and blue) is the first mining step. There are minor variations in the mining sequence across the different designs. The mining sequence for each design option is visualized in Figure 5.17. The yellow stopes have a width of 10m and the purple stopes are 15m wide. The red solids below the stopes are the slices that were mined and backfilled using the cut-and-fill mining method.

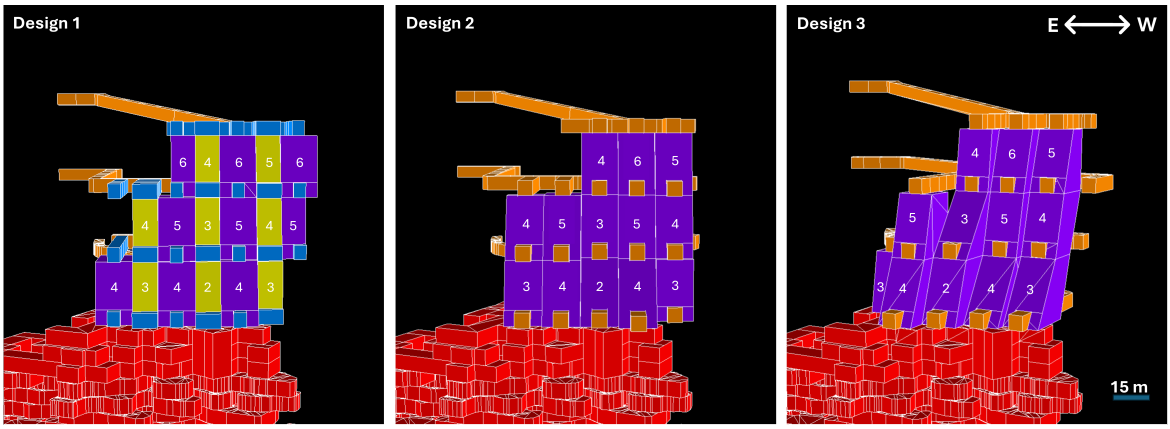

Figure 5.17: Stope design options containing the mining sequence (indicated by numbering) in Map3D.

5.2.2. Overall stress changes through steps

The greatest differential stresses occur in the bottom grid (Figure 5.18). This can be explained by the redistribution of stresses from the slices excavated below. Since the slices are more extensive under the east side of the stope designs, higher stress accumulations compared to the pre-excavation stress state are built up here. Towards the upper sections of the designs, the stress accumulations are lower. It can also be noted that stress is accumulated on the front and back side of the stopes, while stress relaxation takes place at the sidewalls. This occurs because the major principal stress, which is initially perpendicular to the stope sidewalls, arches around the stopes after excavation. At the corners of the excavated stopes, the stresses reach high values. However, in reality the corners will be less sharp, and therefore the stress accumulations will be lower.

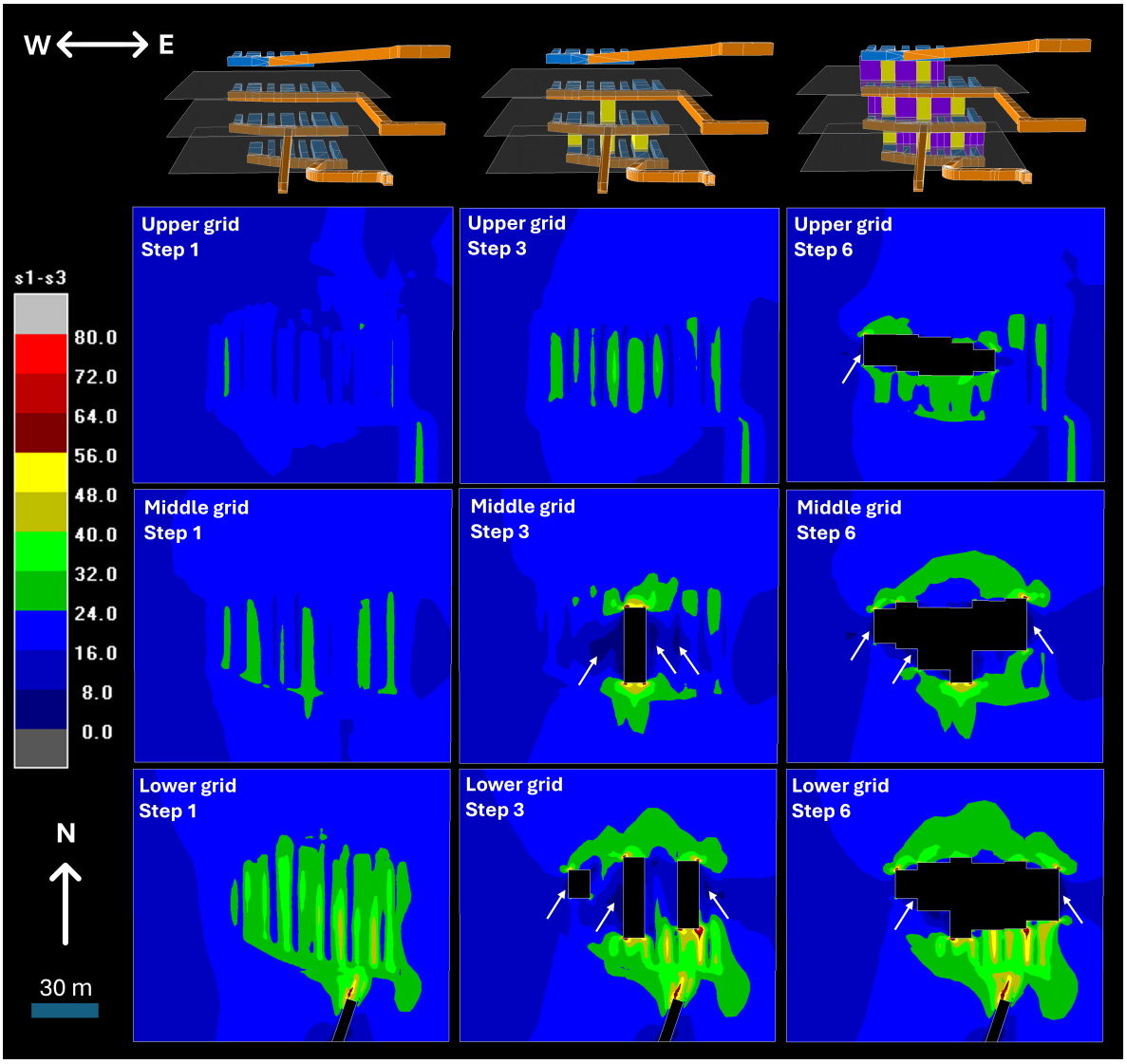

Figure 5.18: Stress distribution through mining steps 1, 3 and 6 for design option 1 on horizontal grids located one meter above the access drifts. The stope model is seen from the south side. The stress levels are displayed on a scale ranging from 0 MPa (blue) to 80 MPa (red). The arrows point at relaxation zones.

Above a selection of the access drifts and in the sidewalls the minor principal stress turns tensile (Figure 5.19), relaxing the discontinuities in the rock mass further, increasing the risk of failure.

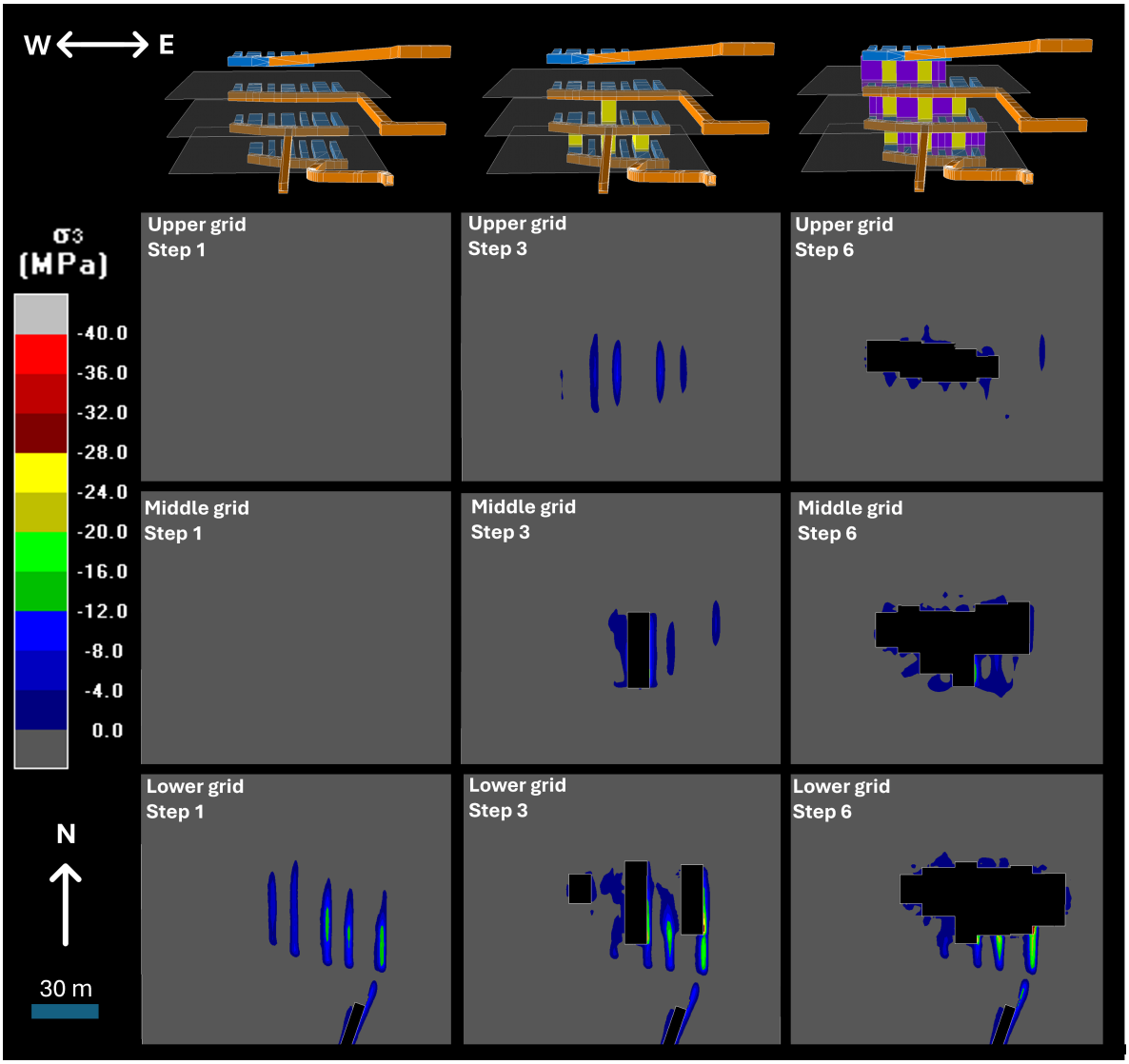

Figure 5.19: Minor principal stress distribution through mining steps 1, 3 and 6 for design option 1 on horizontal grids located one meter above the access drifts. The stope model is seen from the south side. The stress levels are displayed on a scale ranging from 0 MPa (blue) to -40 MPa (red). The coloured areas indicate tensile stresses.

Contradicting to the observations from Figure 5.18, the vertically positioned grids show stress accumulations in the sidewalls (Back grid step 3 and 6, front grid step 6), instead of stress relaxation (Figure 5.20). This deviation from the main trend can be explained by the proximity of the grid to the front face of the stope, where stress tends to build up. The accumulation extends only a short distance along the sidewalls of the stope, after which relaxation initiates. This also leads to the stress accumulations in the floors and roofs of the excavated areas.

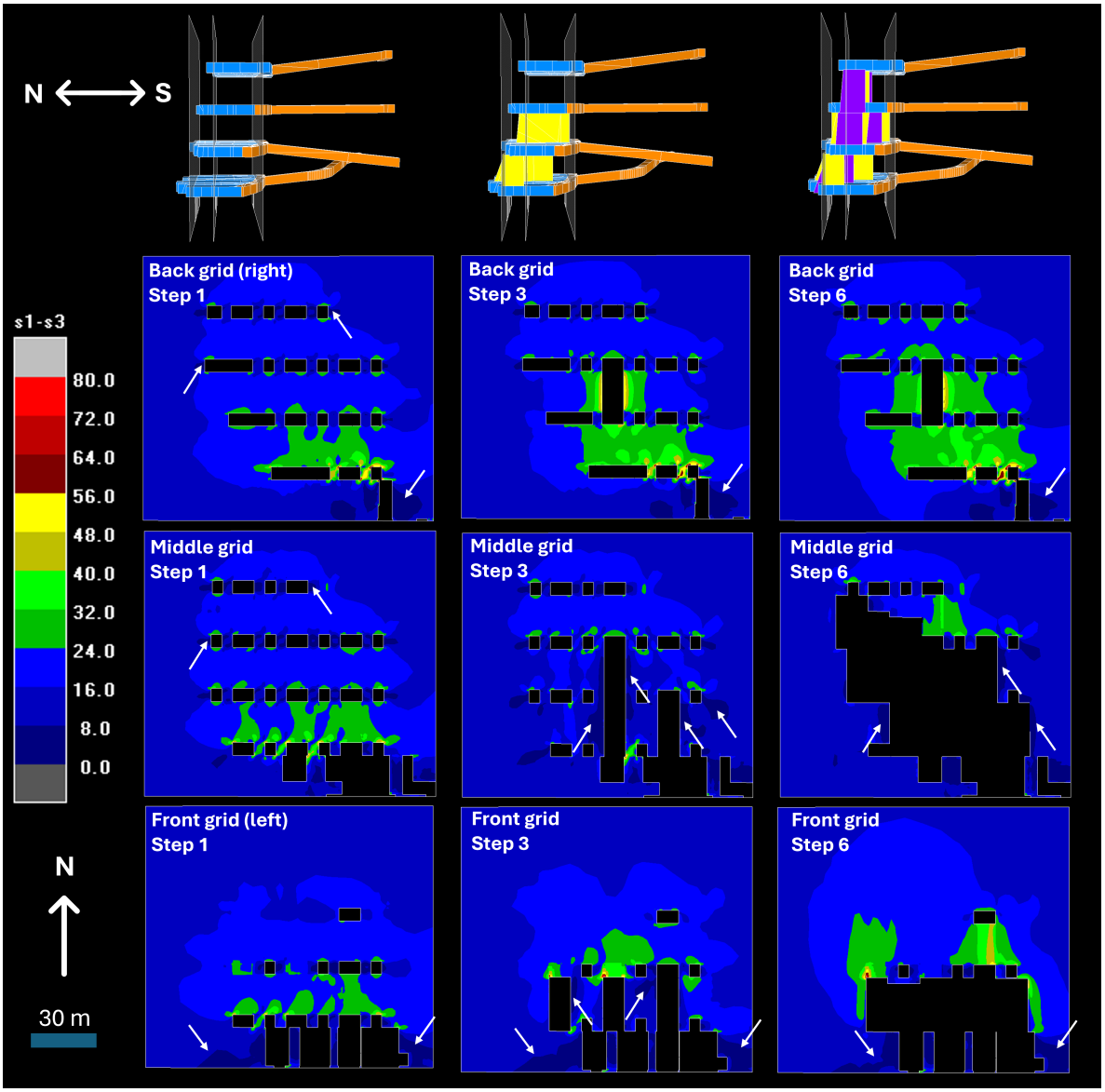

Figure 5.20: Stress distribution through mining steps 1, 3 and 6 for design option 1 on vertical grids that are positioned through the access drifts (right grid), the middle of the stopes (middle grid) and at the back end of the stopes (left grid). The stope model is seen from the west side. The stress levels are displayed on a scale ranging from 0 MPa (blue) to 80 MPa (red). The arrows point at relaxation zones.

Overall, Figure 5.18 and 5.20 show a general differential stress build-up at the front and back side of the stopes up to 56 MPa and in small areas at the corners of the excavations even up to 80 kPa. A differential stress relaxation is encountered along the sidewalls of the stopes.

5.2.3. Differences between models

After mining step 3, design option 1 and 2 experience more extensive relaxation in the sidewalls than design option 3 (Figure 5.21). Moreover, the front and back face of the stopes in the first two design options are subjected to a higher stress. This is caused by the extent of the stress redistribution. Since the stopes in design option 3 are not aligned perpendicular to the major principal stress, unlike the other designs, reduced stress redistribution around the stopes takes place and the zones of stress relaxation and accumulation are less pronounced.

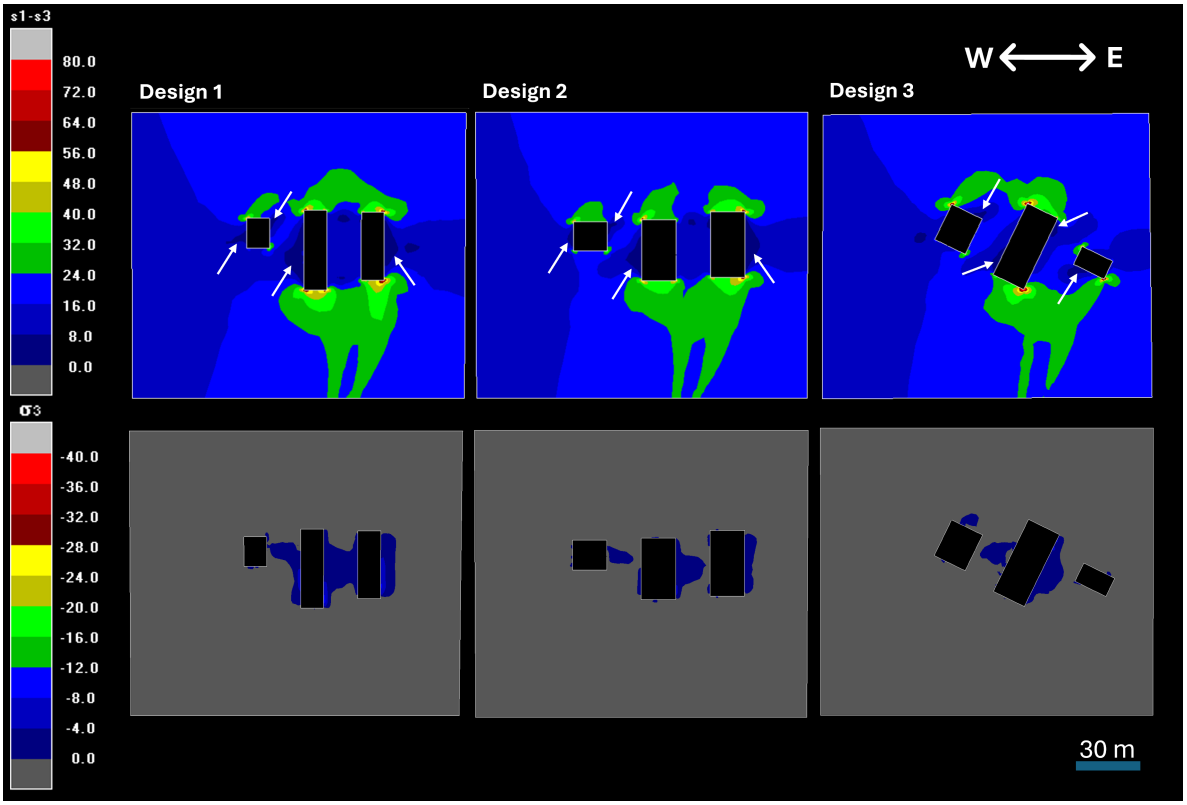

Figure 5.21: Stress accumulation and relaxation variation between models after mining step 3, the excavation of the primary stopes of the first production level. Top row: Differential stress. Bottom row: tensile stress. Note the different scale. The grids are positioned at mid-height of the stopes. The arrows point at relaxation zones.

After the sixth and therefore final step of the mining sequence, there is increased relaxation around the excavated area in option 3, due to its irregular shape (Figure 5.22). Furthermore, it is observed that the accumulated stresses above the stope access drifts are greater in options 1 and 2 compared to option 3. In option 1 and 2, the drifts are located right above the underlying slices. In option 3, the drifts are oriented under the same angle as the stope, and are therefore not aligned with the drifts of the underlying slices. This results in lower stress accumulations.

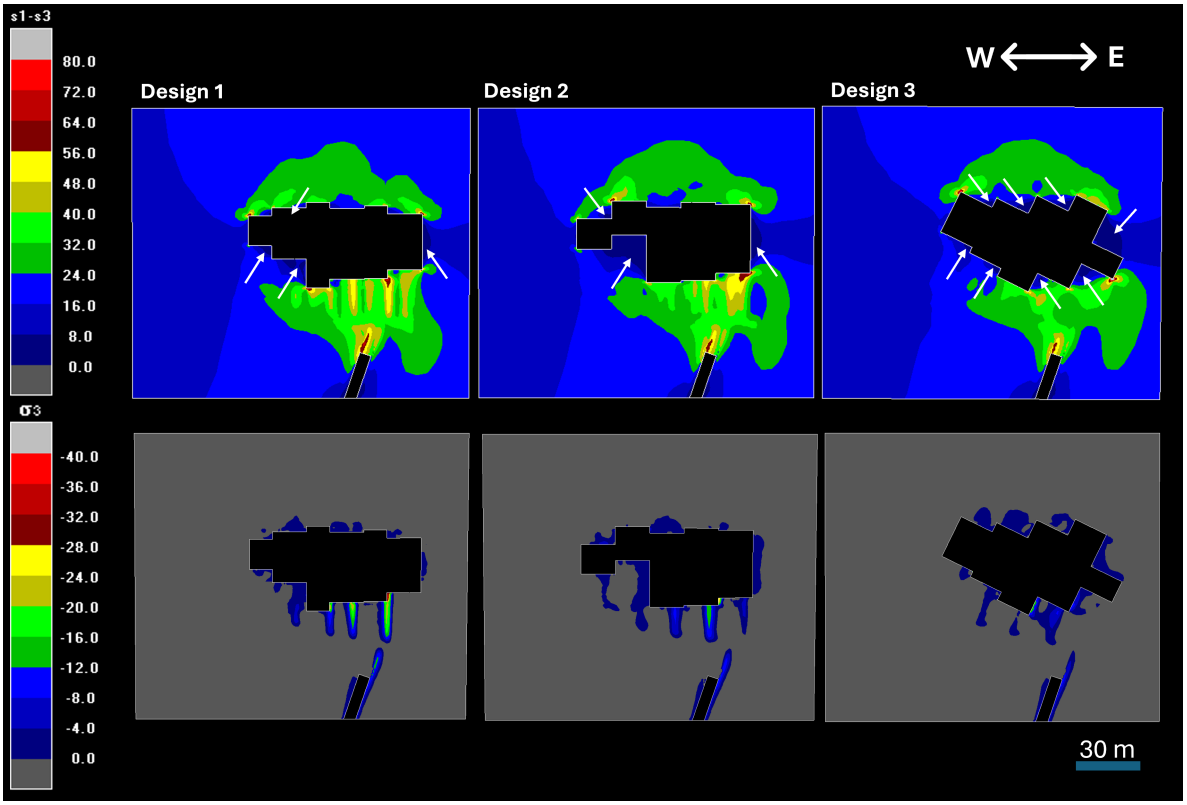

Figure 5.22: Stress accumulation above stope access drifts after mining step 6. Top row: Differential stress. Bottom row: tensile stress. Note the different scale. The grid level is 1m above the stope access drifts of the first production level. The arrows point at relaxation zones.

5.2.4. Results evaluation

This section answered sub-question 2: 'How will the stress distribution in the rock mass develop during excavation?'. It has been concluded that the largest stress accumulation occurs in the lower part of the design, primarily due to the underlying excavations. Additionally, stresses tend to build up in the front and back walls of the stope, as well as in the roof, while relaxation compared to the pre-mining stress state predominantly occurs along the sidewalls of the stopes. Tensile stresses build up above the access drifts and in the sidewalls. After mining the primary stopes at the first production level, the stress disruption is largest for design option 1 and lowest for design option 3. Consequently, the lowest stress accumulation at the front and back faces and the smallest relaxation zone along the sidewalls are observed in the third design. Furthermore, the stress accumulation and tensile stress build-up above the stope access drifts is smallest in option 3. However, this design exhibits more relaxation zones post-mining around the stopes due to its irregular shape.

Tensile stresses in the rock mass result in a reduced stability of the discontinuities and therefore higher risk of failure. The rock material itself will likely not be affected, since the tension will be absorbed by the discontinuities.

It is recognized that the model tends to overestimate stress accumulations at the stope corners due to their modeled sharp angularity. In reality it is not feasible to mine such sharp corners, and therefore they will act less strongly as stress concentration points. The exact degree of this overestimation is unknown and could be decreased by reducing the grid size or blunting the corners in the design. However, this increases computational and manual working time.

Since Map3D does not consider the anisotropy of the rock mass, it does not account for varying rock type parameters. Moreover, linear elasticity is presumed. Due to these assumptions the results could deviate from the real stress redistribution behaviour, which should be considered when interpreting the resulting stress distribution models.

5.3. Geotechnical challenges

5.3.1. Stress-induced failure

To analyze the possibility of stress-induced failure, the deviatoric stress distribution calculated with Map3D is compared with the geological model from Leapfrog. In the geological model the rock types are colour-coded according to their average yield strength (σ_c) (Table 5.3). Areas where the stresses exceed the yield strength are identified. The lower boundary of stress-induced failure is defined by sericite schist, which has a yield strength of 42 MPa. This indicates that the green-blue areas in the stress distribution model are not prone to stress-induced failure. Since the σ_3 values around the excavation are low and even turn negative, their impact on the yield strength is disregarded. Therefore, the yield strength is uniformly assumed to be 0.4*UCS. Figure 5.23 shows a cross-sectional view of the geology at a similar z-elevation as the grids plotting stress distribution per mining step, one meter above the access drifts to the stopes. There are no areas that contain sericite schist where the differential stresses exceeding 40 MPa. Sericite-quartzite, the next weakest rock type, is observed in various areas exceeding its yield strength of 50 MPa, particularly at the front and back walls of the stopes and above the development drifts. Siltstone has a yield strength of 61 MPa. Since the rock is situated at the front side of the stopes while stress accumulations above 60 MPa only occur at the back side, no stress-controlled damage will take place.

Rock type	σ_c [MPa]	Rock type colour
Sericite schist	42	Red
Sericite-quartzite	50	Dark orange
Siltstone	61	Orange
Volcanclastics	67	Dark yellow
Dacite	71	Yellow
Breccia	81	Light green
Andesite	82	Light green
Andalusite-quartzite	94	Green
Quartz-feldspar-porphyry	122	Dark green

Table 5.3: Colour-coding of the geological model per rock type based on yield strength, where rock types with a low yield strength have a colour towards red and rock types with a high yield strength a colour towards green.

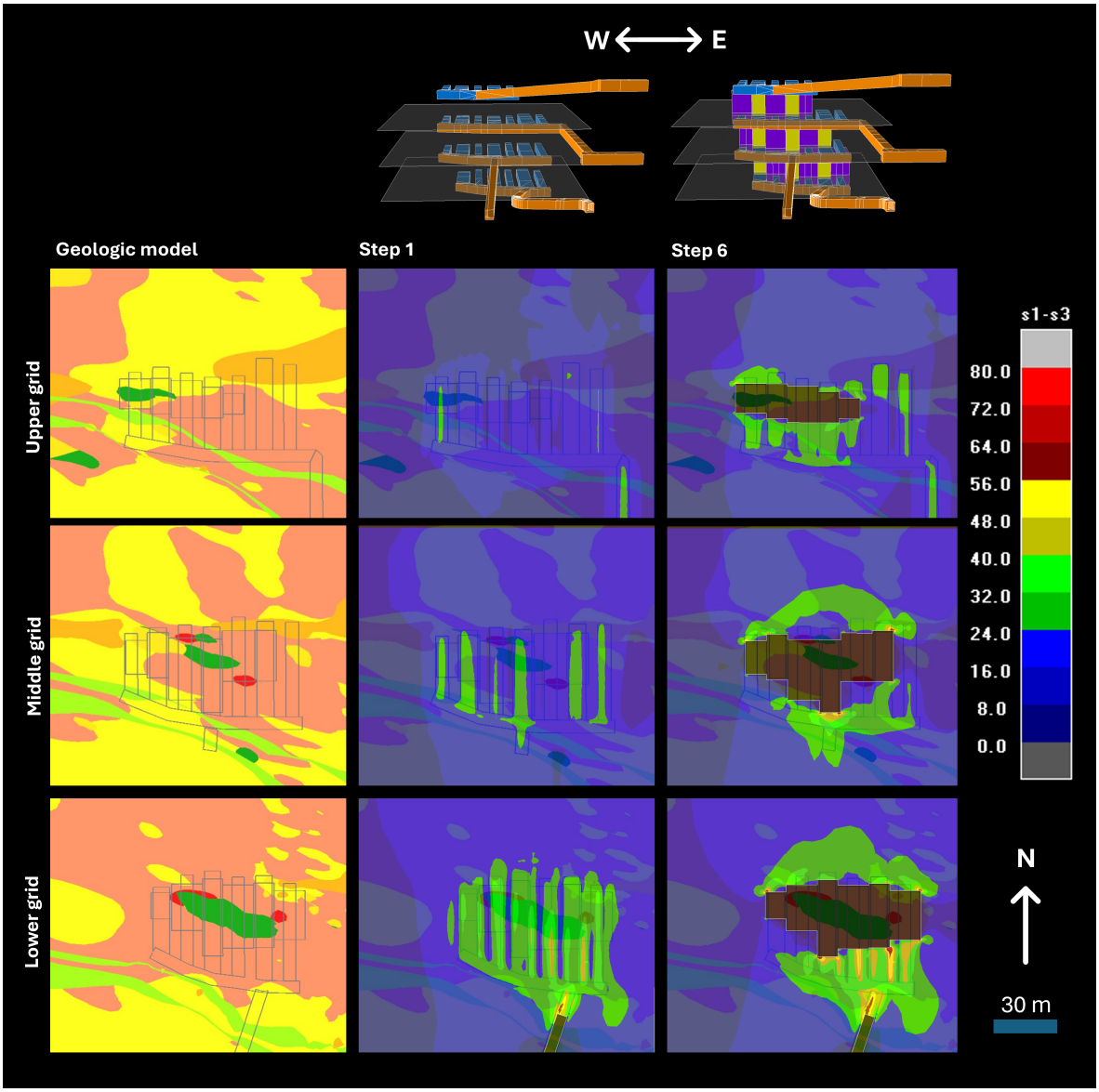

Figure 5.23: Geology (left column) and stress distribution (middle and right column) through mining steps for design option 1. The stress distribution images overlay the geology images. Horizontal grids one meter above the stope access drifts.

Comparing the geologic model and the stress distribution for the second stope design option indicate that the critical area above the access drifts on the east side is more extensive than for design option 1, which could lead to more severe stability issues in the roof of the access drifts and in the back wall of the stopes (Figure 5.24). On the middle production level sericite schist is located in one of the back walls and in the roof of the access drift. As the stress accumulation does not reach 40 MPa, this should not cause stress-related problems. Only the lowest two production levels are shown in Figure 5.24, since Figure 5.23 indicated that the stress accumulation around the upper access drift is minimal.

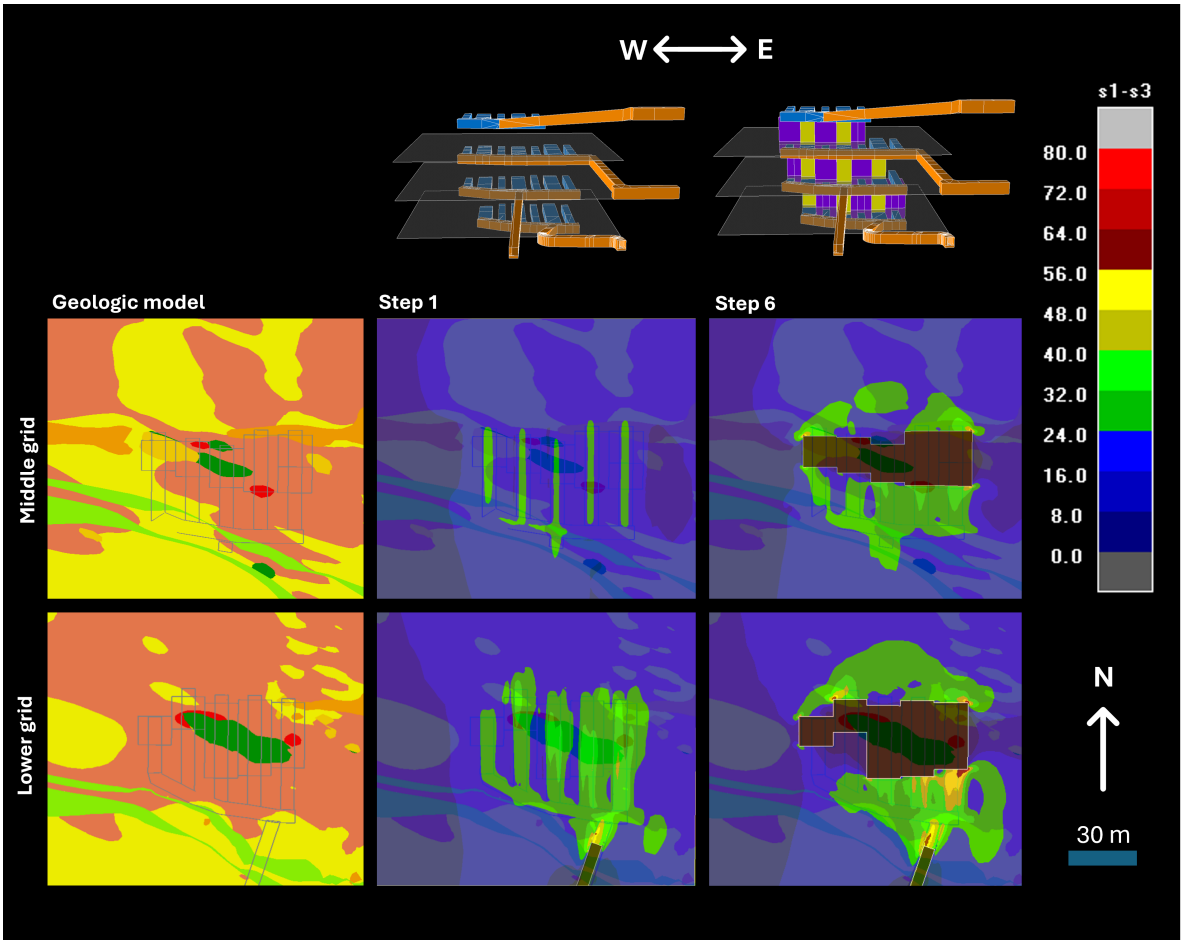

Figure 5.24: Geology (left column) and stress distribution (middle and right column) through mining steps for design option 2. The stress distribution images overlay the geology images. Horizontal grids one meter above the stope access drifts.

In stope design option 3, the critical area above the access drifts on the east side is less pronounced than for design option 1 and 2 and hardly reaches the critical strength of sericite-quartzite (Figure 5.25). This makes this design the best option to prevent stress-induced failure.

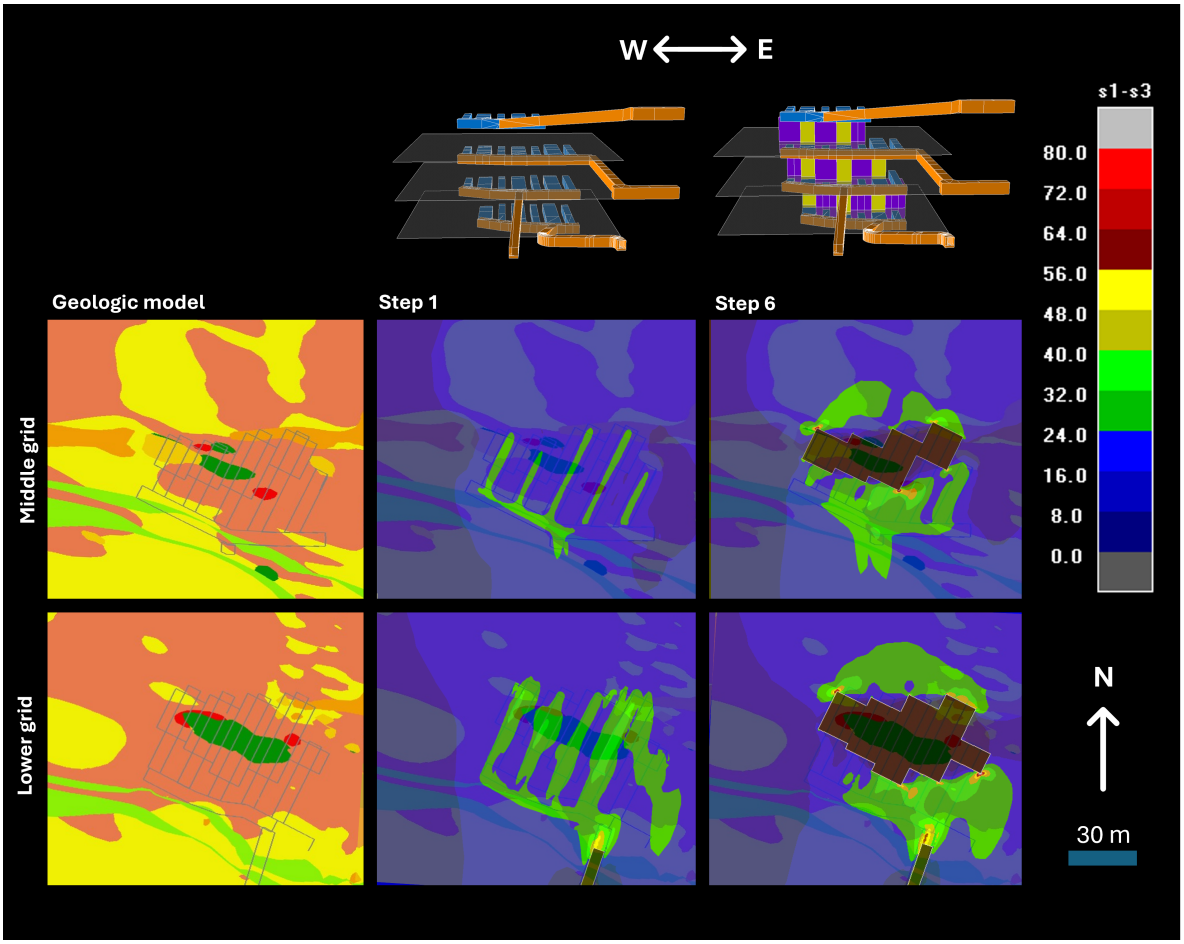

Figure 5.25: Geology (left column) and stress distribution (middle and right column) through mining steps for design option 3. The stress distribution images overlay the geology images. Horizontal grids one meter above the stope access drifts.

5.3.2. Structure-induced failure

Major wedge fall-outs

The main structural condition leading to failure has been established to be a fracture at the boundary between weak and competent rock with a strike from east to west, which is parallel to the main principal stress. This is visualized in the geological model as the boundary between the bright red and any green shape. Such a boundary has been encountered in the geological model between sericite schist and quartz-feldspar-porphyry (SERSCH-QFP) between 285m and 257m depth (Figure 5.26a), where the first level of stopes is planned to be excavated. At 282 meter depth the SERSCH-QFP boundary cuts through the roof of the access drifts, which creates risk of failure (Figure5.26b). At 257m depth it ends at the roof of the access drift of the second stope level, which will not lead to excessive failure. In between, the SERSCH-QFP boundary cuts through the stope walls. These locations are prone to failure during mining. Within the stope, the critical boundary is of low concern for stability.

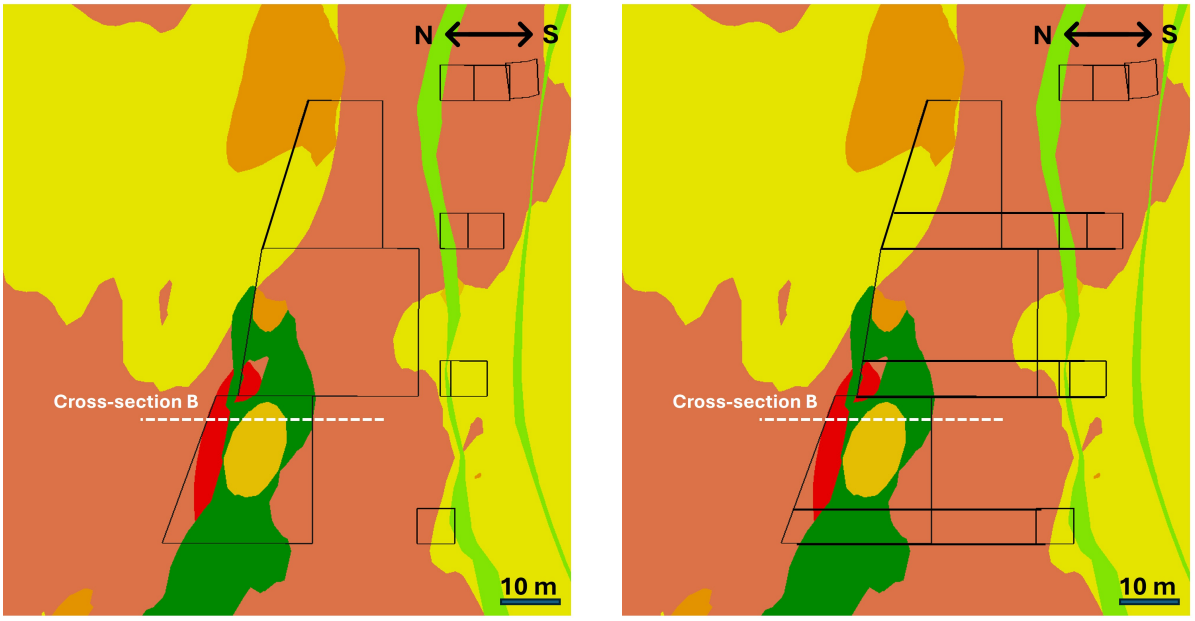

(a) Cross-section A: Vertical view.

(b) Cross-section B: Top view.

Figure 5.26: Sericite schist (red) - quartz-feldspar-porphyry (dark green) boundary that is prone to failure due to a competence difference between the rock types.

The three design options are positioned differently with respect to the SERSCH-QFP boundary (Figure 5.27). The walls of option 1 and 2 intersect the boundary various times, while option 3 only intersects it once. All walls are prone to tensile stresses after excavation, which enhances instability (Figure 5.21 and 5.22). Option 3 is most favourable due to its single intersection of the SERSCH-QFP boundary.

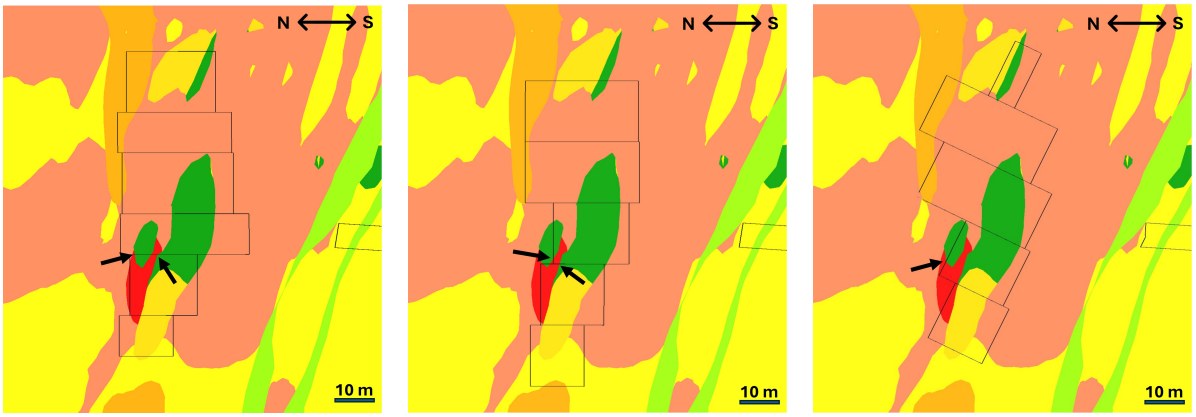

(a) Option 1.

(b) Option 2.

(c) Option 3.

Figure 5.27: Top view, 1m below the roof of the first production level for each design option. The arrows point at the SERSCH-QFP boundary in the stope walls.

Sericite schist presence

In the roof of the access drifts to the second production level, the remainder of the previously discussed sericite schist formation is present, though not in considerable contact with the quartz-feldspar-porphyry (see black arrows in Figure 5.28). A second sericite schist deposit is entering the stope design area on the southeast side (see white arrows in Figure 5.28). It has a maximum width of twelve meters and extends ten meters upward. The rock type has no competent rock in its proximity, but its fractures are generally found to be in unfavourable conditions, which could cause failure. All designs include an access drift through this formation. In design 1 and 2, the back wall of one of the secondary stopes also intersects the schist, making these designs less favourable. No other sericite schist has been encountered in the vicinity of the design options in the geological model.

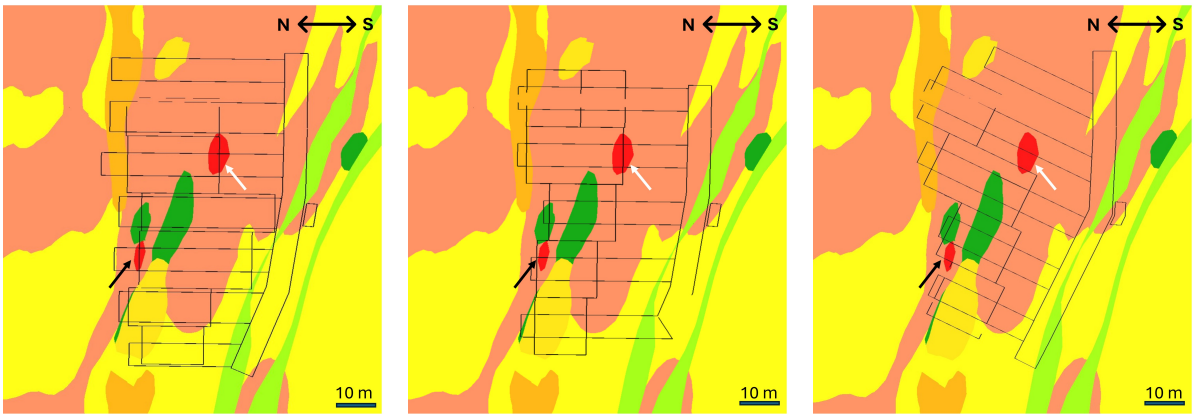

(a) Option 1. **(b)** Option 2. **(c)** Option 3.

Figure 5.28: Top view, top of access drifts into second production level for each design option. The black arrow points at the remainder of the previously covered sericite schist formation. The white arrow points at the second sericite schist formation.

Major fractures

In slice S310 s15, a significant fracture with an orientation of 342/84 cuts into the mined area (Figure 5.29). It caused extensive underbreak due to the dissipation of blasting energy on its surface. Given the the extent of the fracture, it is expected to progress further upwards, reaching the back walls of the stopes across all design options (Figure 5.30). It cuts through design option 2 and 3 more severely than through 1, creating a larger area in which further complications with blasting or stability issues could be encountered. Moreover, as discussed in section 5.2.3, stress accumulates in the back walls for design option 1 and 2, whereas design option 3 experiences stress relaxation due to the orientation of the stopes, releasing the clamping force on the fracture and therefore inducing instability (Figure 5.22).

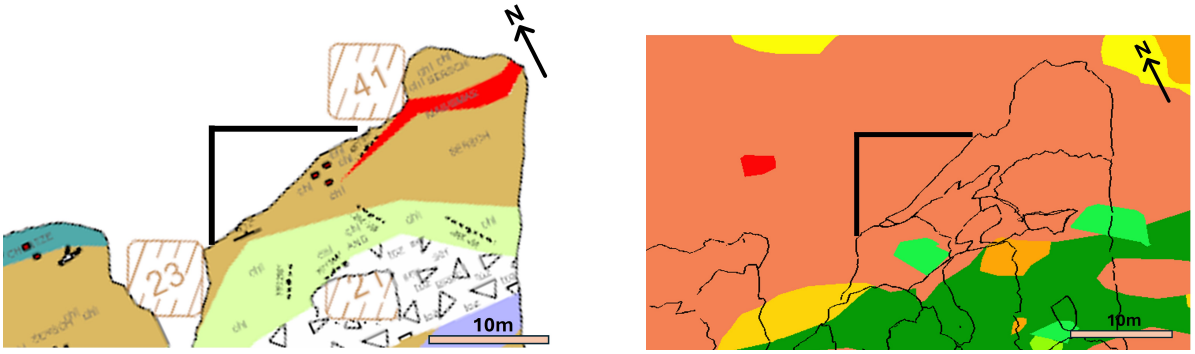

(a) Close-up from geologic map. **(b)** Close-up from geological model.

Figure 5.29: Detail of slice S310 s15, underbreak due to incoming fracture. The black lines indicate the area that was planned to be mined. Due to the dissipation of blasting energy through the discontinuity, the rock behind it did not get damaged enough to fail.

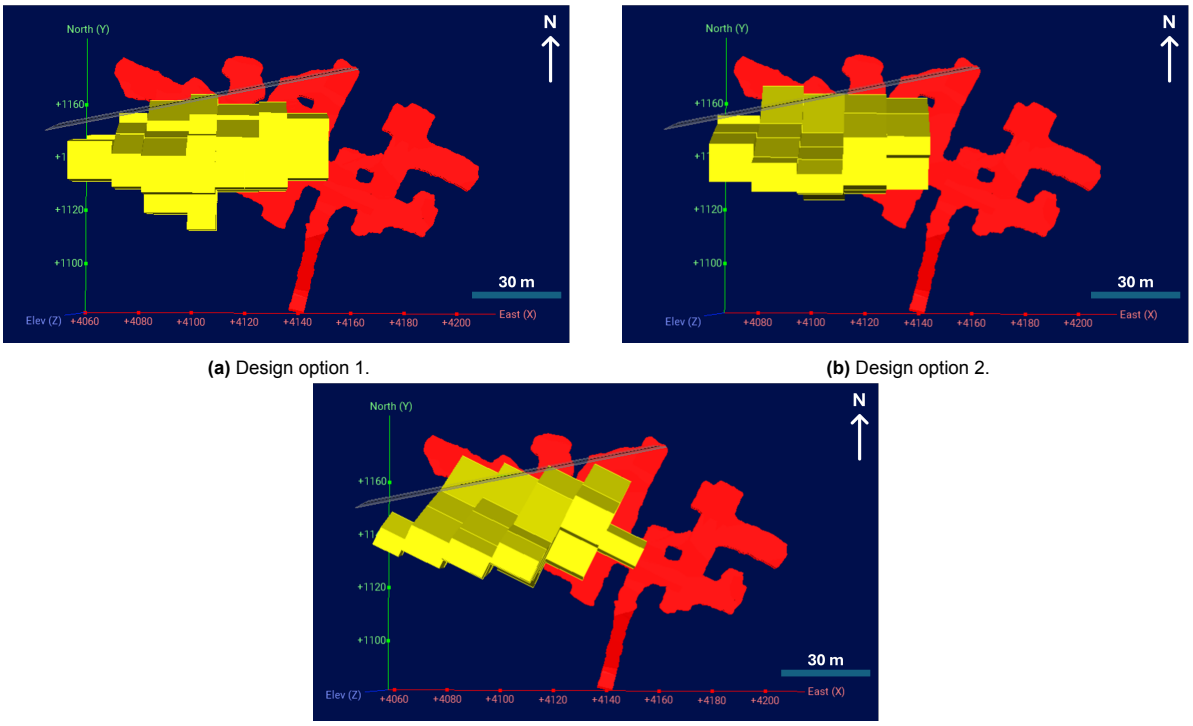

(a) Design option 1.

(b) Design option 2.

(c) Design option 3.

Figure 5.30: Incoming fracture with respect to each design option. The stopes are yellow and slice S310 s15 is red.

The discontinuities responsible for major wedge failure in the previous slices are expected to progress upwards, potentially causing further failure in the access drifts or stopes. Especially the discontinuity with orientation 174/46 has a chance of intersecting the above-mentioned incoming fracture, potentially resulting in wedge failure. Combining their dip angle and direction indicates that these discontinuities will intersect approximately 13 meters above the roof of slice S310 s15, which will be at 293 meters depth. Given that the bottom level of the stopes will be at 288 meters depth, this discontinuity intersection should not cause issues. However, other significant discontinuities could emerge and cause failures, as their appearance is hard to predict.

Figure 5.29 also indicates a difference between the geologic maps and the geological model. Where the geologic map shows an extensive amount of sericite schist, the geologic model only indicates minimum presence. However, the differentiation between weak and strong rocks shows the same pattern in the model and the map. This indicates that the exact rock type distribution is not accurate in the geologic model, but it provides an indication of the global strength trend of the rock mass.

Andesite dykes

Andesite dykes cause alterations in the surrounding material, leading to the formation of features such as fuchsite sheets that could act as slip faces. Also the boundaries of the dykes themselves could serve as slip faces. Figure 5.31 illustrates the location of the designed access drifts in relation to the present andesite dykes. It can be noted that the differences between the designs are minimal. Only in design option 3 the upper access drifts are located more extensively through the andesite dykes compared to the other designs, which could complicate their development.

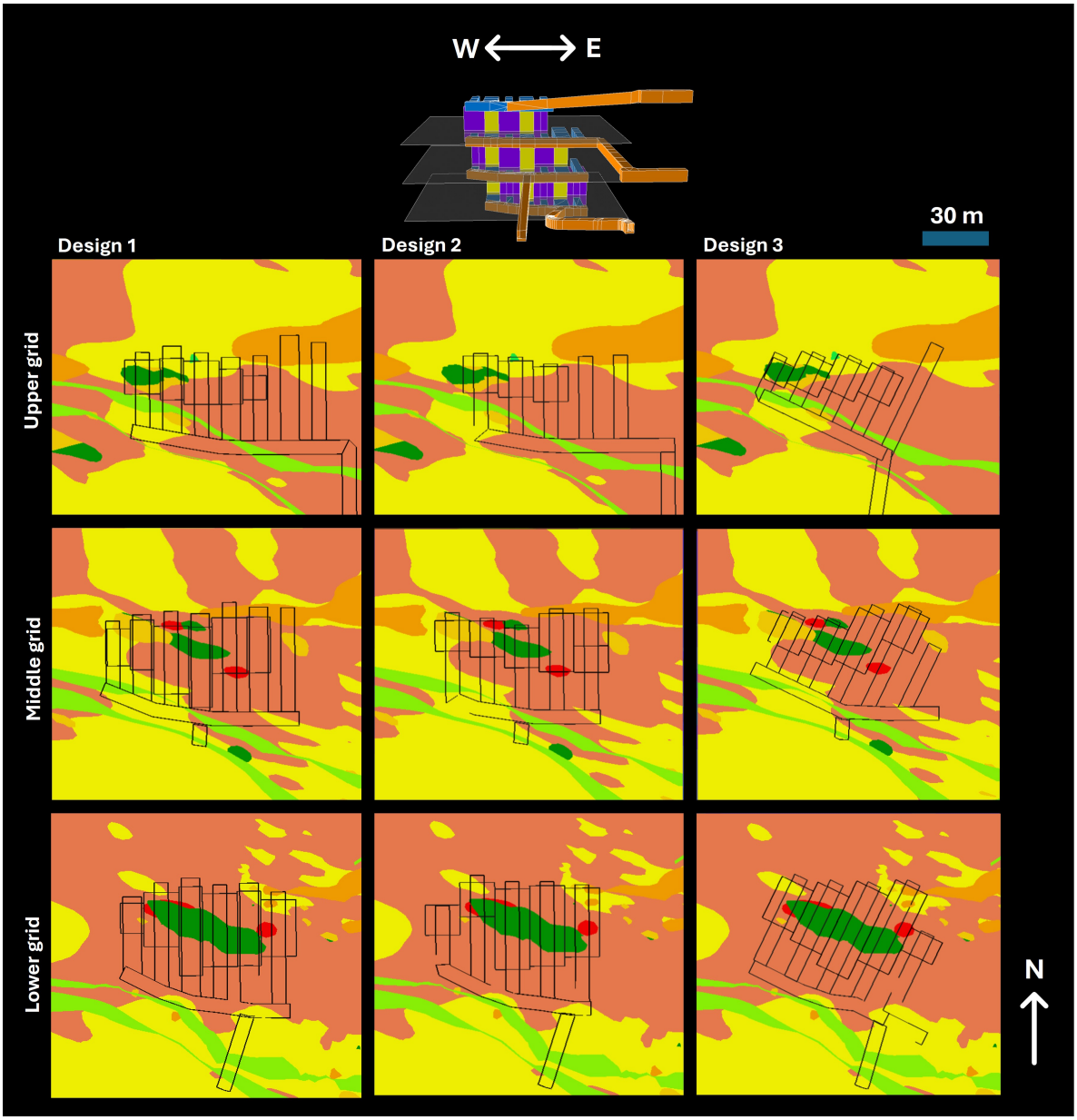

Figure 5.31: Andesite dykes (light green) through access drifts of the designs.

Tensile stresses

Tensile stresses are encountered by Map3D above the access drifts and along the stope walls. The tension generally does not affect the rock material itself, but relaxes the fractures in the rock mass and therefore stimulates structurally-induced rock failure. Tensile stresses are most pronounced above the access drifts in design option 1 and 2 (Figure 5.22).

5.3.3. Overhang

Before transitioning from cut-and-fill to stope mining, the upper slice will be backfilled with cemented backfill. The stopes will be excavated right above the backfill, without the presence of a horizontal sill pillar in between. Since the control over the distribution of cemented backfill cannot be fully guaranteed, a space between the backfill and the rock mass might be left. Another risk could be that the the bearing capacity of the backfill is not sufficient enough to support the rock mass. A result could be that the stopes are not sufficiently supported and settlements may occur.

Due to the mining of the primary stopes, the risk of settlements increases in the secondary stopes. After the mining and backfilling of the primary stopes, the rock mass in between the primary stopes experiences less frictional force from the sides, due to the replacement of rock with cemented backfill. In case of large overhang of the rock mass or insufficient bearing capacity of the backfill, the rock in the secondary stope might slide down or settle. This could increase the fracturing of the rock mass, and affect the access drift that is located through it. The position of the pillars in the underlying cut-and-fill slices could decrease the overhang and increase the bearing capacity, and therefore limit the settlements. In design 1 their position is most optimal relative to the other designs, since they are located next to the access drifts through the stopes, which will have been excavated before the mining of the stopes is initiated (Figure 5.32). Only the east side of secondary stope 3 is not located above undisturbed rock mass or a pillar. In design 2 and 3, the pillars are either located below the primary stopes or in the middle of a secondary stope, under the access drift.

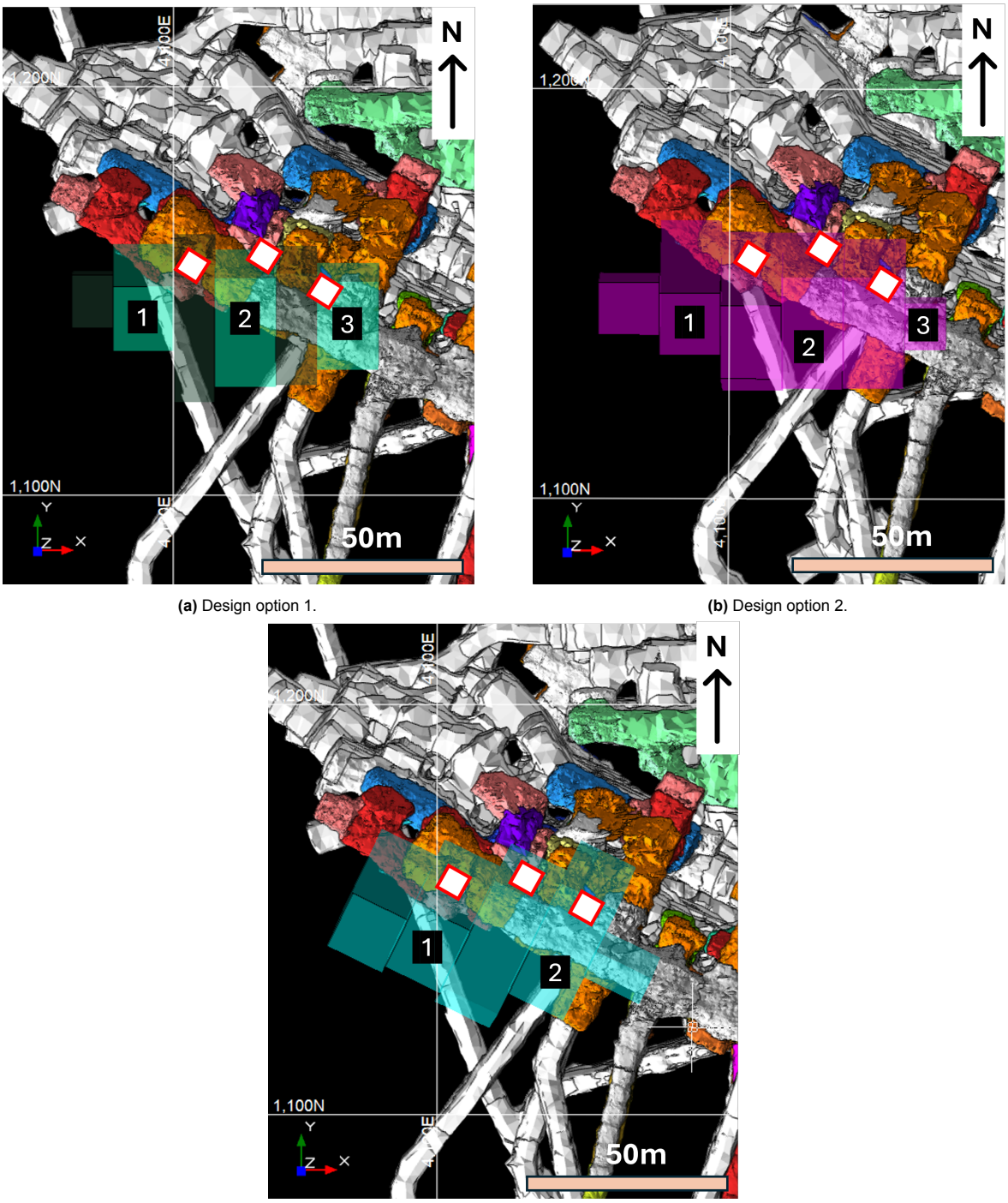

(a) Design option 1.

(b) Design option 2.

(c) Design option 3.

Figure 5.32: Position of the pillars in the underlying cut-and-fill slice with respect to the different stope designs. The secondary stopes are numbered.

5.3.4. Critical areas

The critical areas prone to stress-controlled and structure-controlled failure have been manually investigated for each design option. Areas that will need to be investigated further are shown in Figure 5.33, where area A is related to the boundary of sericite schist and quartz-feldspar-porphyry and the incoming fracture, and area B to the stress accumulations above the lowest access drifts and the sericite schist in the stope wall.

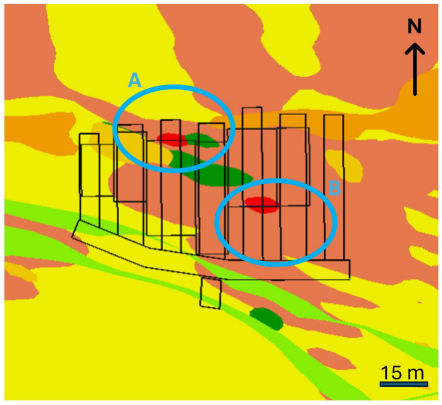

Figure 5.33: Areas to be investigated further.

5.3.5. Results evaluation

It was found that the susceptibility to stress-controlled failure is low across all stope design options. Option 1 and 2 only show a critical zone right above the lowest access drifts, whereas option 3 shows no critical zones. This could be explained by the shallow depth of the stope designs, which results in low in-situ stresses due to the relatively thin overburden, and therefore minimal stress accumulation during and after excavation. However, the sensitivity to structure-controlled failure is more dominant. This can be explained by the lacking clamping force around discontinuities due to the low stress regime, causing rock blocks to easily slide or fall out.

Two regions have been selected for further investigation into their stability. Both areas are characterized by the presence of sericite schist, a primary factor contributing to instability. However, it is plausible that sericite schist is also encountered in other regions during excavation of the drifts and stopes. It was noticed that the geological model and geologic maps show differences regarding rock type distribution. While the geologic maps indicate a substantial presence of sericite schist, the geological model shows only limited appearance. The inaccuracy of the geological model makes it challenging to draw reliable conclusions on the stability of the rock mass. Since the presence of sericite schist adjacent to a competent rock type was found to lead to an increased risk of extensive failure and sericite-quartzite was not, it is important to make the differentiation between the two weak rock types. The stress-induced stability will not be affected by more widely distributed sericite schist than shown in the geological model, since the stress accumulations around the excavations barely exceed 40 MPa, while the yield strength of sericite schist is 42 MPa.

5.4. Geotechnical feasibility of the stope designs

5.4.1. Stope selection

Given that secondary stopes are excavated in between primary stopes that are backfilled with cement, their sidewalls are artificial. Therefore, they are not of concern in this stope stability assessment, as backfill strength requirements are outside the scope of this study. Consequently, generally only primary stopes are investigated. Since it was found in Section 5.3 that the accumulated deviatoric stresses were highest in the lower production level, it was decided to investigate each primary stope in this row. Additionally, due to the presence of sericite schist in the back wall of one of the secondary stopes at the second level, this stope has also been investigated. The artificial sidewalls made of cemented backfill of the adjacent primary stopes have been disregarded.

5.4.2. Q'-parameters

The values for each parameter required to determine Q' are listed per occurring rock type (Table 5.4). They have been calculated for several scenarios: a normal scenario based on average rock type and rock mass parameter values, a pessimistic scenario where one standard deviation is subtracted of these values, another negative scenario where all stopes are encompassed by sericite schist, and lastly, a worst-case scenario where one standard deviation is subtracted from the sericite schist parameter values. The last two scenarios are included because the geological model and the geologic maps do not correspond regarding sericite schist presence, with the geological model indicating a much smaller occurrence. This suggests that the extent of sericite schist may be greater than currently assumed.

	Sericite-quartzite	Sericite schist	Dacite	Siltstone	Vulcanoclastics
Mean RQD	94	90	93	82	83
RQD - 1*st.dev	89	65	85	65	68
Jn	6	12	6	6	6
Mean Jr	1.5	1	3	3	3
Jr - 1*st.dev	1	0.5	2	2	2
Mean Ja	1	3	1	3	1
Ja - 1*st.dev	2	4	1.5	4	1.5

Table 5.4: Standardized parameters for occurring rock types to obtain Q'

5.4.3. N'-parameters

The parameters required to calculate the Modified Stability Number N' are the Modified Q-system Q', the rock stress factor A, the joint orientation factor B and the surface inclination factor C (Chapter 3.2.3). Q' and factor C are calculated individually for each case, as described in Section 3.2.3. The individual values for these parameters per stope wall and scenario can be found in Appendix C. Factor A could be standardized by dividing the UCS of each occurring rock type over the stress level steps in the stress model legend, which increase with 8 MPa since there are ten steps and the stress legend goes up to 80 MPa. Using Figure 3.3c, the corresponding A-value was found and stated in Table 5.5. Factor B could be standardized by determining for each stope wall and the roof which discontinuity set is most poorly oriented and subsequently determining the corresponding B-value. Since only one discontinuity set is taken into account in the method, the assumed failure method is sliding. This is done for each rock type that is occurring in more than one wall. The results are stated in Tables 5.6 and 5.7. For inclined walls the B-values in these tables are not applicable. For these faces the B-factor is determined individually.

	Sericite-quartzite	Sericite schist	Dacite
σ= 8 MPa	1	1	1
σ= 16 MPa	0.75	0.6	0.9
σ= 24 MPa	0.4	0.3	0.5
σ= 32 MPa	0.3	0.2	0.35
σ= 40 MPa	0.2	0.15	0.25
σ= 48 MPa	0.15	0.1	0.2
σ= 56 MPa	0.1	0.1	0.15
σ= 64 MPa	0.1	0.1	0.1
σ= 72 MPa	0.1	0.1	0.1
σ= 80 MPa	0.1	0.1	0.1

Table 5.5: A-values induced stress for each occurring rock type.

	Design option 1 and 2		Design option 3	
	Unfav. disc. orientation	B-value	Unfav. disc. orientation	B-value
Sidewall west	025/36	0.92	177/37	0.67
Sidewall east	177/37	1.00	025/36	1.00
Front wall	177/37	0.63	177/37	0.67
Back wall	025/36	0.67	025/36	0.63
Roof	177/37	0.32	025/36	0.32

Table 5.6: B-values for walls containing sericite-quartzite.

	Design option 1 and 2		Design option 3	
	Unfav. disc. orientation	B-value	Unfav. disc. orientation	B-value
Sidewall west	003/52	1.00	178/53	0.85
Sidewall east	280/41	0.60	280/41	0.65
Front wall	178/53	0.42	202/41	0.42
Back wall	003/52	0.42	003/52	0.45
Roof	354/33	0.20	354/33	0.40

Table 5.7: B-values for walls containing sericite schist.

5.4.4. Stability charts

The Modified Stability graphs for each analysed stope across the different design options display multiple points per stope face (Figure 5.34, 5.35 and 5.36). Each point represents a scenario outcome for a particular stope face as follows:

- First point (top), first scenario: normal case, based on the in-situ rock type, provided by the geological model
- Second point, second scenario: worse case, one standard deviation subtracted from the rock mass parameters assumed in the normal case scenario
- Third point, third scenario: worse case, the stope walls are assumed to be fully covered in sericite schist
- Fourth point (bottom), fourth scenario: worst case, one standard deviation is subtracted from the rock mass parameters assuming full sericite schist coverage.

When multiple rock types are present in a wall, the weakest rock type is selected for the stability analysis for the first two scenarios. However, if a weak rock type covers less than 10% of a wall, it is disregarded. It can be noted that only two or three dots are plotted for the roof. In that case N' for scenario 3 and/or 4 is below 0.1 and therefore outside the range of the graph as designed by Potvin (1988). In these instances, the roofs are assumed to fail. Since the method only takes into account one discontinuity set, the failure is assumed to take place through sliding. Since the analyzed secondary stope has one wall that consists fully of sericite schist, its line in the plot only consists of two dots. The stress distribution

grids that were used to determine the maximum induced stress in each stope face to calculate the A-factor can be found in Appendix B.

Design option 1

In design option 1, where the primary stopes have a width of 10m, the walls and roof fall within the stable or transition zones for scenario one and two (Figure 5.34). In the worst-case scenario the walls will require reinforcement to ensure stability. However, since reinforcement is solely applied to the roof, these walls would be considered to fail. The stability values for the sidewall in the central primary stope are significantly high, even with the large hydraulic radius (Figure 5.34b). This is attributed to the relatively low σ_1 values being normal to the stope sidewall, leading to a favourable stress factor A. This is explained by the orientation of the stope perpendicular to the main principal stress, which redirects the stresses around the stopes. The high stability values of the roof in the western primary stope also stand out compared to the other stope roofs (Figure 5.34a). This difference is explained by the presence of dacite, which has a better rock mass quality than the sericite-quartzite found in the other roofs. Because a structural analysis could not be performed on dacite due to its absence in the areas covered by LiDAR scans, the poorest discontinuity set direction from sericite schist has been used to determine the B-value for the dacite roof. The dacite-specific values for the Q'-parameters could be retrieved from the boreholes, which resulted in the high stability values. Figure 5.34d shows that the back wall of the secondary stope is expected to go to failure since reinforcement is required for its stability, which will not be applied.

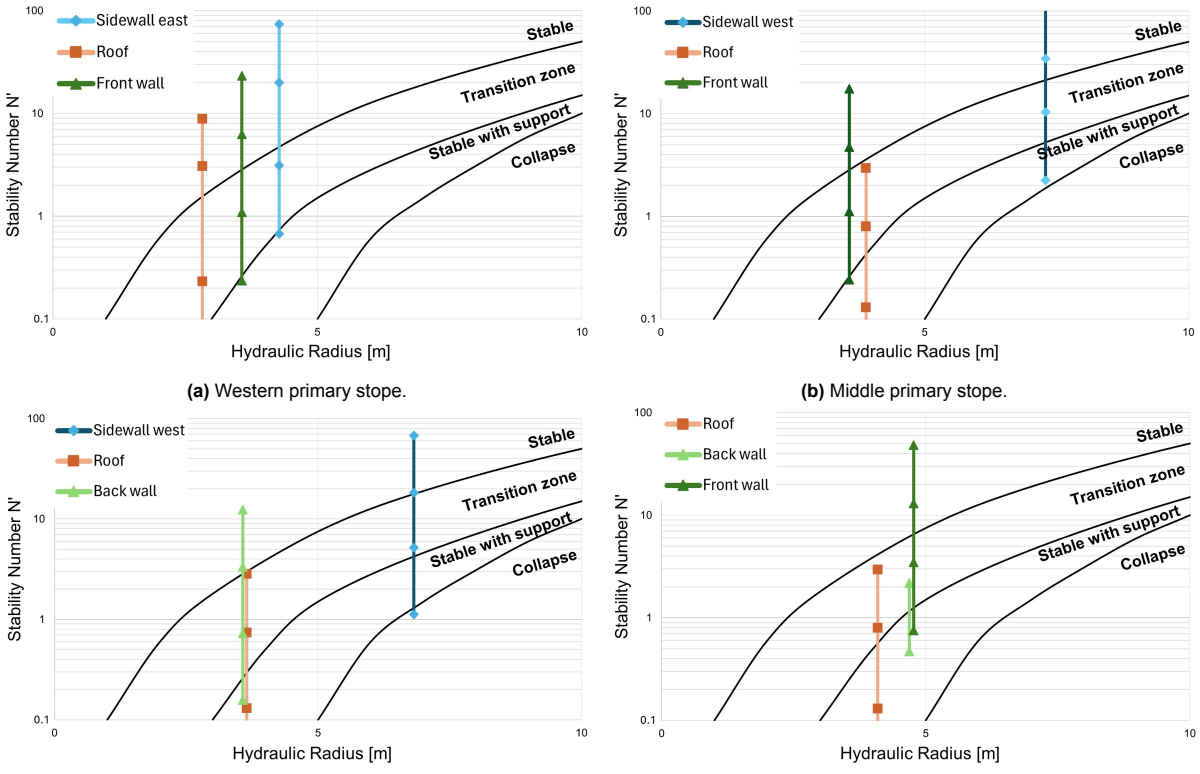

(a) Western primary stope.

(b) Middle primary stope.

(c) Eastern primary stope.

(d) Secondary production level 2.

Figure 5.34: Stability graphs following Potvin (1988), design option 1. In case that N' is below 0.1 no dot is presented and the face is assumed to fail.

Design option 2

In design option 2, where the primary stopes have a width of 15m, the increased hydraulic radius leads to a slightly lower overall stability compared to option 1 (Figure 5.35). Furthermore, there are notable differences in stress distribution, with results in a variation in the critical walls compared to option 1. Also for this design the stopes are expected to stay stable in the first and second scenario. The roof of the western stope is more stable than the other roofs, here due to the presence of volcanoclastics (Figure 5.35a). In this option, the stability of the sidewalls of the eastern primary stope (Figure 5.35c) instead of the middle one (Figure 5.35b) is exceptional, caused by the slightly different stress distribution compared to option 1. The stability of the back wall of the secondary stope has decreased compared to option 1 (Figure 5.35d), which is caused by a larger stress accumulation at this wall due to the underlying access drifts. In case of the third and fourth scenario, the stopes are expected to fail.

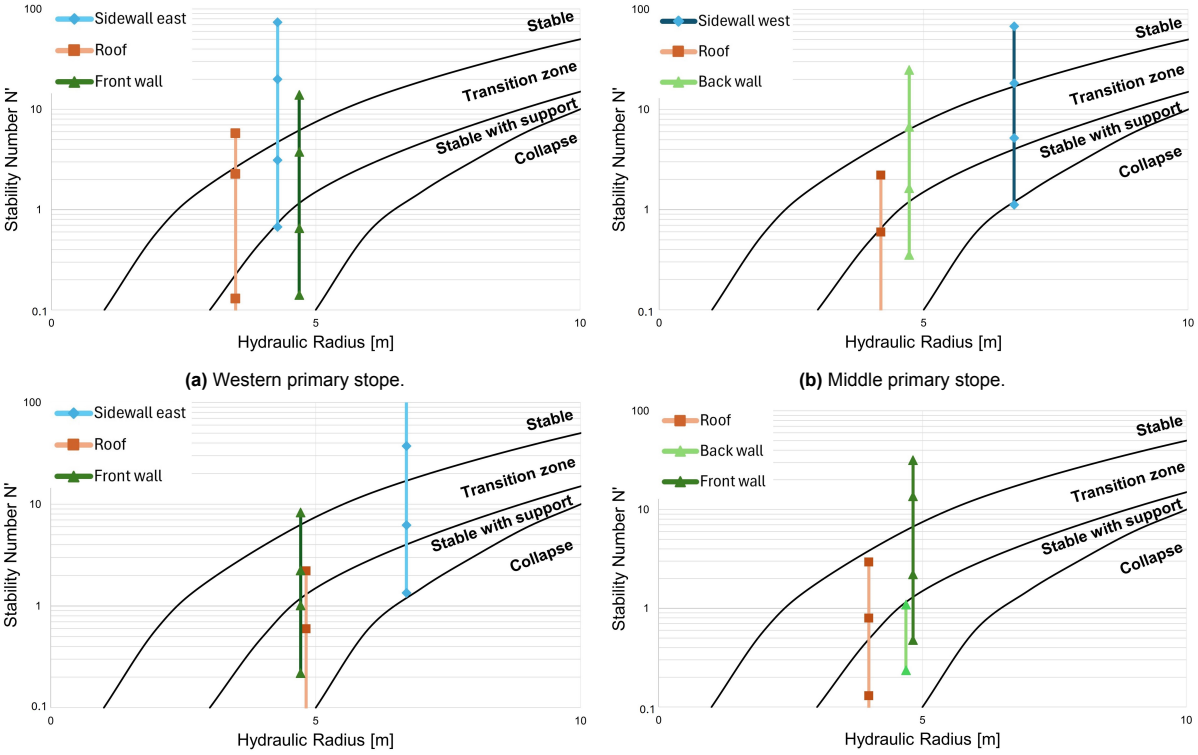

(a) Western primary stope.

(b) Middle primary stope.

(c) Eastern primary stope.

(d) Secondary production level 2.

Figure 5.35: Stability graphs following Potvin (1988), design option 2. In case that N' is below 0.1 no dot is presented and the face is assumed to fail.

Design option 3

In design option 3, where the stopes have a strike of 26°, there is a slight increase in stress accumulation in the sidewalls, which are therefore less stable compared to other design options (Figure 5.36). However, the smaller hydraulic radius of the faces mitigates this effect, maintaining wall stability for scenario 1 and 2. In the worst-case scenario, the stopes are expected to experience failure. The results for the third scenario are distributed around the boundary between the transition zone and the zone where reinforcement is required. This makes it difficult to draw a conclusion. In this design the back face of the secondary stope does not contain sericite schist, which improves its expected stability (Figure 5.36d). Due to the angled orientation of the stopes, the sidewalls of this secondary stope do not consist of the cemented backfill of the primary stope. Therefore, they are included in the stability chart, contradictory to the other design options.

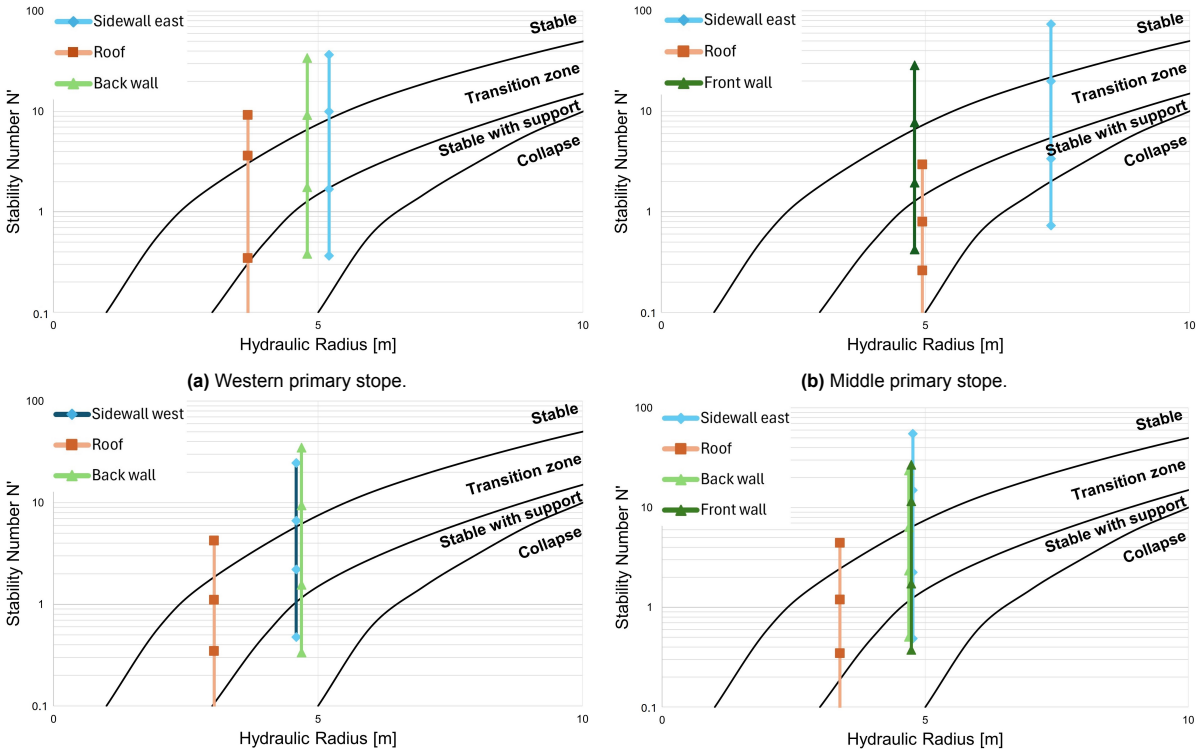

(a) Western primary stope.

(b) Middle primary stope.

(c) Eastern primary stope.

(d) Secondary production level 2.

Figure 5.36: Stability graphs following Potvin (1988), design option 3. In case that N' is below 0.1 no dot is presented and the face is assumed to fail.

5.4.5. Optimal design option

Optimal design following the Modified Stability method

Stope roofs will be reinforced, and since all roofs have a stability in the range of 'stable with support' or better for scenario 1 and 2, they are unlikely to cause issues in any of the designs. However, the walls will go without reinforcement. When focusing solely on the first two scenarios, stability issues arise with the front walls of the eastern and western stopes in the second option, as well as with the back wall in the secondary stope of the first and second options, as their stability is plotted to be in the transition zone and the zone that requires reinforcement. Design option 3 does not indicate unstable walls for these scenarios. In the third scenario, all walls are in or close to the section 'stable with support' for each design option. In the worst-case scenario all walls are expected to show failure. Consequently, based on this analysis the third design option appears to be most favourable.

Optimal design combining the Modified Stability method and the geotechnical challenges

The geotechnical challenges and the standardized Modified Stability analysis results are combined (Table 5.8). To determine which stope design option is most feasible, the encountered geotechnical

challenges are weighted based on the risk that they impose. The accumulated deviatoric and tensile stress above the access drifts are deemed most high-risk. This is due to the long stand-up time of the access drifts, and their frequent usage by employees. Therefore, it got the maximum weight of 3. The SERSCH-QFP boundary, sericite schist presence in the stope wall and the incoming fracture are weighted 2, since their risk of disrupting the regularity of the stope shape due to under- or overbreak is high, but they will not affect human safety, since no personnel will enter the stopes after blasting. The andesite dykes are weighted 1, since no major failures have been documented in the past, but the access drifts that they intersect are intensely used by personnel. The appearance of relaxation zones got the weight of 1, since they may cause production disruptions by inducing overbreak of the stopes. The weight is not higher, because the difference between the models is small. The location of pillars underneath the stopes is also weighted 1, since the presence of overhang is tried to be minimized by using cemented backfill and the location of the pillars only has a limited impact. Both the desk study and the Modified Stability method favour design option 3.

	Advantages [weight]	Disadvantages [weight]
Design 1	1. More favourable position of access drifts with respect to andesite dykes [1] 2. Relatively little relaxation zones around the stopes [1] 3. Favourable position of pillars underneath stopes, reducing possible overhang [1] 4. Favourable orientation of stopes with respect to incoming fracture [2]	1. High deviatoric and tensile stresses above access drifts [3] 2. Prone to SERSCH-QFP boundary failure [2] 3. Unstable back wall following the desk study and Modified Stability analysis due to sericite schist presence [2]
Design 2	1. More favourable position of access drifts with respect to andesite dykes [1]	1. High deviatoric and tensile stresses above access drifts [3] 2. Prone to SERSCH-QFP boundary failure [2] 3. Unstable back wall following the desk study and Modified Stability analysis due to sericite schist presence [2] 4. Unfavourable orientation of stopes with respect to incoming fracture[2] 5. Unstable front walls following the Modified Stability Method 6. Unfavourable position of pillars underneath stopes [1]
Design 3	1. Low deviatoric and tensile stresses above access drifts [3] 2. Less prone to SERSCH-QFP boundary failure [2] 3. No sericite schist presence in back wall of secondary stope [2] 4. Stable stopes following the Modified Stability Method	1. Unfavourable position of access drifts with respect to andesite dykes [1] 2. Relatively many relaxation zones around the stopes [1] 3. Unfavourable position of pillars underneath stopes [1] 4. Unfavourable orientation of stopes with respect to incoming discontinuity [2]

Table 5.8: Geotechnical advantages and disadvantages per stope design, desk study and Modified Stability analysis combined. The geotechnical challenges are weighted based on the risk that they impose.

5.4.6. Results evaluation

Both the desk study and the standardized Modified Stability analysis resulted that design option 3 is most feasible from a geotechnical perspective. The Modified Stability method focuses on global rock type distribution and general rock mass parameters such as discontinuity orientations, and stope dimensions. The desk study emphasizes the in-situ anomalies such as the interaction between adjacent rock types and individual major discontinuities. Combining these two approaches provides a more complete overview of the possible risks that arise for each stope design.

The results of this section have shown the significant effect of sericite schist presence on the stability of a stope face. To ensure the reliability of the design, it is important to improve the insight in the distribution of this rock type, making it possible to adjust the model accordingly.

6

Discussion

It has been concluded that design option 3 is most feasible from a geotechnical perspective. However, also this design is not free of risks. They could be mitigated by elongating the access drifts of the third production level, such that they cut through the andesite dykes perpendicularly (Figure 6.1, upper grid). The second and third stope in the first production level could be made slightly shorter, to avoid the incoming fracture in the stope and more importantly, in the access drift. Stope 1 could also be shortened, but it will need to reduce more than half in size, which will have a large financial impact.

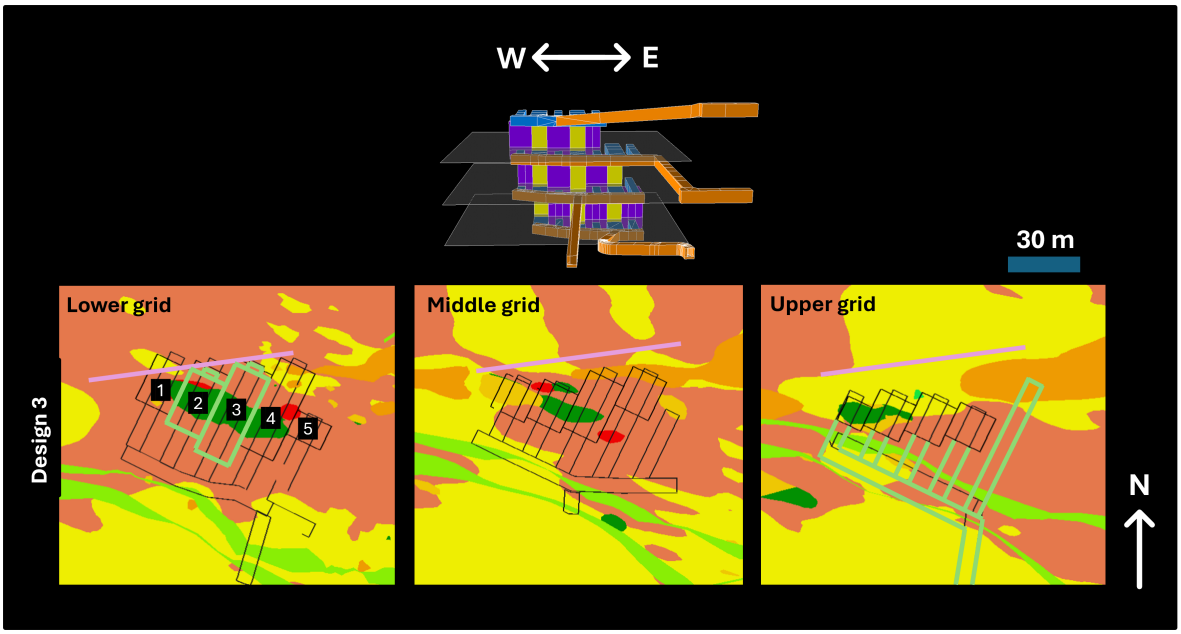

Figure 6.1: Updated design option 3, where the green lines indicate the opted adjustment on the design and the purple line indicates the incoming fracture that cuts through a selection of the stopes in the first production level.

A more rigorous adjustment to the stope design could be made to optimize the location of the secondary stopes with respect to the cut-and-fill pillars below (Figure 6.2). The stopes are shifted approximately seven meters southeast. The most eastern stope is deleted and a stope could possibly be added on the west side to excavate the ore that is located there.

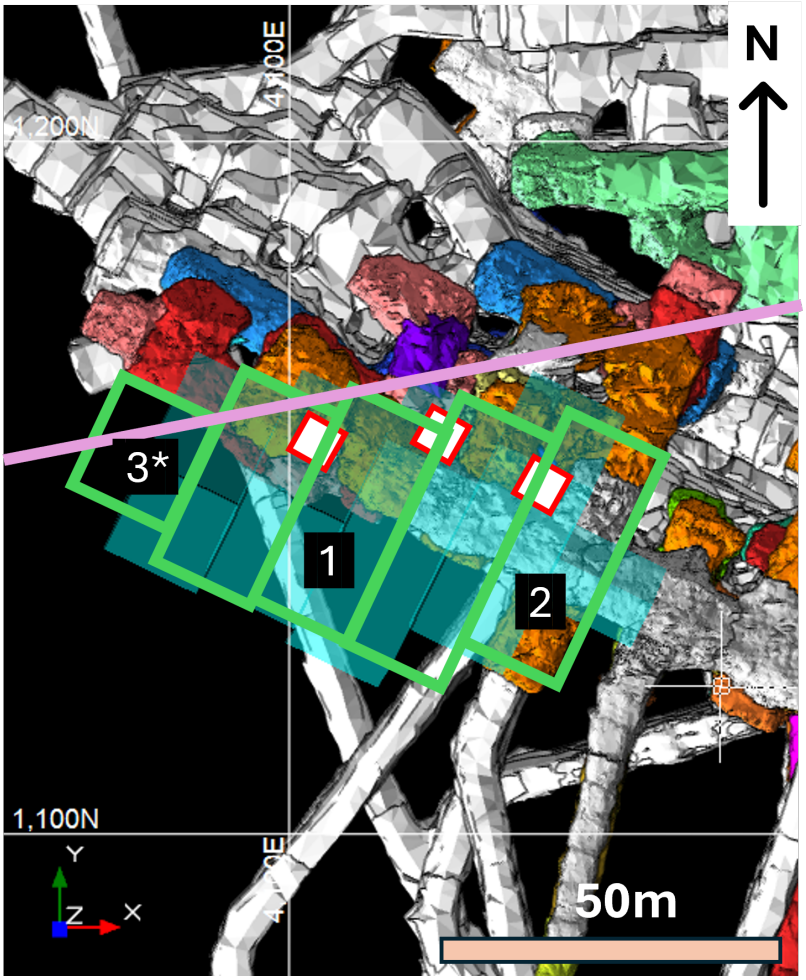

Figure 6.2: Further geotechnically optimized design option 3, where the stopes are moved such that the cut-and-fill pillar location is more favourable with respect to the secondary stopes. Secondary stope 3* could be added to account for the relocation of the stopes out of that place. The green lines indicate the opted adjustment on the stope location and the purple line indicates the incoming discontinuities that cuts through a selection of the stopes in the first production level. The secondary stopes are numbered. Stope 3* has been added to the design. The eastern primary stope is removed.

Lastly, an optimal angle for the strike of the stopes could be found, such that the incoming fracture is avoided, the stress relaxation areas are decreased, but the tensile stresses above the access drifts stay below a critical level. New stress models need to be created to determine this optimum.

Boliden and many other mining companies use the Modified Stability Method as a stability assessment for stope designs. In this project, the Modified Stability method and the desk study on individual geotechnical risks favoured the same design option. However, the approaches have different focus points. The Modified Stability method investigates the overall stability of a stope wall of specific dimensions with respect to the global rock mass characteristics, but does not take into consideration the specific rock type distribution and their interconnected behaviour, and tensile stress build-up. Moreover, it solely focuses on the stopes, and not on the development or possible transition between mining methods. The study on individual geotechnical risks covers the effect of rock type interactions with competence differences, extensive fractures and tensile stresses. Also the stability of the development, and the possible instability caused by overhang above underlying excavations is taken into account, but the effect of the size of the stopes is neglected. Since the two risk determination methods have different focus points, their agreement on stope design 3 is attributed to luck in this case. Only the sericite schist presence in the back wall of the secondary stope which stability has been investigated is covered in both approaches. If the access drifts would have been oriented differently, such that high tensile stresses would build up in option 3, and the SERSCH-QFP boundary would be located slightly to the

northwest, design option 3 could be less favourable, leading to a disagreement between the two methods. Therefore, it is stressed to complement the Modified Stability method with an investigation on geotechnical risks based on heterogeneities to account for both the anticipated general behaviour and the impact of locally occurring anomalies that may induce failure, in order to make an informed decision.

Not only does the desk study on geotechnical risks provide the option to make both minor and major adjustments on a stope design prior to mining in order to improve safety and reduce the risk of production disruptions, it also offers an insight in potential challenges that could be encountered during production. This enables a proactive preparation and anticipation rather than reactive measures.

Various modifications of the Modified Stability method have been developed, adjusting the boundaries between the zones on the chart, or the parameters that are taken into account for the determination of Modified Stability Number N' (Mawdesley et al., 2001a, Mortazavi and Osserbay, 2022). Examples are the implementation of the effect of present faults by Suorineni, (1998) and the impact of tensile stresses by Mitri et al., (2011). These adjustments implement a part of the performed desk study on geotechnical risks into the stability method. It is suggested to find the most optimal modification for Boliden.

Geotechnical data is limited in the not yet excavated area of interest in the upper section of the mine. The assumption has been made that the average rock mass and rock type parameters could be extrapolated to this region to describe the rock mass. As mining in this area progresses, additional data could be collected to update the rock mass description and corresponding stability predictions.

One of the available rock mass parameters is discontinuity orientation, which is extracted from LiDAR scans. Unfortunately, the low resolution of the scans does not allow for persistence determination, which complicates the prediction of large wedge failures. High resolution 3D point clouds, obtained using e.g. digital photogrammetry, can be analyzed using the softwares CloudCompare and Discontinuity Set Extractor to provide fracture characteristics such as persistence (Dewez et al., 2016, Riquelme et al., 2018). It is advised to further investigate the possible integration of this method.

Usage of the software Map3D introduces major assumptions and limitations. The rock mass is assumed to be homogeneous, isotropic and linearly elastic, and standardized values for the Young's Modulus and Poisson's ratio have been used. These standardized elastic parameters lead to an potential overestimation of the stability, since stress could concentrate in weaker zones and lead to localized failure (Mahmoodzadeh et al., 2022). Nontheless, the software is widely used in the mining industry due to its ability to manage large scale problems with 3D complex geometries, and its capacity of simulating a mining sequence (Bruneau et al., 2003). It is strongly advised to investigate the options of other stress distribution software, or methods to account for the assumptions that are made in Map3D. To enhance the understanding and prediction of failure mechanisms, a 3D elasto-plastic model should be developed. This model would simulate failure scenarios while considering various factors such as different rock type characteristics adjacent to each other, rock mass properties, and the in-situ stress field. By including these elements, the model can provide a comprehensive and realistic representation of the conditions leading to failure. This will enhance the ability to optimize the design, achieving the highest productivity with minimal disruptions.

Another factor of uncertainty in this project is caused by the geological model, which does not properly differentiate between sericite-quartzite and sericite schist. The presence of the weaker sericite schist is underestimated. Since this rock type plays an important role in the formation of major wedge failures, an attempt should be made to improve the differentiation of the model between the two rock types.

7

Conclusion

This study investigated the transition from small-scale post-pillar mining to large-scale longhole open stoping at the Kankberg mine, focusing on the geotechnical risks that are encountered in different stope design options. The primary objective was to identify the most geotechnically favourable design among the three proposed options, considering the geological and structural characteristics of the area of interest.

The area of interest was investigated by performing a structural analysis that provided discontinuity set orientations for each rock type. Additionally, geological borehole data was used to describe the rock type and rock mass properties. Lastly, the characteristics of major wedge failures that occurred recently were identified both visually and using LiDAR scans made after excavation.

It was found that the main discontinuity clusters have an east-west strike, which is parallel to the major present day principal stress direction. Moreover, a boundary between weak and competent rock was established to form one of the major failure planes over which wedge failure took place, especially when oriented parallel to the major principal stress direction. The other major failure plane is located in the competent rock, which underwent fracturization due to pure shear. The wedges fail through free fall by gravity after excavation of the rock mass underneath.

An linear elastic stress model assuming homogeneity and isotropy was developed to assess the stress distribution around each design. An aes for the Young's Modulus and Poisson's ratio were presumed. Some differences in stress distribution between the models were encountered. The study concluded that stress-induced failure (meaning failure caused by σ_1 stresses exceeding the rock mass strength) is not a major concern. This is explained by the shallow depth at which the stopes will be located, which results in a low overburden pressure and therefore relatively low in-situ stresses. However, tensile stresses develop above the access drifts of the first production level, which could destabilize the in-situ fractures and induce failure. Design 1 and 2 show high tensile stress build-up, whereas design option 3 does not.

Structural failure was found to occur in various ways, particularly around the boundary between weak and competent rock types with an approximately east-west strike, especially if this boundary intersects a large open area. Additionally, extensive fractures were observed to cut through the area, and sericite schist was identified in some stope faces. In terms of structure-induced failure, design option 3 was found to be the most favourable. For both stress-induced failure and structure-induced failure, areas of potential failure were identified that require additional investigation to analyse their stability. These areas were analysed by using the Modified Stability method. The outcome provides an indication of the stability conditions of the stope walls. The analysis revealed that design option 3 is the most stable, while design options 1 and 2 exhibited a tendency for failure in certain stope walls. However, the Modified Stability Method does not take into account the rock type distributions with respect to each other, thereby not investigating the interconnected behaviour of the rock types. Therefore, the desk study and Modified Stability analysis should be combined to get a complete insight into the stability of

each stope design.

Based on the findings, it was concluded that design option 3, with certain adjustments, could offer the most favourable stability conditions. A fourth design option has been provided, containing adjustments regarding the location and length of the stopes, and location of the access drifts. Additionally, further investigations should be conducted to improve the understanding of the geological and geotechnical conditions and their impact on stope stability. Also the possibility of using an improved stress distribution calculation method should be investigated.

References

Bark, G., & Weihed, P. (2012). Geodynamic settings for paleoproterozoic gold mineralization in the svecofennian domain: A tectonic model for the fäboliden orogenic gold deposit, northern sweden. *Ore Geology Reviews*, *48*, 403–412.

Bauer, T., Skyttä, P., Allen, R., & Weihed, P. (2011). Syn-extensional faulting controlling structural inversion – insights from the palaeoproterozoic vargfors syncline, skellefte mining district, sweden. *Precambrian Research*, *191*, 166–183.

Bergman, J. (2001). Palaeoproterozoic mineralized volcanic arc systems and tectonic evolution of the fennoscandian shield: Skellefte district sweden. *Weihed, P. (Ed.), Economic Geology Research*, *Sver. Geol. Unders. C833*, 46–68.

Bieniawski, Z. (1976). Rock mass classification in rock engineering. *Symposium of Exploration for Rock Engineering*, 97–106.

Bieniawski, Z. (1989). *Engineering rock mass classifications: A complete manual for engineersand geologists in mining, civil and petroleum engineering*. Wiley.

Blom, J. (2017). Scandinavia & the alps.

Blomberg, M. (2024). Present rock types in kankberg and their geological features.

Bogdanova, S., Gorbatschev, R., Skridlaite, G., Soesoo, A., Taran, L., & Kurlovich, D. (2015). Trans-baltic palaeoproterozoic correlations towards the reconstruction of supercontinent columbia/-nuna. *Precambrian Research*, *259*, 5–33.

Brace, W. F., Paulding, B. W., & Scholz, C. H. (1966). Dilatancy in the fracture of crystalline rocks. *Journal of Geophysical Research*, *71*, 3939–3953.

Bruneau, G., Hudyma, M., Hadjigeorgiou, J., & Potvin, Y. (2003). Influence of faulting on a mine shaft—a case study: Part ii—numerical modelling. *International Journal of Rock Mechanics and Mining Sciences*, *40*, 113–125.

Deere, D., & Deere, D. (1988). The rock quality designation (rqd) index in practice. *Rock classification systems for engineering purposes, ASTM Special Publication 984.*, 91–101.

Deere, D., Hendron, A., Patton, F., & Cording, E. (1967). Design of surface and near surface construcrtion in rock. *The 8th U.S. Symposium on Rock Mechanics (USRMS)*.

Dehghannejad, M., Bauer, T., Malehmir, A., Juhlin, C., & Weihed, P. (2012). Crustal geometry of the central skellefte district, northern sweden – constraints from reflection seismic investigations. *Tectonophysics*, *524-525*, 87–99.

Dewez, T., Girardeau-Montaut, D., Allanica, C., & Rohmer, J. (2016). Facets: A cloudcompare plugin to extract geological planes from unstructured 3d point clouds. *The International Archives of the Photogrammetry, Remote Sensing and Spatial Information Sciences*, *XLI-B5*.

Diederichs, M. S. (2003). Rock fracture and collapse under low confinement conditions. *Rock Mechanics and Rock Engineering*.

Fernberg, H. (2007). *Mining methods in underground mining*. Atlas CopCo.

Groves, D., Santosh, M., Goldfarb, R., & Zhang, L. (2018). Structural geometry of orogenic gold deposits: Implications for exploration of world-class and giant deposits. *Geoscience Frontiers*, *9*, 1163–1177.

Guitreau, M., Blichert-Toft, J., & Billström, K. (2014). Hafnium isotope evidence for early-proterozoic volcanic arc reworking in the skellefte district (northern sweden) and implications for the svecofennian orogen. *Precambrian Research*, *252*, 39–52.

Haldar, S. (2018). *Mineral exploration: Principles and applications*. Elsevier.

Heapa, M., Villeneuve, M., Albinoc, F., Farquharsond, J., Brothelandee, E., Amelung, F., Gotf, J.-L., & Baud, P. (2020). Towards more realistic values of elastic moduli for volcano modelling. *Journal of Volcanology and Geothermal Research*, *390*.

Hustrulid, W., & Bullock, R. (2007). *Underground mining methods: Engineering fundamentals and international case studies*. SME.

Jönsson, H., Koorem, B., Heden, H., Hedman, H., Rigg, D., & Mattsson, B. (1999). *Status report 1999 åkulla östra mine investigation – geology*. Boliden.

Korja, A., Lahtinen, R., & Nironen, M. (2006). The svecofennian orogen: A collage of microcontinents and island arcs. *Geological Society, London, Memoirs*, *32*, 561–578.

Lahtinen, R., Köykkä, J., Salminen, J., Sayab, M., & Johnston, S. (2023). Paleoproterozoic tectonics of fennoscandia and the birth of baltica. *Earth-Science Reviews*, *246*.

Lahtinen, R., Nironen, M., Korja, A., & Heikkinen, P. (2009). Paleoproterozoic accretionary processes in fennoscandia. *Geological Society London Special Publications*, *318*, 237–256.

Larsson, P. (2019). *Rock mechanical prestudy for sub-level stoping of fw1 level 325-249*. Boliden.

Latta, T. (2024). Present rock types in kankberg and their geotechnical features.

Mahmoodzadeh, A., Nejati, H., Mohammadi, M., Mohammed, A., Ibrahim, H., & Rashidi, S. (2022). Numerical and machine learning modeling of hard rock failure induced by structural planes around deep tunnels. *Engineering Fracture Mechanics*, *271*.

Martin, C. D. (1997). The effect of cohesion loss and stress path on brittle rock strength. *Seventeenth Canadian Geotechnical Colloquium*.

Martin, C. D. (2005). Preliminary assessment of potential underground stability (wedge and spalling) at forsmark, simpevarp and laxemar sites. *Svensk Kärnbränslehantering AB*.

Martin, C. D., Kaiser, P. K., & McCreath, D. R. (1998). Hoek-brown parameters for predicting the depth of brittle failure around tunnels. *Canadian Geotechnical Journal*.

Mawdesley, C., Trueman, R., & Whiten, W. (2001a). Extending the mathews stability graph for open-stope design. *Mining Technology*, *110*, 27–39.

Mawdesley, C., Trueman, R., & Whiten, W. (2001b). Extending the mathews stability graph for open-stope design. *Transactions of the Institution of Mining and Metallurgy, Section A: Mining Technology*.

Mitri, H., Hughes, R., & Zhang, Y. ((2011)). New rock stress factor for the stability graph method. *International Journal of Rock Mechanics Mining Sciences*, *48*, 141–145.

Mortazavi, A., & Osserbay, B. (2021). The consolidated mathews stability graph for open stope design. *Nazarbayev University, School of Mining Geosciences*.

Mortazavi, A., & Osserbay, B. (2022). The consolidated mathews stability graph for open stope design. *Geotechnical and Geological Engineering*, *40*, 2409–2424.

Nironen, M. (1997). The svecofennian orogen: A tectonic model. *Precambrian Research*, *86*, 21–44.

Nordfeldt, P., Allen, R., Pitcairn, I., & Gibson, H. (2019). Topaz-rich breccias at the 1.9 ga kankberg au-te deposit, skellefte district, sweden. In *Life with ore deposits on earth, 15th sga biannial meeting*.

Pabst, S. (2022). *Boliden summary report laver project*. Boliden.

Potvin, Y. (1988). Empirical open stope design in canada. *University of British Columbia, Department of Mining and Mineral Process Engineering*.

Purser, R., Mohmoud, M., Serati, M., & Chen, Z. (2021). Determining rock elastic parameters using a new true-triaxial-based technique. *Resource Operators Conference*.

Ragnarsson, E. (2024). Present rock types in kankberg and their geotechnical features.

Riquelme, A., Tomás, R., Cano, M., Pastor, J., & Abellán, A. (2018). Automatic mapping of discontinuity persistence on rock masses using 3d point clouds. *Rock Mechanics and Rock Engineering*, *51*, 3005–3028.

Sadeghi, M., Morris, G., Carranza, E., Ladenberger, A., & Andersson, M. (2013). Rare earth element distribution and mineralization in sweden: An application of principal component analysis to foregs soil geochemistry. *Journal of Geochemical Exploration*, *133*, 160–175.

Scholz, C. H. (1968). Microfracturing and the inelastic deformation of rock in compression. *Journal of Geophysical Research*, *73*, 1417–1432.

SGU. (2020). *The bedrock of sweden*. Retrieved December 25, 2023, from https://www.sgu.se/en/geology-of-sweden/rocks/the-bedrock-of-sweden/

Sjöberg, J., & Sjöström, J. (2000). *Rock mechanics core logging - boliden standard*. Boliden.

Stewart, S., & Forsyth, W. (1995). The mathew's method for open stope design. *Rock Mechanics*, *88*, 45–53.

Suorineni, F. ((1998)). *Effects of faults and stress on open stope design*. University of Waterloo.

Tavakoli, S., Elming, S., & Thunehed, H. (2012). Geophysical modelling of the central skellefte district, northern sweden; an integrated model based on the electrical, potential field and petrophysical data. *Journal of Applied Geophysics*, *82*, 84–100.

Wagner, T., & Wenzel, T. (2007). Remobilization processes in the metamorphosed boliden massive sulfide deposit: Insights from la-icp-ms analysis of invisible gold in arsenopyrite and pyrite. In C. Andrew (Ed.), *Mineral exploration and research: Digging deeper* (pp. 589–592). SGA.

Wiles, T. (2012). Rock mechanics/model interpretation.

A

Conversion sheet RMR data to Q parameters

4	Joint Alteration Number	Φ_r approx.	J_a
a) Rock-wall contact (no mineral fillings, only coatings)			
A	Tightly healed, hard, non-softening, impermeable filling, i.e., quartz or epidote.		0.75
B	Unaltered joint walls, surface staining only.	25-35°	1
C	Slightly altered joint walls. Non-softening mineral coatings; sandy particles, clay-free disintegrated rock, etc.	25-30°	2
D	Silty or sandy clay coatings, small clay fraction (non-softening).	20-25°	3
E	Softening or low friction clay mineral coatings, i.e., kaolinite or mica. Also chlorite, talc gypsum, graphite, etc., and small quantities of swelling clays.	8-16°	4
b) Rock-wall contact before 10 cm shear (thin mineral fillings)			
F	Sandy particles, clay-free disintegrated rock, etc.	25-30°	4
G	Strongly over-consolidated, non-softening, clay mineral fillings (continuous, but <5 mm thickness).	16-24°	6
H	Medium or low over-consolidation, softening, clay mineral fillings (continuous, but <5 mm thickness).	12-16°	8
J	Swelling-clay fillings, i.e., montmorillonite (continuous, but <5 mm thickness). Value of J_a depends on percent of swelling clay-size particles.	6-12°	8-12
c) No rock-wall contact when sheared (thick mineral fillings)			
K	Zones or bands of disintegrated or crushed rock. Strongly over-consolidated.	16-24°	6
L	Zones or bands of clay, disintegrated or crushed rock. Medium or low over-consolidation or softening fillings.	12-16°	8
M	Zones or bands of clay, disintegrated or crushed rock. Swelling clay. J_a depends on percent of swelling clay-size particles.	6-12°	8-12
N	Thick continuous zones or bands of clay. Strongly over-consolidated.	12-16°	10
O	Thick, continuous zones or bands of clay. Medium to low over-consolidation.	12-16°	13
P	Thick, continuous zones or bands with clay. Swelling clay. J_a depends on percent of swelling clay-size particles.	6-12°	13-20

Figure A.1: Conversion sheet Ja

2	Joint set number	J_n
A	Massive, no or few joints	0.5-1.0
B	One joint set	2
C	One joint set plus random joints	3
D	Two joint sets	4
E	Two joint sets plus random joints	6
F	Three joint sets	9
G	Three joint sets plus random joints	12
H	Four or more joint sets, random heavily jointed "sugar cube", etc	15
J	Crushed rock, earth like	20

Note: i) For tunnel intersections, use 3 x J_n

ii) For portals, use 2 x J_n

Figure A.2: Conversion sheet Jn

3	Joint Roughness Number	J_r
a) *Rock-wall contact, and* ***b)*** *Rock-wall contact before 10 cm of shear movement*		
A	Discontinuous joints	4
B	Rough or irregular, undulating	3
C	Smooth, undulating	2
D	Slickensided, undulating	1.5
E	Rough, irregular, planar	1.5
F	Smooth, planar	1
G	Slickensided, planar	0.5
Note: i) Description refers to small scale features and intermediate scale features, in that order		
c) *No rock-wall contact when sheared*		
H	Zone containing clay minerals thick enough to prevent rock-wall contact when sheared	1

Note: ii) Add 1 if the mean spacing of the relevant joint set is greater than 3 m (dependent on the size of the underground opening)

iii) J_r = 0.5 can be used for planar slickensided joints having lineations, provided the lineations are oriented in the estimated sliding direction

Figure A.3: Conversion sheet Jr

B

σ_1 distribution around stopes

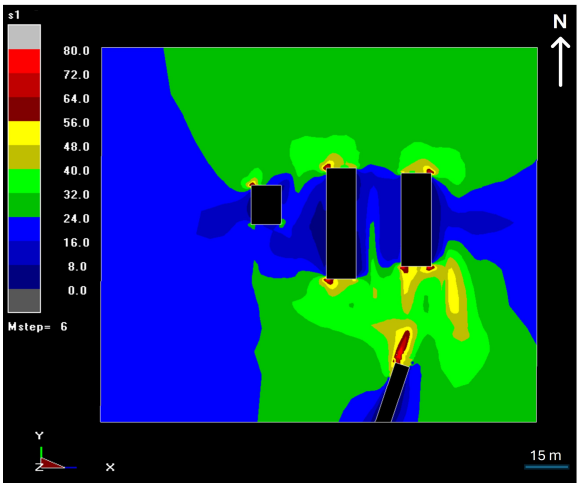

(a) Horizontal grid stope level 1.

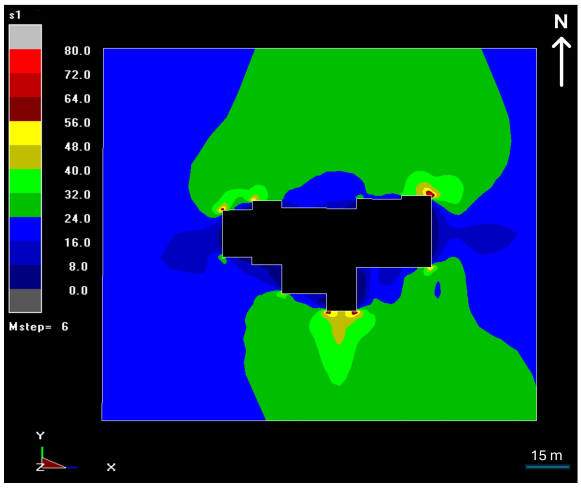

(b) Horizontal grid stope level 2.

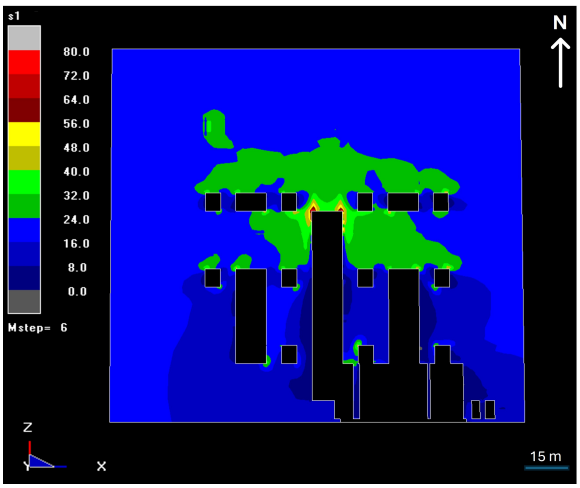

(c) Vertical grid step 3.

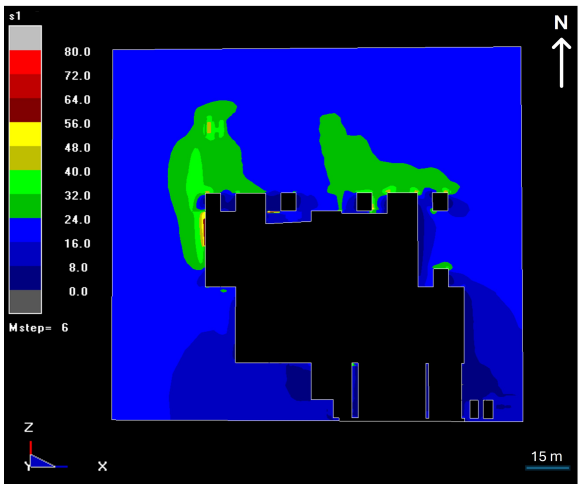

(d) Vertical grid step 6.

Figure B.1: σ_1-distribution around the stopes for design option 1.

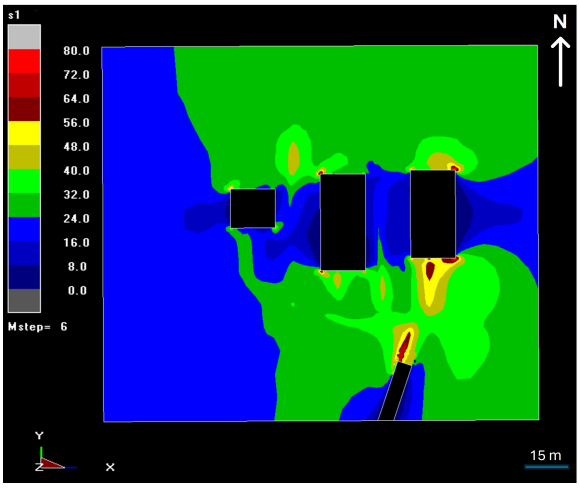

(a) Horizontal grid stope level 1.

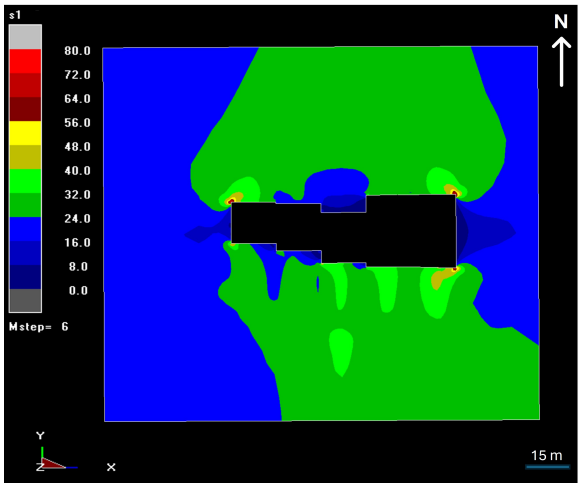

(b) Horizontal grid stope level 2.

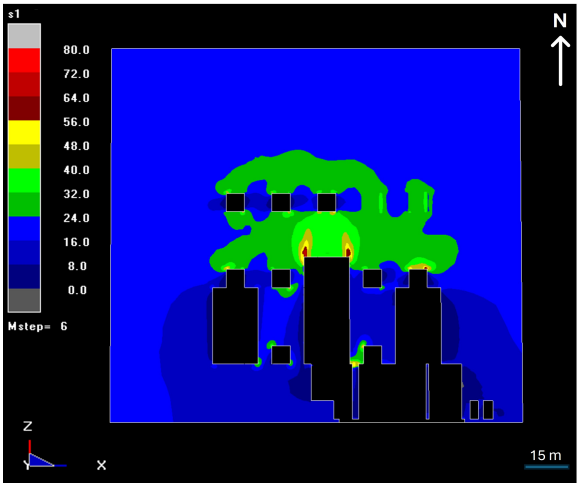

(c) Vertical grid step 3.

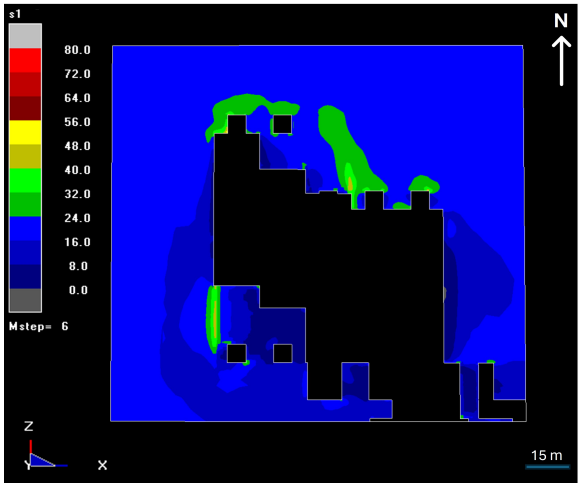

(d) Vertical grid step 6.

Figure B.2: σ_1-distribution around the stopes for design option 2.

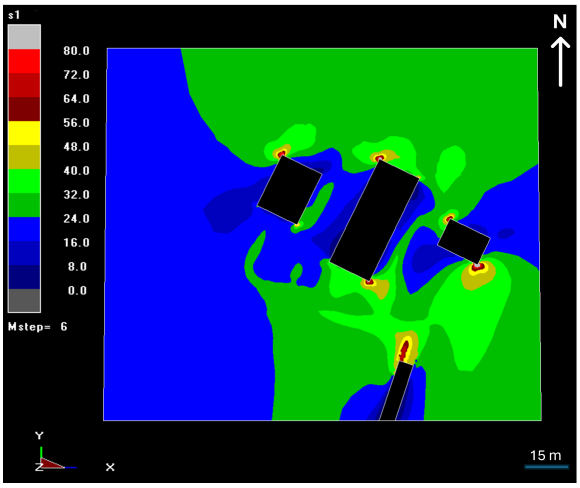

(a) Horizontal grid stope level 1.

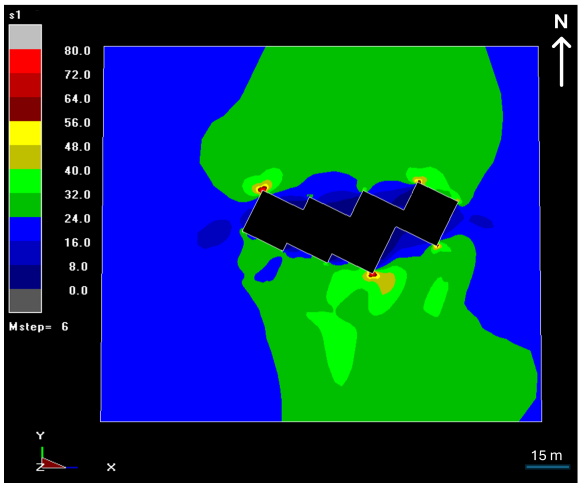

(b) Horizontal grid stope level 2.

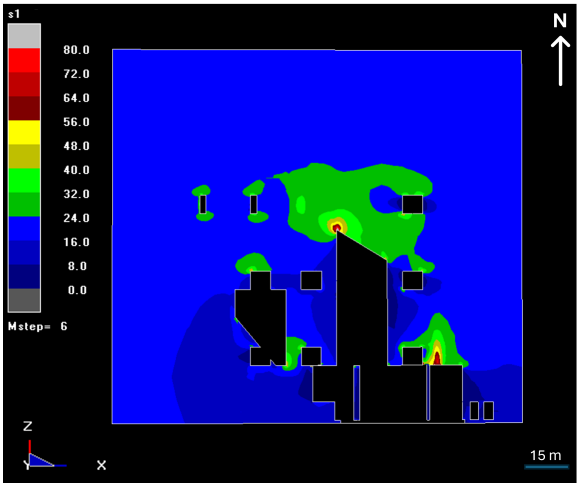

(c) Vertical grid step 3.

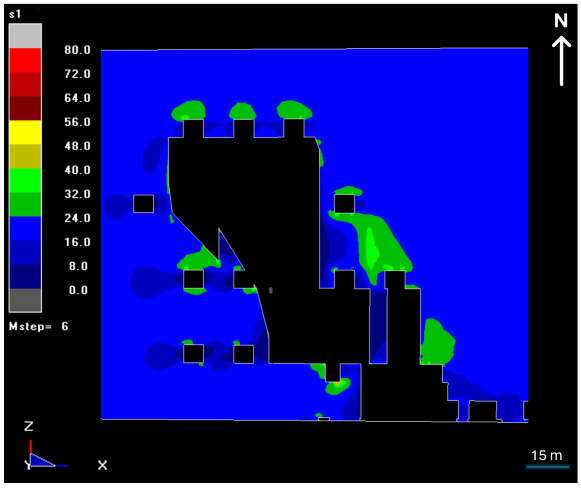

(d) Vertical grid step 6.

Figure B.3: σ_1-distribution around the stopes for design option 3.

C

Excel sheets for Modified Stability number determination

							WESTERN STOPE								
Riktning	Bergyta	Scenario	BRQD	Conversio	RQD	Jn	Jr	Ja	Q´	A	B	C	N´	H	B	L
Transverse	Long wall west shortest stope	Full serqtze	77	1.20	92.14	6	1.5	1	23.03	0.75	0.92	8	127.1	25.0		13.0
		Full serqtze less fav conditions	58	1.29	74.69	6	1	2	6.22	0.75	0.92	8	34.4	25.0		13.0
		Full SERSCH	61	1.28	77.91	12	1	3	2.16	0.6	1	8	10.4	25.0		13.0
		Full SERSCH stdev -1	34	1.32	44.89	12	0.5	4	0.47	0.6	1	8	2.2	25.0		13.0
Transverse	Long wall East shortest stope	Full serqtze	77	1.20	92.14	6	1.5	1	23.03	0.4	1	8	73.7	25.0		13.0
		Full serqtze less fav conditions	58	1.29	74.69	6	1	2	6.22	0.4	1	8	19.9	25.0		13.0
		Full SERSCH	61	1.28	77.91	12	1	3	2.16	0.3	0.6	8	3.1	25.0		13.0
		Full SERSCH stdev -1	34	1.32	44.89	12	0.5	4	0.47	0.3	0.6	8	0.7	25.0		13.0
Transverse	Roof	Full dacite	72	1.23	88.28	6	3	1	44.14	0.5	0.2	2	8.8		10.0	13.0
		Full dacite less fav conditions	53	1.30	69.02	6	2	1.5	15.34	0.5	0.2	2	3.1		10.0	13.0
		Full SERSCH	61	1.28	77.91	9	1	3	2.89	0.2	0.2	2	0.2		10.0	13.0
		Full SERSCH stdev -1	34	1.32	44.89	9	0.5	4	0.62	0.2	0.2	2	0.0		10.0	13.0
Transverse	Short front wall	Full serqtze	77	1.20	92.14	6	1.5	1	23.03	0.2	0.63	8	23.2	25.0		
		Full serqtze less fav conditions	58	1.29	74.69	6	1	2	6.22	0.2	0.63	8	6.3	25.0	10.0	
		Full SERSCH	61	1.28	77.91	12	1	3	2.16	0.15	0.42	8	1.1	25.0	10.0	
		Full SERSCH stdev -1	34	1.32	44.89	12	0.5	4	0.47	0.15	0.42	8	0.2	25.0	10.0	
Transverse	Short wall back	Full serqtze	77	1.20	92.14	6	1.5	1	23.03	0.4	0.67	8	49.4	25.0	10.0	
		Full serqtze less fav conditions	58	1.29	74.69	6	1	2	6.22	0.4	0.67	8	13.3	25.0	10.0	
		Full SERSCH	61	1.28	77.91	12	1	3	2.16	0.3	0.42	8	2.2	25.0	10.0	
		Full SERSCH stdev -1	34	1.32	44.89	12	0.5	4	0.47	0.3	0.42	8	0.5	25.0	10.0	
							MIDDLE STOPE									
Riktning	Bergyta	Scenario	BRQD	Conversio	RQD	Jn	Jr	Ja	Q´	A	B	C	N´	H	B	L
Transverse	Long wall (Sidewall) longest stope	Average case	77	1.20	92.14	6	1.5	1	23.03	0.75	0.92	8	127.1	25.0		35.0
		BRQD std dev (-1)	58	1.29	74.69	6	1	2	6.22	0.75	0.92	8	34.4	25.0		35.0
		Full SERSCH	61	1.28	77.91	12	1	3	2.16	0.6	1	8	10.4	25.0		35.0
		Full SERSCH stdev -1	34	1.32	44.89	12	0.5	4	0.47	0.6	1	8	2.2	25.0		35.0
Transverse	Long wall East shortest stope	Full serqtze	77	1.20	92.14	6	1.5	1	23.03	0.75	1	8	138.2	25.0		35.0
		Full serqtze less fav conditions	58	1.29	74.69	6	1	2	6.22	0.75	1	8	37.3	25.0		35.0
		Full SERSCH	61	1.28	77.91	12	1	3	2.16	0.6	0.6	8	6.2	25.0		35.0
		Full SERSCH stdev -1	34	1.32	44.89	12	0.5	4	0.47	0.6	0.6	8	1.3	25.0		35.0
Transverse	Roof	Full serqtze	77	1.20	92.14	6	1.5	1	23.03	0.2	0.32	2	2.9		10.0	35.0
		BRQD std dev (-1)	58	1.29	74.69	6	1	2	6.22	0.2	0.32	2	0.8		10.0	35.0
		Full SERSCH	61	1.28	77.91	12	1	3	2.16	0.15	0.2	2	0.1		10.0	35.0
		Full SERSCH stdev -1	34	1.32	44.89	12	0.5	4	0.47	0.15	0.2	2	0.0		10.0	35.0
Transverse	Front wall	Average case	77	1.20	92.14	6	1.5	1	23.03	0.15	0.86	5.9	17.5	26.6	10.0	
		BRQD std dev (-1)	58	1.29	74.69	6	1	2	6.22	0.15	0.86	5.9	4.7	26.6	10.0	
		Full SERSCH	61	1.28	77.91	12	1	3	2.16	0.1	0.88	5.9	1.1	26.6	10.0	
		Full SERSCH stdev -1	34	1.32	44.89	12	0.5	4	0.47	0.1	0.88	5.9	0.2	26.6	10.0	
Transverse	back wall	Average case	77	1.20	92.14	6	1.5	1	23.03	0.15	0.67	8	18.5	25.0	10.0	
		BRQD std dev (-1)	58	1.29	74.69	6	1	2	6.22	0.15	0.67	8	5.0	25.0	10.0	
		Full SERSCH	61	1.28	77.91	12	1	3	2.16	0.1	0.42	8	0.7	25.0	10.0	
		Full SERSCH stdev -1	34	1.32	44.89	12	0.5	4	0.47	0.1	0.42	8	0.2	25.0	10.0	

EASTERN STOPE

Riktning	Bergyta	Scenario	BRQD	Conversio	RQD	Jn	Jr	Ja	Q`	A	B	C	N`	H	B	L	Area	Omkrets	HR
Transverse	Long wall west shortest stope	Full serqtze	77	1.20	92.14	6	1.5	1	23.03	0.4	0.92	8	67.8	25.0		30.0	750	110	6.8
		Full serqtze less fav conditions	58	1.29	74.69	6	1	2	6.22	0.4	0.92	8	18.3	25.0		30.0	750	110	6.8
		Full SERSCH	61	1.28	77.91	12	1	3	2.16	0.3	1	8	5.2	25.0		30.0	750	110	6.8
		Full SERSCH stdev -1	34	1.32	44.89	12	0.5	4	0.47	0.3	1	8	1.1	25.0		30.0	750	110	6.8
Transverse	Long wall east shortest stope	Full serqtze	77	1.20	92.14	6	1.5	1	23.03	0.75	1	8	138.2	25.0		30.0	750	110	6.8
		Full serqtze less fav conditions	58	1.29	74.69	6	1	2	6.22	0.75	1	8	37.3	25.0		30.0	750	110	6.8
		Full SERSCH	61	1.28	77.91	12	1	3	2.16	0.6	0.6	8	6.2	25.0		30.0	750	110	6.8
		Full SERSCH stdev -1	34	1.32	44.89	12	0.5	4	0.47	0.6	0.6	8	1.3	25.0		30.0	750	110	6.8
Transverse	Roof	Full serqtze	72	1.23	88.28	6	1.5	1	22.07	0.2	0.32	2	2.8		10.0	27.0	270	74	3.6
		Full serqtze less fav conditions	53	1.30	69.02	6	1	2	5.75	0.2	0.32	2	0.7		10.0	27.0	270	74	3.6
		Full SERSCH	61	1.28	77.91	12	1	3	2.16	0.15	0.2	2	0.1		10.0	27.0	270	74	3.6
		Full SERSCH stdev -1	34	1.32	44.89	12	0.5	4	0.47	0.15	0.2	2	0.0		10.0	27.0	270	74	3.6
Transverse	Short front wall	Full serqtze	77	1.20	92.14	6	1.5	1	23.03	0.15	0.8	6.7	18.5	25.6	10.0		256	71.2	3.6
		Full serqtze less fav conditions	58	1.29	74.69	6	1	2	6.22	0.15	0.8	6.7	5.0	25.6	10.0		256	71.2	3.6
		Full SERSCH	61	1.28	77.91	12	1	3	2.16	0.1	0.84	6.7	1.2	25.6	10.0		256	71.2	3.6
		Full SERSCH stdev -1	34	1.32	44.89	12	0.5	4	0.47	0.1	0.84	6.7	0.3	25.6	10.0		256	71.2	3.6
Transverse	Short back wall	Full serqtze	77	1.20	92.14	6	1.5	1	23.03	0.1	0.67	8	12.3	25.0	10.0		250	70	3.6
		Full serqtze less fav conditions	58	1.29	74.69	6	1	2	6.22	0.1	0.67	8	3.3	25.0	10.0		250	70	3.6
		Full SERSCH	61	1.28	77.91	12	1	3	2.16	0.1	0.42	8	0.7	25.0	10.0		250	70	3.6
		Full SERSCH stdev -1	34	1.32	44.89	12	0.5	4	0.47	0.1	0.42	8	0.2	25.0	10.0		250	70	3.6

SECONDARY STOPE

Riktning	Bergyta	Scenario	BRQD	Conversio	RQD	Jn	Jr	Ja	Q`	A	B	C	N`	H	B	L	Area	Omkrets	HR
Transverse	Long wall west shortest stope	-																	
		-																	
		-																	
Transverse	Long wall east shortest stope	-																	
		-																	
		-																	
Transverse	Roof	Full serqtze	77	1.20	92.14	6	1.5	1	23.03	0.2	0.32	2	2.9		15.0	18.0	270	66	4.1
		Full serqtze less fav conditions	58	1.29	74.69	6	1	2	6.22	0.2	0.32	2	0.8		15.0	18.0	270	66	4.1
		Full SERSCH	61	1.28	77.91	12	1	3	2.16	0.15	0.2	2	0.1		15.0	18.0	270	66	4.1
		Full SERSCH stdev -1	34	1.32	44.89	12	0.5	4	0.47	0.15	0.2	2	0.0		15.0	18.0	270	66	4.1
Transverse	Short front wall	Full serqtze	77	1.20	92.14	6	1.5	1	23.03	0.4	0.86	6.1	48.3	26.2	15.0		393	82.4	4.8
		Full serqtze less fav conditions	58	1.29	74.69	6	1	2	6.22	0.4	0.86	6.1	13.1	26.2	15.0		393	82.4	4.8
		Full SERSCH	61	1.28	77.91	12	1	3	2.16	0.3	0.88	6.1	3.5	26.2	15.0		393	82.4	4.8
		Full SERSCH stdev -1	34	1.32	44.89	12	0.5	4	0.47	0.3	0.88	6.1	0.8	26.2	15.0		393	82.4	4.8
Transverse	Short back wall	Full SERSCH	61	1.28	77.91	12	1	3	2.16	0.3	0.42	8	2.2	25.0	15.0		375	80	4.7
		Full SERSCH stdev -1	34	1.32	44.89	12	0.5	4	0.47	0.3	0.42	8	0.5	25.0	15.0		375	80	4.7
		-																	
		-																	

Figure C.2: Design option 1, eastern and secondary stope.

WESTERN STOPE

Riktning	Bergyta	Scenario	BRQD	Conversio	RQD	Jn	Jr	Ja	Q´	A	B	C	N´	H	B	L	Area	Omkrets	HR
Transverse	West face west stope	Sericite-quartzite	77	1.20	92.14	6	1.5	1	23.03	1	0.92	8	169.5	25.0		13.0	325	76	4.3
		Sericite-quartzite-1*st.dev	58	1.29	74.69	6	1	2	6.22	1	0.92	8	45.8	25.0		13.0	325	76	4.3
		Sericite schist	61	1.28	77.91	12	1	3	2.16	1	1	8	17.3	25.0		13.0	325	76	4.3
		Sericite schist-1*st.dev	34	1.32	44.89	12	0.5	4	0.47	1	1	8	3.7	25.0		13.0	325	76	4.3
Transverse	East face west stope	Sericite-quartzite	77	1.20	92.14	6	1.5	1	23.03	0.4	1	8	73.7	25.0		13.0	325	76	4.3
		Sericite-quartzite-1*st.dev	58	1.29	74.69	6	1	2	6.22	0.4	1	8	19.9	25.0		13.0	325	76	4.3
		Sericite schist	61	1.28	77.91	12	1	3	2.16	0.3	0.6	8	3.1	25.0		13.0	325	76	4.3
		Sericite schist-1*st.dev	34	1.32	44.89	12	0.5	4	0.47	0.3	0.6	8	0.7	25.0		13.0	325	76	4.3
Transverse	Roof	Volcanoclastics	83	1.16	95.93	6	3	1	47.96	0.3	0.2	2	5.8			15.0	195	56	3.5
		Volcanoclastics less fav conditions	68	1.25	84.79	6	2	1.5	18.84	0.3	0.2	2	2.3			15.0	195	56	3.5
		Full SERSCH	61	1.28	77.91	12	1	3	2.16	0.15	0.2	2	0.1			15.0	195	56	3.5
		Full SERSCH stdev -1	34	1.32	44.89	12	0.5	4	0.47	0.15	0.2	2	0.0			15.0	195	56	3.5
Transverse	Front wall	Sericite-quartzite	77	1.20	92.14	6	1.5	1	23.03	0.2	0.63	8	13.9	25.0	15.0		375	80	4.7
		Sericite-quartzite-1*st.dev	58	1.29	74.69	6	1	2	6.22	0.2	0.63	8	3.8	25.0	15.0		375	80	4.7
		Sericite schist	61	1.28	77.91	12	1	3	2.16	0.15	0.42	8	0.7	25.0	15.0		375	80	4.7
		Sericite schist-1*st.dev	34	1.32	44.89	12	0.5	4	0.47	0.15	0.42	8	0.1	25.0	15.0		375	80	4.7
Transverse	back wall	Sericite-quartzite	77	1.20	92.14	6	1.5	1	23.03	0.3	0.67	8	31.5	25.0	15.0		375	80	4.7
		Sericite-quartzite-1*st.dev	58	1.29	74.69	6	1	2	6.22	0.3	0.67	8	8.5	25.0	15.0		375	80	4.7
		Sericite schist	61	1.28	77.91	12	1	3	2.16	0.2	0.42	8	1.2	25.0	15.0		375	80	4.7
		Sericite schist-1*st.dev	34	1.32	44.89	12	0.5	4	0.47	0.2	0.42	8	0.3	25.0	15.0		375	80	4.7

MIDDLE STOPE

Riktning	Bergyta	Scenario	BRQD	Conversio	RQD	Jn	Jr	Ja	Q´	A	B	C	N´	H	B	L	Area	Omkrets	HR
Transverse	Long wall West longest stope	Sericite-quartzite	77	1.20	92.14	6	1.5	1	23.03	0.4	0.92	8	67.8	25.0		29.0	725	108	6.7
		Sericite-quartzite-1*st.dev	58	1.29	74.69	6	1	2	6.22	0.4	0.92	8	18.3	25.0		29.0	725	108	6.7
		Sericite schist	61	1.28	77.91	12	1	3	2.16	0.3	1	8	5.2	25.0		29.0	725	108	6.7
		Sericite schist-1*st.dev	34	1.32	44.89	12	0.5	4	0.47	0.3	1	8	1.1	25.0		29.0	725	108	6.7
Transverse	Long wall East shortest stope	Sericite-quartzite	77	1.20	92.14	6	1.5	1	23.03	0.75	1	8	138.2	25.0		29.0	725	108	6.7
		Sericite-quartzite-1*st.dev	58	1.29	74.69	6	1	2	6.22	0.75	1	8	37.3	25.0		29.0	725	108	6.7
		Sericite schist	61	1.28	77.91	12	1	3	2.16	0.6	0.6	8	6.2	25.0		29.0	725	108	6.7
		Sericite schist-1*st.dev	34	1.32	44.89	12	0.5	4	0.47	0.6	0.6	8	1.3	25.0		29.0	725	108	6.7
Transverse	Roof	Sericite-quartzite	77	1.20	92.14	6	1.5	1	23.03	0.15	0.32	2	2.2		15.0	19.0	285	68	4.2
		Sericite-quartzite-1*st.dev	58	1.29	74.69	6	1	2	6.22	0.15	0.32	2	0.6		15.0	19.0	285	68	4.2
		Sericite schist	61	1.28	77.91	12	1	3	2.16	0.1	0.2	2	0.1		15.0	19.0	285	68	4.2
		Sericite schist-1*st.dev	34	1.32	44.89	12	0.5	4	0.47	0.1	0.2	2	0.0		15.0	19.0	285	68	4.2
Transverse	Front wall	Sericite-quartzite	77	1.20	92.14	6	1.5	1	23.03	0.2	0.93	4.8	27.0	29.5	15.0		442.5	89	5.0
		Sericite-quartzite-1*st.dev	58	1.29	74.69	6	1	2	6.22	0.2	0.93	4.8	7.3	29.5	15.0		442.5	89	5.0
		Sericite schist	61	1.28	77.91	12	1	3	2.16	0.15	0.93	4.8	1.9	29.5	15.0		442.5	89	5.0
		Sericite schist-1*st.dev	34	1.32	44.89	12	0.5	4	0.47	0.15	0.93	4.8	0.4	29.5	15.0		442.5	89	5.0
Transverse	back wall	Sericite-quartzite	77	1.20	92.14	6	1.5	1	23.03	0.15	0.8	6.8	24.9	25.6	15.0		384	81.2	4.7
		Sericite-quartzite-1*st.dev	58	1.29	74.69	6	1	2	6.22	0.15	0.8	6.8	6.7	25.6	15.0		384	81.2	4.7
		Sericite schist	61	1.28	77.91	12	1	3	2.16	0.1	0.84	6.8	1.6	25.6	15.0		384	81.2	4.7
		Sericite schist-1*st.dev	34	1.32	44.89	12	0.5	4	0.47	0.1	0.84	6.8	0.4	25.6	15.0		384	81.2	4.7

Figure C.3: Design option 2, western and middle stope.

EASTERN STOPE

Riktning	Bergyta	Scenario	BRQD	Conversio	RQD	Jn	Jr	Ja	Q´	A	B	C	N´	H	B	L	Area	Omkrets	HR
Transverse	Long wall west right stope	Sericite-quartzite	77	1.20	92.14	6	1.5	1	23.03	1	0.92	8	169.5	25.0		29.0	725	108	6.7
		Sericite-quartzite-1*st.dev	58	1.29	74.69	6	1	2	6.22	1	0.92	8	45.8	25.0		29.0	725	108	6.7
		Sericite schist	61	1.28	77.91	12	1	3	2.16	1	1	8	17.3	25.0		29.0	725	108	6.7
		Sericite schist-1*st.dev	34	1.32	44.89	12	0.5	4	0.47	1	1	8	3.7	25.0		29.0	725	108	6.7
Transverse	Long wall east right stope	Sericite-quartzite	77	1.20	92.14	6	1.5	1	23.03	0.75	1	8	138.2	25.0		29.0	725	108	6.7
		Sericite-quartzite-1*st.dev	58	1.29	74.69	6	1	2	6.22	0.75	1	8	37.3	25.0		29.0	725	108	6.7
		Sericite schist	61	1.28	77.91	12	1	3	2.16	0.6	0.6	8	6.2	25.0		29.0	725	108	6.7
		Sericite schist-1*st.dev	34	1.32	44.89	12	0.5	4	0.47	0.6	0.6	8	1.3	25.0		29.0	725	108	6.7
Transverse	Roof	Sericite-quartzite	77	1.20	92.14	6	1.5	1	23.03	0.15	0.32	2	2.2		15.0	27.0	405	84	4.8
		Sericite-quartzite-1*st.dev	58	1.29	74.69	6	1	2	6.22	0.15	0.32	2	0.6		15.0	27.0	405	84	4.8
		Sericite schist	61	1.28	77.91	12	1	3	2.16	0.1	0.2	2	0.1		15.0	27.0	405	84	4.8
		Sericite schist-1*st.dev	34	1.32	44.89	12	0.5	4	0.47	0.1	0.2	2	0.0		15.0	27.0	405	84	4.8
Transverse	Short front wall	SILTSTONE	82	1.16	95.36	6	3	3	15.89	0.2	0.86	6.3	17.2	26.0	15.0		390	82	4.8
		SILTSTONE less fav conditions	65	1.26	81.96	6	2	4	6.83	0.2	0.86	6.3	7.4	26.0	15.0		390	82	4.8
		Full SERSCH	61	1.28	77.91	12	1	3	2.16	0.1	0.88	6.3	1.2	26.0	15.0		390	82	4.8
		Full SERSCH stdev -1	34	1.32	44.89	12	0.5	4	0.47	0.1	0.88	6.3	0.3	26.0	15.0		390	82	4.8
Transverse	Short back wall	Sericite-quartzite	77	1.20	92.14	6	1.5	1	23.03	0.1	0.4	9	8.3	25.4	15.0		381	80.8	4.7
		Sericite-quartzite-1*st.dev	58	1.29	74.69	6	1	2	6.22	0.1	0.4	9	2.2	25.4	15.0		381	80.8	4.7
		Sericite schist	61	1.28	77.91	12	1	3	2.16	0.1	0.52	9	1.0	25.4	15.0		381	80.8	4.7
		Sericite schist-1*st.dev	34	1.32	44.89	12	0.5	4	0.47	0.1	0.52	9	0.2	25.4	15.0		381	80.8	4.7

SECONDARY STOPE

Riktning	Bergyta	Scenario	BRQD	Conversio	RQD	Jn	Jr	Ja	Q´	A	B	C	N´	H	B	L	Area	Omkrets	HR
Transverse	Long wall west shortest stope	-																	
		-																	
		-																	
Transverse	Long wall east shortest stope	-																	
		-																	
		-																	
Transverse	Roof	Sericite-quartzite	77	1.20	92.14	6	1.5	1	23.03	0.2	0.32	2	2.9		15.0	17.0	255	64	4.0
		Sericite-quartzite-1*st.dev	58	1.29	74.69	6	1	2	6.22	0.2	0.32	2	0.8		15.0	17.0	255	64	4.0
		Sericite schist	61	1.28	77.91	12	1	3	2.16	0.15	0.2	2	0.1		15.0	17.0	255	64	4.0
		Sericite schist-1*st.dev	34	1.32	44.89	12	0.5	4	0.47	0.15	0.2	2	0.0		15.0	17.0	255	64	4.0
Transverse	Short front wall	SILTSTONE	82	1.16	95.36	6	3	3	15.89	0.4	0.86	5.8	31.7	27.0	15.0		405	84	4.8
		SILTSTONE less fav conditions	65	1.26	81.96	6	2	4	6.83	0.4	0.86	5.8	13.6	27.0	15.0		405	84	4.8
		Sericite schist	61	1.28	77.91	12	1	3	2.16	0.2	0.88	5.8	2.2	27.0	15.0		405	84	4.8
		Sericite schist-1*st.dev	34	1.32	44.89	12	0.5	4	0.47	0.2	0.88	5.8	0.5	27.0	15.0		405	84	4.8
Transverse	Short back wall	Sericite schist	61	1.28	77.91	12	1	3	2.16	0.15	0.42	8	1.1	25.0	15.0		375	80	4.7
		Sericite schist-1*st.dev	34	1.32	44.89	12	0.5	4	0.47	0.15	0.42	8	0.2	25.0	15.0		375	80	4.7
		-																	
		-																	

Figure C.4: Design option 2, eastern and secondary stope.

WESTERN STOPE

Riktning	Bergyta	Scenario	BRQD	Conversio	RQD	Jn	Jr	Ja	Q´	A	B	C	N´	H	B	L	Area	Omkrets	HR
Transverse	West face west stope	Sericite-quartzite	77	1.20	92.14	6	1.5	1	23.03	0.4	0.67	8	49.4	25.0		17.9	446.25	85.7	5.2
		Sericite-quartzite-1*st.dev	58	1.29	74.69	6	1	2	6.22	0.4	0.67	8	13.3	25.0		17.9	446.25	85.7	5.2
		Sericite schist	61	1.28	77.91	12	1	3	2.16	0.3	0.85	8	4.4	25.0		17.9	446.25	85.7	5.2
		Sericite schist-1*st.dev	34	1.32	44.89	12	0.5	4	0.47	0.3	0.85	8	1.0	25.0		17.9	446.25	85.7	5.2
Transverse	East face west stope	Sericite-quartzite	77	1.20	92.14	6	1.5	1	23.03	0.2	1	8	36.9	25.0		17.9	446.25	85.7	5.2
		Sericite-quartzite-1*st.dev	58	1.29	74.69	6	1	2	6.22	0.2	1	8	10.0	25.0		17.9	446.25	85.7	5.2
		Sericite schist	61	1.28	77.91	12	1	3	2.16	0.15	0.65	8	1.7	25.0		17.9	446.25	85.7	5.2
		Sericite schist-1*st.dev	34	1.32	44.89	12	0.5	4	0.47	0.15	0.65	8	0.4	25.0		17.9	446.25	85.7	5.2
Transverse	Roof	Sericite-quartzite	83	1.16	95.93	6	3	1	47.96	0.3	0.32	2	9.2		15.0	14.4	216	58.8	3.7
		Sericite-quartzite-1*st.dev	68	1.25	84.79	6	2	1.5	18.84	0.3	0.32	2	3.6		15.0	14.4	216	58.8	3.7
		Sericite schist	61	1.28	77.91	12	1	3	2.16	0.2	0.4	2	0.3		15.0	14.4	216	58.8	3.7
		Sericite schist-1*st.dev	34	1.32	44.89	12	0.5	4	0.47	0.2	0.4	2	0.1		15.0	14.4	216	58.8	3.7
Transverse	Front wall	Sericite-quartzite	77	1.20	92.14	6	1.5	1	23.03	0.4	0.94	4.7	51.1	29.7	15.0		445.5	89.4	5.0
		Sericite-quartzite-1*st.dev	58	1.29	74.69	6	1	2	6.22	0.4	0.94	4.7	13.8	29.7	15.0		445.5	89.4	5.0
		Sericite schist	61	1.28	77.91	12	1	3	2.16	0.3	0.92	4.7	3.5	29.7	15.0		445.5	89.4	5.0
		Sericite schist-1*st.dev	34	1.32	44.89	12	0.5	4	0.47	0.3	0.92	4.7	0.8	29.7	15.0		445.5	89.4	5.0
Transverse	back wall	Sericite-quartzite	77	1.20	92.14	6	1.5	1	23.03	0.75	0.29	10	34.1	26.6	15.0		399	83.2	4.8
		Sericite-quartzite-1*st.dev	58	1.29	74.69	6	1	2	6.22	0.75	0.29	10	9.2	26.6	15.0		399	83.2	4.8
		Sericite schist	61	1.28	77.91	12	1	3	2.16	0.6	0.2	10	1.8	26.6	15.0		399	83.2	4.8
		Sericite schist-1*st.dev	34	1.32	44.89	12	0.5	4	0.47	0.6	0.2	10	0.4	26.6	15.0		399	83.2	4.8

MIDDLE STOPE

Riktning	Bergyta	Scenario	BRQD	Conversio	RQD	Jn	Jr	Ja	Q´	A	B	C	N´	H	B	L	Area	Omkrets	HR
Transverse	Long wall West longest stope	Sericite-quartzite	77	1.20	92.14	6	1.5	1	23.03	0.4	0.67	8	49.4	25.0		36.0	900	122	7.4
		Sericite-quartzite-1*st.dev	58	1.29	74.69	6	1	2	6.22	0.4	0.67	8	13.3	25.0		36.0	900	122	7.4
		Sericite schist	61	1.28	77.91	12	1	3	2.16	0.3	0.85	8	4.4	25.0		36.0	900	122	7.4
		Sericite schist-1*st.dev	34	1.32	44.89	12	0.5	4	0.47	0.3	0.85	8	1.0	25.0		36.0	900	122	7.4
Transverse	Long wall East shortest stope	Sericite-quartzite	77	1.20	92.14	6	1.5	1	23.03	0.4	1	8	73.7	25.0		36.0	900	122	7.4
		Sericite-quartzite-1*st.dev	58	1.29	74.69	6	1	2	6.22	0.4	1	8	19.9	25.0		36.0	900	122	7.4
		Sericite schist	61	1.28	77.91	12	1	3	2.16	0.3	0.65	8	3.4	25.0		36.0	900	122	7.4
		Sericite schist-1*st.dev	34	1.32	44.89	12	0.5	4	0.47	0.3	0.65	8	0.7	25.0		36.0	900	122	7.4
Transverse	Roof	Sericite-quartzite	77	1.20	92.14	6	1.5	1	23.03	0.2	0.32	2	2.9		15.0	29.0	435	88	4.9
		Sericite-quartzite-1*st.dev	58	1.29	74.69	6	1	2	6.22	0.2	0.32	2	0.8		15.0	29.0	435	88	4.9
		Sericite schist	61	1.28	77.91	12	1	3	2.16	0.15	0.4	2	0.3		15.0	29.0	435	88	4.9
		Sericite schist-1*st.dev	34	1.32	44.89	12	0.5	4	0.47	0.15	0.4	2	0.1		15.0	29.0	435	88	4.9
Transverse	Front wall	Sericite-quartzite	77	1.20	92.14	6	1.5	1	23.03	0.2	0.89	5.9	28.7	26.6	15.0		399	83.2	4.8
		Sericite-quartzite-1*st.dev	58	1.29	74.69	6	1	2	6.22	0.2	0.89	5.9	7.8	26.6	15.0		399	83.2	4.8
		Sericite schist	61	1.28	77.91	12	1	3	2.16	0.15	0.86	5.9	2.0	26.6	15.0		399	83.2	4.8
		Sericite schist-1*st.dev	34	1.32	44.89	12	0.5	4	0.47	0.15	0.86	5.9	0.4	26.6	15.0		399	83.2	4.8
Transverse	back wall	Sericite-quartzite	77	1.20	92.14	6	1.5	1	23.03	0.2	0.83	6.8	30.6	25.5	15.0		382.5	81	4.7
		Sericite-quartzite-1*st.dev	58	1.29	74.69	6	1	2	6.22	0.2	0.83	6.8	8.3	25.5	15.0		382.5	81	4.7
		Sericite schist	61	1.28	77.91	12	1	3	2.16	0.15	0.56	6.8	1.5	25.5	15.0		382.5	81	4.7
		Sericite schist-1*st.dev	34	1.32	44.89	12	0.5	4	0.47	0.15	0.56	6.8	0.3	25.5	15.0		382.5	81	4.7

Figure C.5: Design option 3, western and middle stope.

EASTERN STOPE

Riktning	Bergyta	Scenario	BRQD	Conversio	RQD	Jn	Jr	Ja	Q´	A	B	C	N´	H	B	L	Area	Omkrets	HR
Transverse	Long wall west right stope	Sericite-quartzite	77	1.20	92.14	6	1.5	1	23.03	1	0.92	8	169.5	25.0	15.0	29.0	725	108	6.7
		Sericite-quartzite-1*st.dev	58	1.29	74.69	6	1	2	6.22	1	0.92	8	45.8	25.0		29.0	725	108	6.7
		Sericite schist	61	1.28	77.91	12	1	3	2.16	1	1	8	17.3	25.0		29.0	725	108	6.7
		Sericite schist-1*st.dev	34	1.32	44.89	12	0.5	4	0.47	1	1	8	3.7	25.0		29.0	725	108	6.7
Transverse	Long wall east right stope	Sericite-quartzite	77	1.20	92.14	6	1.5	1	23.03	0.75	1	8	138.2	25.0	15.0	29.0	725	108	6.7
		Sericite-quartzite-1*st.dev	58	1.29	74.69	6	1	2	6.22	0.75	1	8	37.3	25.0		29.0	725	108	6.7
		Sericite schist	61	1.28	77.91	12	1	3	2.16	0.6	0.6	8	6.2	25.0		29.0	725	108	6.7
		Sericite schist-1*st.dev	34	1.32	44.89	12	0.5	4	0.47	0.6	0.6	8	1.3	25.0		29.0	725	108	6.7
Transverse	Roof	Sericite-quartzite	77	1.20	92.14	6	1.5	1	23.03	0.15	0.32	2	2.2		15.0	27.0	405	84	4.8
		Sericite-quartzite-1*st.dev	58	1.29	74.69	6	1	2	6.22	0.15	0.32	2	0.6		15.0	27.0	405	84	4.8
		Sericite schist	61	1.28	77.91	12	1	3	2.16	0.1	0.2	2	0.1		15.0	27.0	405	84	4.8
		Sericite schist-1*st.dev	34	1.32	44.89	12	0.5	4	0.47	0.1	0.2	2	0.0		15.0	27.0	405	84	4.8
Transverse	Short front wall	SILTSTONE	82	1.16	95.36	6	3	3	15.89	0.2	0.86	6.3	17.2	26.0	15.0		390	82	4.8
		SILTSTONE less fav conditions	65	1.26	81.96	6	2	4	6.83	0.2	0.86	6.3	7.4	26.0	15.0		390	82	4.8
		Full SERSCH	61	1.28	77.91	12	1	3	2.16	0.1	0.88	6.3	1.2	26.0	15.0		390	82	4.8
		Full SERSCH stdev -1	34	1.32	44.89	12	0.5	4	0.47	0.1	0.88	6.3	0.3	26.0	15.0		390	82	4.8
Transverse	Short back wall	Sericite-quartzite	77	1.20	92.14	6	1.5	1	23.03	0.1	0.4	9	8.3	25.4	15.0		381	80.8	4.7
		Sericite-quartzite-1*st.dev	58	1.29	74.69	6	1	2	6.22	0.1	0.4	9	2.2	25.4	15.0		381	80.8	4.7
		Sericite schist	61	1.28	77.91	12	1	3	2.16	0.1	0.52	9	1.0	25.4	15.0		381	80.8	4.7
		Sericite schist-1*st.dev	34	1.32	44.89	12	0.5	4	0.47	0.1	0.52	9	0.2	25.4	15.0		381	80.8	4.7

SECONDARY STOPE

Riktning	Bergyta	Scenario	BRQD	Conversio	RQD	Jn	Jr	Ja	Q´	A	B	C	N´	H	B	L	Area	Omkrets	HR
Transverse	Long wall west shortest stope	-																	
		-																	
		-																	
Transverse	Long wall east shortest stope	-																	
		-																	
		-																	
Transverse	Roof	Sericite-quartzite	77	1.20	92.14	6	1.5	1	23.03	0.2	0.32	2	2.9		15.0	17.0	255	64	4.0
		Sericite-quartzite-1*st.dev	58	1.29	74.69	6	1	2	6.22	0.2	0.32	2	0.8		15.0	17.0	255	64	4.0
		Sericite schist	61	1.28	77.91	12	1	3	2.16	0.15	0.2	2	0.1		15.0	17.0	255	64	4.0
		Sericite schist-1*st.dev	34	1.32	44.89	12	0.5	4	0.47	0.15	0.2	2	0.0		15.0	17.0	255	64	4.0
Transverse	Short front wall	SILTSTONE	82	1.16	95.36	6	3	3	15.89	0.4	0.86	5.8	31.7	27.0	15.0		405	84	4.8
		SILTSTONE less fav conditions	65	1.26	81.96	6	2	4	6.83	0.4	0.86	5.8	13.6	27.0	15.0		405	84	4.8
		Sericite schist	61	1.28	77.91	12	1	3	2.16	0.2	0.88	5.8	2.2	27.0	15.0		405	84	4.8
		Sericite schist-1*st.dev	34	1.32	44.89	12	0.5	4	0.47	0.2	0.88	5.8	0.5	27.0	15.0		405	84	4.8
Transverse	Short back wall	Sericite schist	61	1.28	77.91	12	1	3	2.16	0.15	0.42	8	1.1	25.0	15.0		375	80	4.7
		Sericite schist-1*st.dev	34	1.32	44.89	12	0.5	4	0.47	0.15	0.42	8	0.2	25.0	15.0		375	80	4.7
		-																	
		-																	

Figure C.6: Design option 3, eastern and secondary stope.